Ghent University

Faculty of Engineering and Architecture

Academic Year 2019 – 2020

INTERACTIVE TOOL FOR STRUCTURAL FIRE ENGINEERING AWARENESS

Kevin Kurniawan

Supervisor:

Ruben Van Coile

Counsellors:

Balša Jovanović

Ranjit Kumar Chaudhary

Master thesis submitted in the Erasmus + Study Programme

International Master of Science in Fire Safety Engineering

Disclaimer

This thesis is submitted in partial fulfilment of the requirements for the degree of The International Master of Science in Fire Safety Engineering (IMFSE). This thesis has never been submitted for any degree or examination to any other University/programme. The author(s) declare(s) that this thesis is original work except where stated. This declaration constitutes an assertion that full and accurate references and citations have been included for all material, directly included and indirectly contributing to the thesis. The author(s) gives (give) permission to make this master thesis available for consultation and to copy parts of this master thesis for personal use. In the case of any other use, the limitations of the copyright have to be respected, in particular with regard to the obligation to state expressly the source when quoting results from this master thesis. The thesis supervisor must be informed when data or results are used.

Read and approved,

Kevin Kurniawan

IMFSE Master Thesis Declaration

This form has been developed in the context of the unforeseen circumstances due to Covid-19, necessitating a reduction of practical project work (whether it be laboratory based, computational, or fieldwork) during the master thesis semester. It acts as a record of the impact on the master thesis. The form has been completed by the student and verified by the supervisor. **A copy of the signed form is included behind the abstract in the dissertation.**

Name: Kevin Kurniawan

Work completed

All items of wholly, or partially completed work must be listed, indicating the percentage completion for each task. **Please take care to provide a full detailed list of all work done.**

Regression Analysis	100%
Structural Behaviour Anomaly Analysis	90%

Work not commenced

Any items of outstanding work that have not been started should be listed here.

Declaration

To the best of our knowledge, this form is an accurate record of the project status on 30 April 2020

Student: Kevin Kurniawan _____

Supervisor: Ruben Van Coile _____

Abstract

When designing a structure it is important to make sure that all external load, including fire, are accounted for. The probability of a fire happens in a building is highly uncertain, yet the effect is not negligible. In order to increase this structural fire safety awareness, structural and fire engineers need to be exposed to this serious problem, and an accurate and interactive tool is required.

Since the effect of fire to structure is very non-linear, finite element method is used in structural fire software and often it takes too much time to run. So, machine learning methods are developed in this research to "bypass" the long computational time by the software by predicting the wanted outputs by several inputs. By using machine learning method, it is expected that the structural behaviour under thermal load can be accurately predicted within a short period of time.

The machine learning methods used are polynomial regression and gradient boosting on decision trees, the results of which are compared and explained in this research. With the help of Latin Hypercube Sampling (LHS), the amount of simulations needed for this research can be minimized, and hence improving efficiency in the process.

During the analysis, uncommon behaviour of concrete structure is observed where a concrete beam may deflect upwards when heated from underneath. An unexpected turn is made in this research to further investigate and validate this behaviour using M-χ diagram and virtual work method to calculate the beam deflection.

Abstrak

Saat mendesain suatu gedung, sangatlah penting untuk memastikan bahwa semua beban luar, termasuk api, sudah diperhitungkan. Walaupun kemungkinan terjadinya kebakaran di gedung tidak menentu, dampak dari kejadian tersebut tidak bisa diremehkan. Untuk meningkatkan kesadaran akan hal ini, insinyur struktur dan api perlu diinformasikan akan hal ini, dan oleh sebab itu, alat bantu yang akurat dan interaktif diperlukan.

Karena dampak dari kebakaran ke suatu elemen struktur sangat tidak linear, kebanyakan program perhitungan struktur dan api menggunakan metode finite element dan memakan banyak waktu. Jadi, riset ini menggunakan algoritma machine learning untuk memangkas waktu perhitungan dari program tersebut dengan cara memprediksi hasil yang diinginkan dengan sejumlah input. Dengan cara ini, perilaku struktur yang terdampak oleh kebakaran dapat diprediksi secara akurat dengan waktu yang singkat.

Metode machine learning yang digunakan di riset ini adalah polynomial regression dan gradient boosting on decision trees, yang hasilnya akan dibahas dan dibandingkan. Dengan bantuan metode pengambilan sampel Latin Hypercube Sampling (LHS), banyaknya simulasi yang perlu dijalankan di riset ini dapat diminimalisir dan membuat riset ini lebih efisien.

Di riset ini, perilaku menyimpang dari struktur dapat diamati di mana balok beton yang seharusnya melendut ke bawah saat dipanaskan dari bawah, berbalik melendut ke atas. Kejadian ini lantas diamati secara lebih mendalam di riset ini dengan menggunakan diagram momen kurvatur (M-χ diagram) dan metode virtual work untuk menghitung lendutan balok.

Acknowledgement

First of all, I would like to thank Ruben Van Coile as the promotor of this thesis for giving me the opportunity to work on this interesting topic and throughout the semester providing me with his guidance, knowledge, and patience. Without his help, this thesis would not have been possible.

I would also like to thank Ranjit Kumar Chaudary as the counsellor of this thesis for giving me inputs and recommendations and especially Балша Јовановић (Balša Jovanović) as my counsellor and my housemate as well whom I can bother until 2AM in the morning for thesis questions.

My eternal gratitude goes to my family back in Indonesia for their constant support from the first day I stepped my foot in Europe. Especially during this corona pandemic, they never stop giving me encouragements and supports even from miles away.

Furthermore, many thanks to my IMFSE friends with whom I went through thick and thin for the last two years. Especially with the meme battle going on in the group chat that really cheers everyone up.

Last but not least, I dedicate my thesis to my fiancée, Martina Megasari, for being very supportive the whole 2 years of IMFSE programme and for being the person I can really count on during this hard period.

Table of Contents

1 Introduction & Objectives

1.1 Background

As structural fire engineering lies between structural engineering and fire engineering disciplines, it is often over-simplified by either discipline [1]. Traditional structural engineers often neglect, for example the effect of cooling phase in a fire exposed structure, while fire engineers often assess a structure based on a temperature limit and tend to overlook other structural behaviour under fire. These simplifications will result in a less successful structural fire engineering design [1]. As also emphasized by Thienpont et al., cooling phase should also be considered when calculating structural strength under fire [2]. Therefore, if each of the disciplines could be more acquainted with the complexity of the opposite area of knowledge and its influence, a more comprehensive solution would be achieved. [3]

One of the important measures to help achieving this goal is to raise awareness amongst structural and fire engineers. This can be done by creating an interactive tool that can instantaneously show structural fire performance by integrating the complexities from both disciplines, allowing structural or fire engineer to have an immediate and clear visualization of the structural behaviour. In order to achieve this, reliable and fast solutions are needed. So, a large number of structural fire engineering calculations will be conducted and the results of which will be generalized with the help of machine learning methods. The model created by machine learning method allows to accurately predict the output with negligible waiting time.

1.2 Objective

The objectives of this thesis are to study structural response in case of fire; to find a relationship between parameters (from structural and fire engineering fields) and beam behaviours, such as deflection and internal forces; and to provide a real-time visualization of the outputs without having to model the beam in a computer programme with the help of statistical and machine learning method.

Additionally, this research has taken an unexpected turn and a deeper structural analysis is carried out to analyse unusual behaviour of a beam with double pinned support when exposed to fire. Initially, it was expected that a beam would deflect downwards when heated from underneath because the exposed side of the beam will elongate more than the opposite side [4]. However, in some of the simulations, it was observed that the beam will deflect downwards at first and after reaching one point, the beam would change its deflection direction and start deflecting upwards. A more detailed analysis and will be discussed in Section 4.

1.3 Research Outline

The remainder of this thesis will be organized as follow. Chapter 2 presents some related works on the similar problems to this project. SAFIR simulations and regression analysis are conducted and the overall methodology of the project is presented in Chapter 3. In Chapter 4, the anomaly of the beam behaviour observed in Chapter 3 is discussed further. Finally, the research conclusions and ideas for future work are presented in Chapter 5.

2 Literature Review

In this section, some works related to reinforced concrete beam behaviour under fire load and beam analysis using regression are discussed to give more explanation about the background of this research.

2.1 Concrete Beam Behaviour Under Thermal Load

Concrete is one of the most used structural material in the world and there have been many researches in this field regarding its strength and behaviour. However, when exposed to fire, concrete will experience strength loss and its responses might vary.

In one of his papers, Usmani et al. [4] discussed the behaviour of structural materials under fire load. Since most materials will expand while heated, he analysed that the temperature difference in the material will affect its behaviour which is dependent on the thermal conductivity of the material itself. For example, unlike steel, concrete has a very low conductivity, meaning that the temperature on the exposed side will be much higher than the one on the other side. This difference in the temperature will create a thermally induced displacement which is called "thermal bowing". Figure 1 below shows the thermal bowing effect due to temperature difference in a simply supported beam.

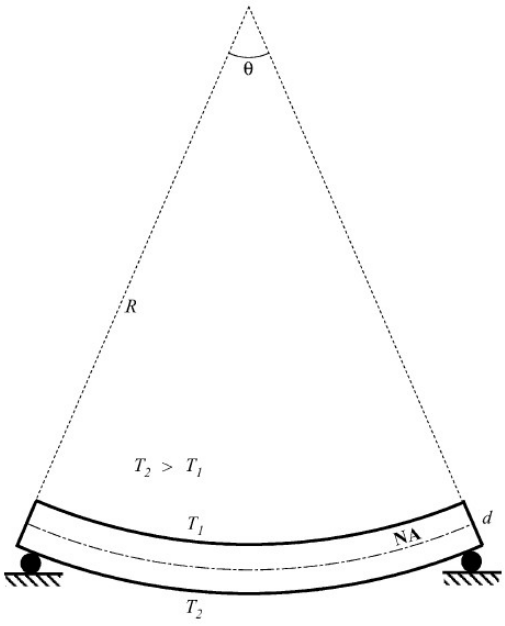

Figure 1. Thermal bowing due to linear temperature difference in a simply supported beam [4]

Furthermore, if the beam is axially restrained, the thermal elongation of the beam will be restrained by the supports and make the beam deflects vertically, hence making the displacement bigger. However, it is important to note that the thermal gradient between the exposed side and the opposite side is assumed to be linear, where in reality, for concrete beam, the thermal gradient is far from being linear.

Another research was conducted by Kodur et al. [5] to predict the behaviour of reinforced concrete under thermal load. In this research, he assumed that the thermal gradient is non-linear and he used finite element model to predict the beam deflections which involves moment-curvature relationships and non-linear stiffness equation.

2.2 Regression Analysis

Regression analysis has been a popular research area in fire engineering field due to the big number of uncertainties. Not only can it help predicting the structural behaviour, but it can also help to predict response time and evacuation time of a model. Lin et al. [6] conducted a research about doing a regression model to predict response time and evacuation time based on variables such as floor area, number of evacuation exits, and the occupant load per floor. Those variables were then analysed using Microsoft Excel as the regression method. It was found that, when compared to software simulations, the performance of the prediction model could have less than ten percent error.

Another type of regression analysis is with multiple linear regression. This approach needs more than one variables but they cannot be too closely correlated to each other [7]. A study by Johansson et al. [8] used this method at first to predict the temperature of the smoke layer in an adjacent room before the fire reaches flashover. However, at a later stage the regression method was changed to exponential regression because the result of the multiple linear regression was not satisfactory. SPSS (Statistical Package for the Social Sciences) software was used in this research to analyse both regression analyses.

3 Structural Fire Tool Development

3.1 Methodology

This section consists of two main stages. The first stage involves variable selection, where the inputs are carefully considered and selected from its relevance to the outputs, and data analysis where the selected variables are processed with structural fire software, SAFIR to get the structural fire response.

SAFIR is a finite element based computer programme developed by University of Liege that can model structure behaviour when exposed to fire. There are two methods of inputting parameter values to this software. First is with GiD, a pre-processing software with a GUI (Graphical User Interface) where you can draw the structure and run SAFIR directly. The second method uses a plain text file as an input file. This method is more difficult than the first one because it needs a proper knowledge of SAFIR and the input file takes longer time to build from scratch. But, this method allows repeated simulations with the help of a programmable tool. As multiple simulations need to be analysed with SAFIR in this research, the second method will be adopted.

In the second stage, the obtained responses are then analysed using Python programming language for doing statistical calculation and creating machine learning models. In this stage, correlations between the inputs and the outputs are produced in the form of equations. By

using these equations, an instant output can be accurately predicted and hence, making the tool interactive and easy to use for either structural or fire engineers. The whole procedure is illustrated in a flowchart in Figure 2 below.

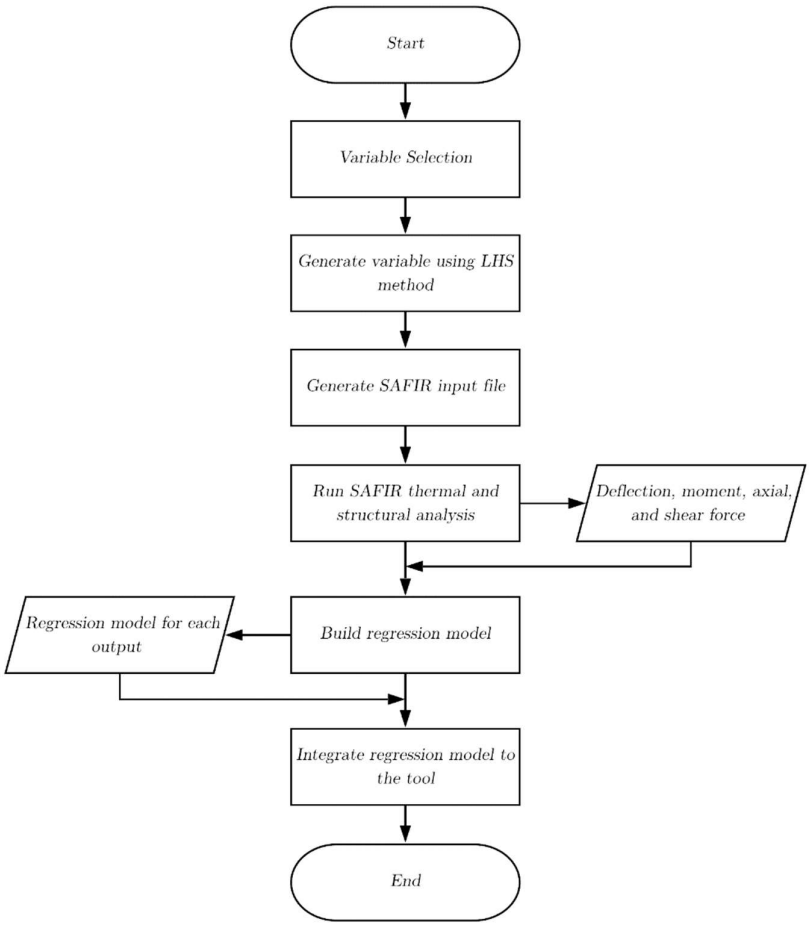

Figure 2. Flowchart for structural fire tool development

3.1.1 Variable Selection

Since the results of the machine learning largely depend on the selection of inputs, this part is very crucial to building a strong foundation to this research. First of all, several inputs are selected based on the relevance to the desired outputs which are beam deflection and the internal forces of the beam (axial, moment, and shear load). In this proof-of-concept study, the inputs selected for the outputs are:

3.1.1.1 Concrete compressive strength (f_c')

Compressive strength of the concrete will determine the concrete modulus (E_c) which will later affect the beam deflection. This can be seen from the stress-strain relationship in accordance with the Eurocode [9]. Additionally, when the beam is axially restrained and subjected to thermal load, it will expand and the concrete modulus will have an effect on the restraining force.

3.1.1.2 Steel yield strength (f_y)

As the reinforced concrete beam is comprised of concrete and steel rebar, steel yield strength, like concrete compressive strength, will also affect the deflection of the concrete beam.

3.1.1.3 Beam section (depth and width)

Depth and width of the beam will have an influence in the temperature of the beam. These will also affect the moment of inertia of the beam which will affect whether the beam will deflect downwards or upwards. This will be explained in depth in Section 4. In terms of internal forces, the area of the beam section will affect the restraining force in the support.

3.1.1.4 Concrete cover

Concrete cover will affect how fast the steel rebar will be heated when the beam is exposed to fire. Because concrete has much lower conductivity than steel, the concrete cover will protect the steel rebar from the heat.

3.1.2 Variables Generation

After selecting all the required inputs, the values of each input are then generated randomly using Latin Hypercube Sampling (LHS). It is based on Latin square model, which maps n different numbers into a square of size n x n in a way that each row and column has exactly one occurrence of each number. and Figure 4 below show an example of a Latin square with 3 columns and 3 rows [10] and a mapping of an LHS sampling respectively.

A	B	C
C	A	B
B	C	A

Figure 3. Latin square model [14]

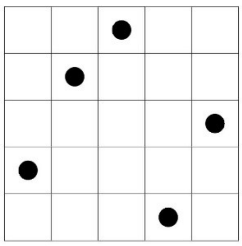

Figure 4. LHS Sampling

The advantage of this method is that the data can be distributed evenly so that, when compared to a normal random sampling method, the amount of simulations needed can be reduced to produce results of similar quality [11]. With the number of simulations being reduced, since this research will do multiple analyses with SAFIR, the computational time can be reduced as well. Under this consideration, LHS method will be adopted in this research. The sampling range of the input values and the descriptions are shown in Table 1 and Figure 5.

Table 1. Input value distribution

Variables	Min	Max	Units
Concrete strength	30	80	MPa
Steel strength	300	600	MPa
Depth (D)	300	600	mm
Width (w)	300	400	mm
Concrete cover (c)	20	40	mm

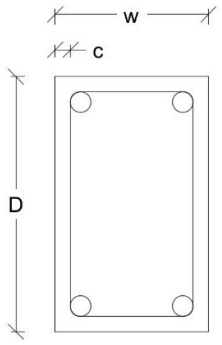

Figure 5. Section description

3.1.3 Data Analysis

From the sets of input data acquired from the previous step, a Python program will be used to convert all of them into SAFIR plain text input file. There are two files that are needed to be generated per simulation using Python program, thermal input file for SAFIR thermal analysis and structural input file for SAFIR structural analysis. For both analyses, the calculation time is set to be 180 minutes and the output will be recorded each minute.

3.1.3.1 SAFIR Thermal Analysis

This analysis is carried out to calculate the temperature of the beam section depending on the fire type and where the fire is located. The fire curve used in this analysis is ISO 834 fire curve. Since the purpose of this research is to demonstrate the behaviour of a concrete beam, the fire will be located below the beam and therefore, the sides of the beam that are exposed to the heat are the right side, bottom side, and left side; leaving the top side exposed to ambient temperature which is assumed to be 20°C (Figure 6).

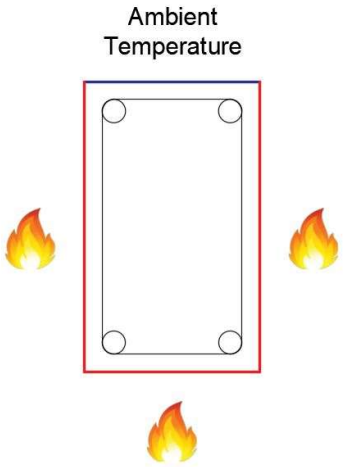

Figure 6. Boundary conditions of the beam

Apart from the fire exposure to the beam, other inputs that are used for this analysis are shown in Table 2 below. It can be seen in the table that reinforcement bars are also included in the thermal input variables. It is not the strength of the steel rebar that is analysed but the location of the steel rebar will affect the conductive heat transfer in the beam as the thermal conductivity of the steel is much bigger than that of concrete. It is also assumed that heat transfer by conduction is done directly from elements to elements (no heat transfer in the cavity) [12]

As SAFIR is a finite element based computer programme, the beam section needs to be meshed into smaller parts for the input file. A Python program will be used to divide the section with the help of matplotlib plotting library from Python. The temperature of each section will then be analysed per minute.

Table 2. SAFIR Thermal Analysis Inputs

Variables	Value	Units
Beam depth	vary[1]	mm
Beam width	vary[1]	mm
Mesh size	10	mm
# of rebar	4	pcs
Rebar diameter	32	mm
Concrete specifications:[2]		
Specific mass	2400	kg/m^3
Moisture content	48	kg/m^3
Convection coefficient (hot surfaces)	25	W/m^2K
Convection coefficient (cold surfaces)	4	W/m^2K
Relative emissivity	0.7	-
Parameter of thermal conductivity	0.5	-
Steel rebar specifications:[2]		
Convection coefficient (hot surfaces)	25	W/m^2K
Convection coefficient (cold surfaces)	4	W/m^2K
Relative emissivity	0.7	-

[1] Beam depth and width value will be generated randomly from the range listed in Table 1
[2] Concrete and steel rebar specifications use the default value of SAFIR

After the analysis has finished, the programme will create two files, a *.OUT and *.TEM file which consist of all the temperature values of each section of the beam throughout the calculation time. The latter will also be needed as an input file for SAFIR structural analysis which will be described in the following section.

3.1.3.2 SAFIR Structural Analysis

SAFIR structural analysis is the last step of this SAFIR analysis. After getting *.TEM output file from SAFIR thermal analysis, it will be used as an input file in SAFIR structural analysis to take into account the effect of temperature rise in the beam.

In this analysis, it is assumed that there is no external load working on the beam, be it a distributed load or a point load. So, the deflections and internal forces recorded in the outputs are purely caused by the thermal load. Table 3 below lists the other inputs that are used in SAFIR structural analysis.

It can be seen from the table that there is another mesh input in SAFIR structural analysis. The difference of the mesh between thermal and structural analysis is that in thermal analysis, the section of the beam will be meshed, while in structural analysis, the beam length. The maximum temperature listed in the rebar specification is the temperature where irreversible behaviour takes place during the cooling phase and the yield strength starts to decrease.

However, since the temperature of the beam does not reach 1200°C throughout the 3 hours of calculation time, both of these behaviour do not apply to this analysis.

Table 3. SAFIR Structural Analysis Inputs

Variables	Value	Units
Beam depth	vary[1]	mm
Beam width	vary[1]	mm
Beam length	10	m
Maximum mesh size	0.2	m
# of rebar	4	pcs
Rebar diameter	32	mm
Concrete specifications:[2]		
Poisson ratio (v)	0.3	-
Compressive strength	vary[1]	N/m^2
Tensile strength	0	N/m^2
Steel rebar specifications:[2]		
Young's modulus	2×10^{11}	N/m^2
Poisson ratio (v)	0.3	-
Yield strength	vary[1]	N/m^2
Maximum temperature	1200	°C
Decrease rate of yield strength	0	MPa/°C

[1] The value will be generated randomly from the range listed in Table 1
[2] Concrete and steel rebar specifications use the default value of SAFIR

After the analysis, the output file will be created comprising all the necessary structural outputs; namely, beam deflections, mechanical strains, stresses, and beam internal forces (moment, shear, and axial forces). These responses are then stored in a plain text file with *.OUT extension.

However, as it is difficult to observe the data in a plain text file type, Python will be used to extract the necessary information from the *.OUT file into a Microsoft Excel file.

3.1.4 Regression Model

After the results from SAFIR simulations have been obtained, they are used as data sources for building regression models. In this research, the methods used to build the models are polynomial regression and gradient boosting on decision trees.

3.1.4.1 Polynomial Regression

Polynomial regression is a type of machine learning method that use polynomial function to model a relationship between independent variables (x) and dependent variables (Y). The complexity of the relationship depends on the degree of polynomial used and the amount of

(3.1)

variables. Equation 3.1 below is the example of a polynomial equation with two variables and two degree of polynomial with theta (θ) as a coefficient for each polynomial terms.

$$Y = f(x)$$

$$Y = \theta_0 + \theta_1.x_1 + \theta_2.x_1^2 + \theta_3.x_1x_2 + \theta_4.x_2 + \theta_5.x_2^2$$

In this analysis, independent variables are divided into three samples comprising a training set, a validation set, and a testing set. Training set and validation set consist of variables that has been randomized using LHS method described in Section 3.1.2 while the testing set will be randomized normally using random distribution. This is because the regression model will train a training set and a validation set, while the testing set will be used to determine the prediction accuracy of the model.

In order to produce a good regression model, a set of regression parameter needs to be defined. The parameters are degree of polynomials (D), regularization parameter (λ), and number of training instances (n). Those parameters, together with the variable sets, will then be used to calculate the cost function, which is: (3.2)

$$J_{(\theta)} = \frac{1}{2n}\sum_{i=1}^{n}(f(x) - Y)^2$$

However, before the variables sets can be used in Equation 3.2 above, they need to be 'standardized' so as to make the convergence easier to reach. Standardized, in this case, means that all the randomized variables are converted, so that each group of variable has a mean value of zero. [13]

After the variable values have been standardized, the D is then defined by calculating the cost function of the training set using Equation 3.2 for each polynomial, from which, the most optimal D will be selected. From 1000 simulations trained, Figure 7 below shows the cost function for each polynomial from 1 to 6. It can be seen that the error drastically drops from 1st to 2nd degree polynomial, but from 2nd to 3rd degree polynomial, there is no significant improvement on the cost function and therefore, 2nd degree polynomial is chosen.

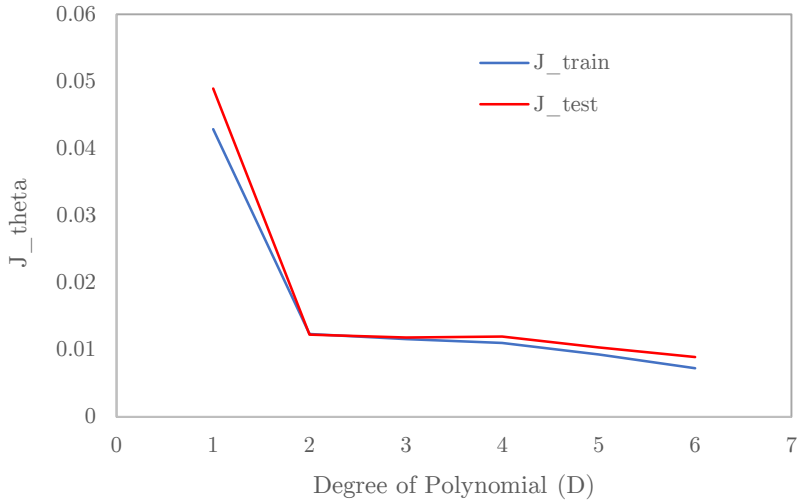

Figure 7. Cost function value for each degree of polynomial

After the degree of polynomial has been defined, the next step is to see whether or not 1000 simulations that has been trained is enough or not as well as to calculate the regularization parameter (λ) needed for 1000 simulations.

Similar to the step mentioned above, the number of simulations are tested per increment, and the cost function for each increment is calculated. Figure 8 shows that 100 simulations will be insufficient since the cost function for the testing set (J_{test}) is too big and from 300 simulations, the cost function is considered good enough. Hence for this research, 600 simulations is selected for the n value.

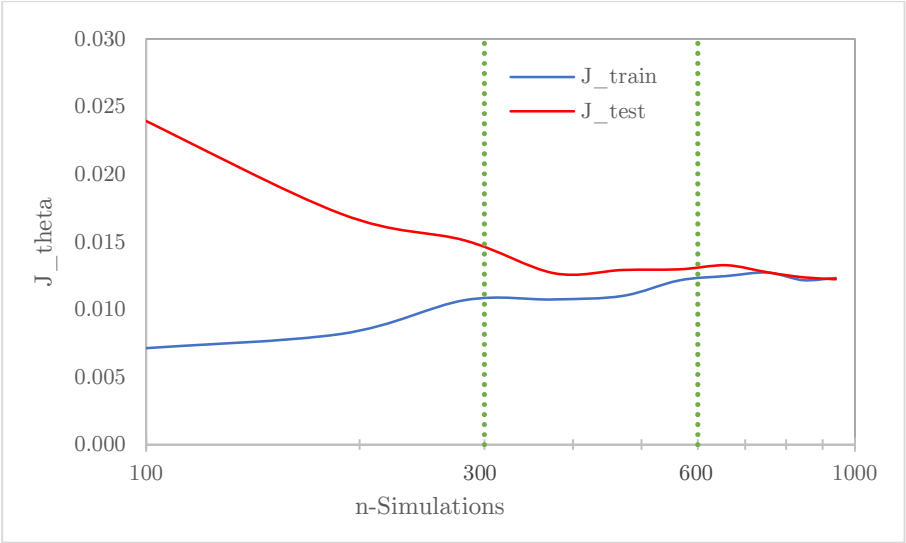

Figure 8. Cost function value for n number of simulations

With regards to the regularization parameter, the same method applies and the cost function of each of the λ value is calculated. Figure 9 below shows that the bigger the λ, the bigger the cost function as well. So, the λ value of zero is used in this analysis.

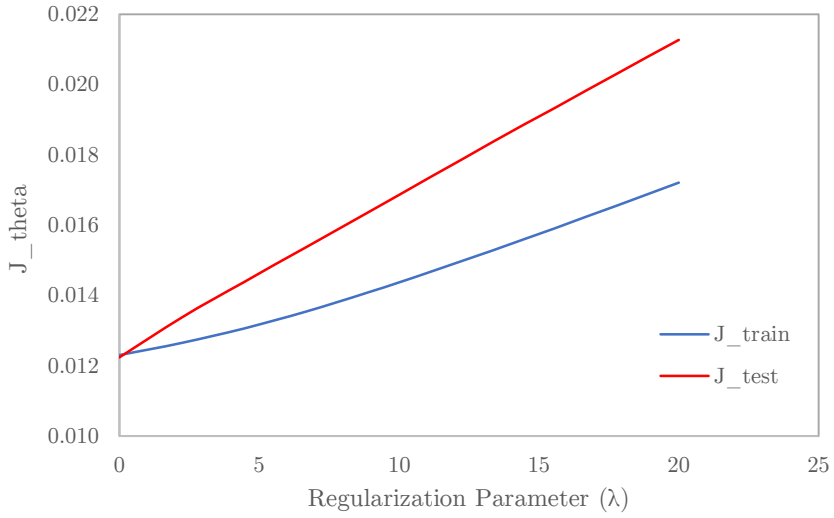

Figure 9. Cost function value for each λ value

With all the learning parameters defined, the next step is to run the regression analysis to get the regression coefficient (θ) for each polynomial terms.

3.1.4.2 Gradient Boosting on Decision Trees

Decision tree is one of machine learning methods that is simple and fast. Unlike polynomial regression, this method does not require the variables to be standardized. Decision tree consists of three different parts, namely root node, internal node, and leaf nodes, all of which are connected with branches (Figure 10). In each node, the variable is classified before being passed on to the next node. Finally, when the variable reaches the leaf node, it will not be passed anymore and its numerical value is evaluated [14]. However, a single decision tree usually does not have strong predictive power. So, in order to increase accuracy of the prediction, many decision trees can be combined. This method is called ensemble [15].

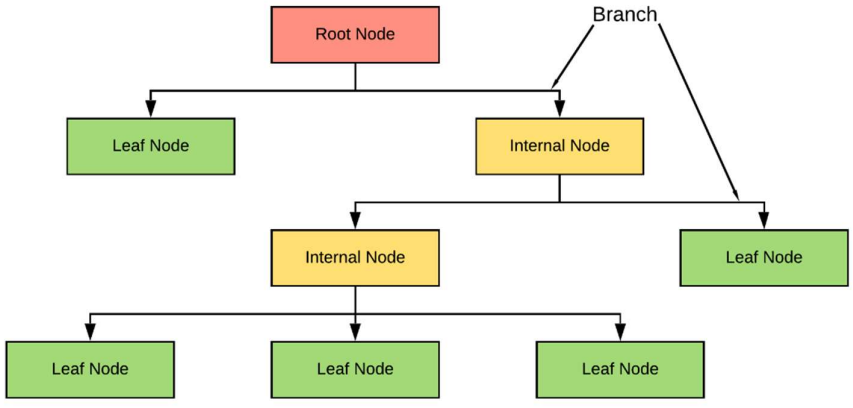

Figure 10. Decision tree example

Additionally, a variant of ensemble methods which is called gradient boosting, is used to strengthen the model even more. This method combines weak models, typically decision trees, to produce one stronger model. Building a gradient boosting model involves building decision trees sequentially. Each of which is built with an objective to improve the accuracy of the previous group of trees. This is done by focusing more on the training simulation that are poorly predicted by the previous trees [16]. In this research, a gradient boosting algorithm variant, Light Gradient Boosting Machine (LGBM) which is created by Ke et al. [16] is used. A schematic diagram of how gradient boosting works on decision trees is displayed in Figure 11 below.

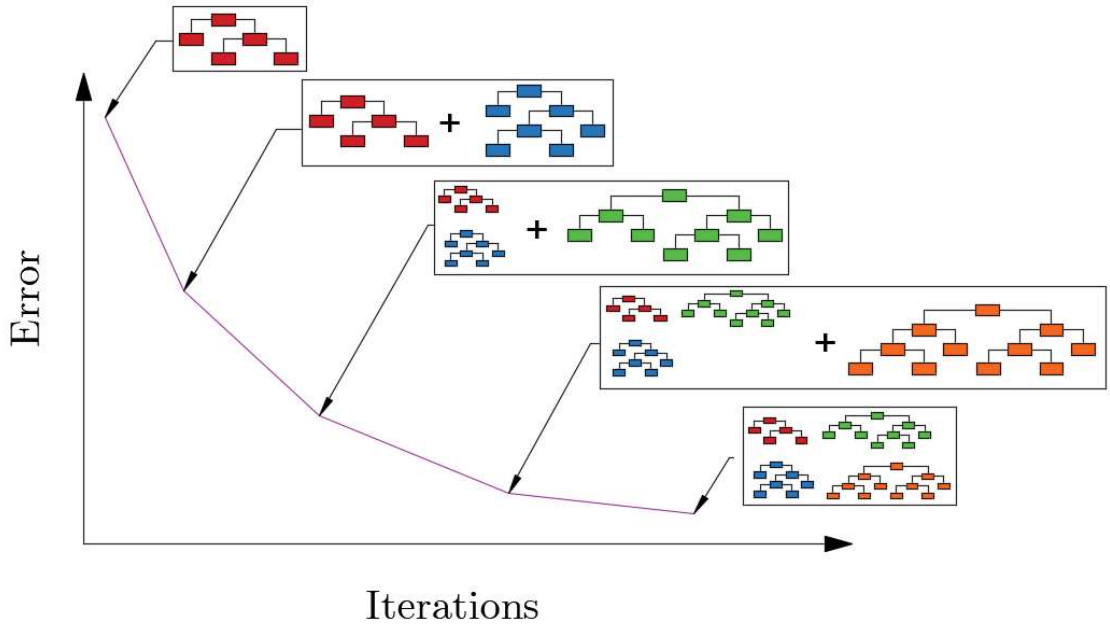

Figure 11. Diagram of gradient boosting method on decision trees

3.1.4.2.1 Learning Parameter Tuning

In order to build a gradient boosting model, there are some learning parameters [17] that can be set to define the training process and manage the model complexity, and in this project, only several basic learning parameters are tuned. A Python library, which was created by Bergstra et al [18], called "Hyperopt" is utilised to tune the learning parameters. This algorithm finds the optimal set of learning parameters value from the training history. It will need some time to run to get a good idea of what combinations of parameters that is likely to produce minimal errors and avoid overfitting.

After selecting the learning parameters, a value range for each learning parameter is then defined. Table 4 below lists the selected learning parameters with descriptions, and the range of value selected for this analysis.

Table 4. Gradient boosting parameter values

Parameters	Min	Max	Description
boosting_type	'gbdt'		Gradient Boosting Decision Tree
num_leaves	30	150	Number of leaves per tree
min_data_in_leaf	1	10	Number of data in a leaf
learning_rate	0.01	0.2	Learning rate of the model
lambda_l1	e^{-16}	e^{2}	Regularization parameter 1
lambda_l2	e^{-16}	e^{2}	Regularization parameter 2
feature_fraction	50	100	% of parameter used when boosting
bagging_fraction	50	100	% of data used when training

After the learning parameter range has been set, the same variables generated for polynomial regression will be used for the Hyperopt library.

3.1.4.3 Error metrics

To evaluate the accuracy of the regression model, a quantitative assessment is necessary to "score" the predicted value in comparison with the target value. In this research, MAPE (Mean Absolute Percentage Error), in conjunction with RMSE (Root Mean Squared Error), will be used to quantify the error of the prediction. Each of the mentioned method has its own advantages and disadvantages and when combined, they will complement each other.

3.1.4.3.1 MAPE (Mean Absolute Percentage Error)

MAPE has been widely chosen when it comes to forecast accuracy measurement. This is due to its independency of the variable scaling and high interpretability. MAPE calculation is defined in Equation 3.2 below:

$$MAPE = \frac{1}{N}\sum_{i=1}^{N}\left|\frac{A_i - P_i}{A_i}\right| \tag{3.3}$$

where A_i is the actual target value, P_i is the predicted target value and N is the amount of data points. However, its main and biggest disadvantage is that it will give infinite or very high value when calculating errors with actual value of zero or close to zero [19]. This can be overcome by pairing this calculation with RMSE calculation.

3.1.4.3.2 RMSE (Root Mean Squared Error)

RMSE is a method to quantify the performance of a regression model. It is one of the methods that is scale dependent, meaning that the results will depend on how big the actual value is [20]. It is a square root of the average squared differences between the actual and predicted values as shown in Equation 3.1.

$$RMSE = \sqrt{\frac{1}{N}\sum_{i=1}^{N}(A_i - P_i)^2} \tag{3.4}$$

The downside of this method is, due to its scale dependency, one cannot simply regard the value as good or not. It needs to be compared with actual values beforehand. On the other hand, unlike MAPE, the advantage of RMSE is that it is able to calculate error value when the value is 0 or close to 0. Additionally, it also penalizes more on bigger values which is the opposite of MAPE (explained in the following section). As it is a square root of the squared difference of the values, the unit for this method also depends on the variable.

3.1.5 Data Visualization

After getting the prediction model from regression analysis, a GUI is developed using Python Tkinter toolkit to make the calculation interactive. The prediction model will then be used according to the needs of the users which can be chosen from deflection, moment, shear, or axial force. Using the model in the calculation means that it does not require a huge computational effort to calculate the wanted outputs. Therefore, quick and accurate responses from the tool can be achieved. A schematic diagram visualizing how this tool works can be seen in Figure 12.

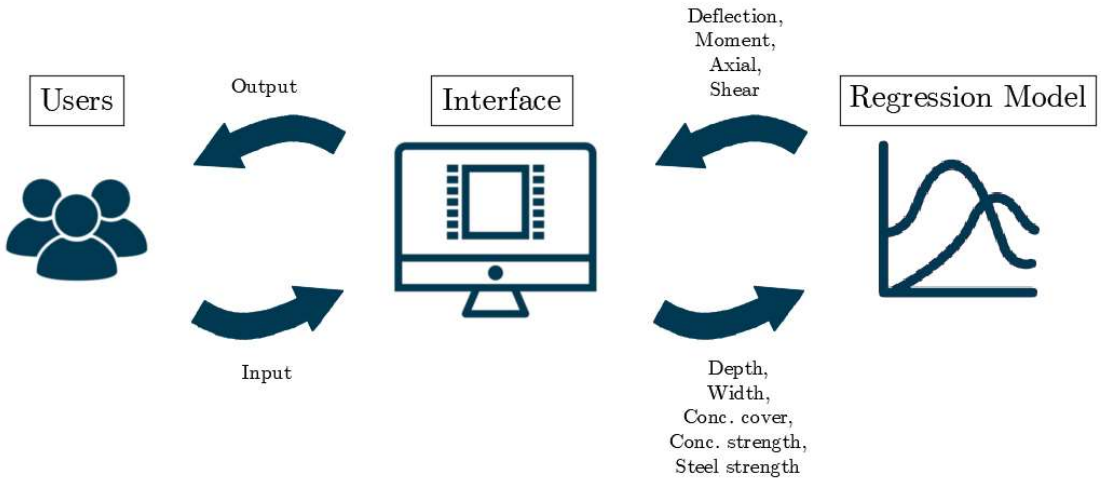

Figure 12. Schematic diagram of the tool process

3.2 Results and Discussions

The results from SAFIR analysis and regression analysis will be presented in this section and discussed. In this analysis, the studied beam configurations are double pinned support beam and simply supported beam (pinned and roller). Finally, the GUI for the calculation tool will be displayed.

3.2.1 SAFIR and Regression Analysis

3.2.1.1 Variable Modification

After running all the simulations with variables listed in Table 1 using SAFIR, it was observed that there are beams that deflect upwards under thermal load. Figure 13 below shows the comparison between two types of beams that deflect downwards and upwards, which will later be addressed as Beam A and Beam B respectively.

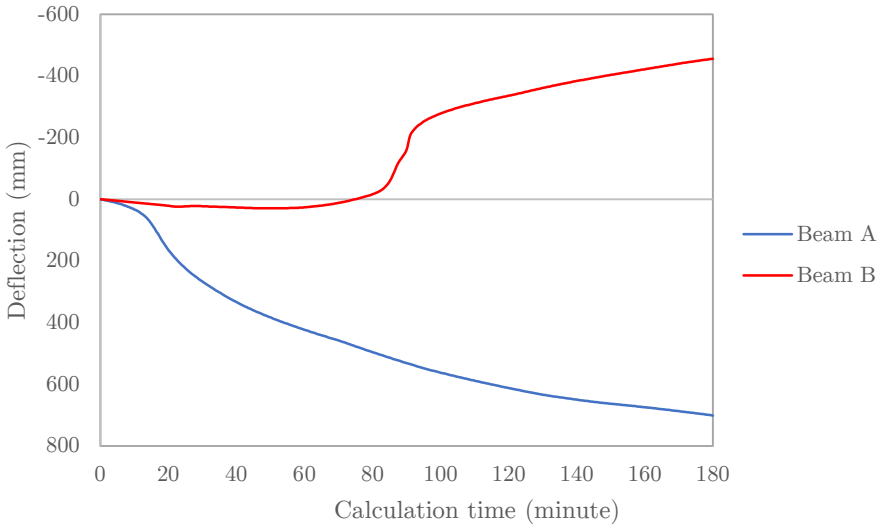

Figure 13. Deflection graph comparison from SAFIR between Beam A and Beam B (positive value for downward deflection and negative for upward deflection)

These two behaviours are discussed in Section 4 and it can be seen that if the thermal load is not enough to create certain amount of moment, which can cause a beam to continue deflecting downwards, the deflection direction will change its direction upwards. So, in order to make a better prediction, the original variable range is adjusted so that all the beams in the new range will deflect downwards. The ranges of input variables from Table 1 are then modified into new ranges shown in Table 5 below.

Table 5. Modified input variable range

Variables	Min	Max	Units
Concrete strength	30	80	MPa
Steel strength	300	600	MPa
Depth (D)	300	**500**[1]	mm
Width (w)	**200**[1]	**300**[1]	mm
Concrete cover (c)	20	40	mm

[1] Bolded values are modified

In this new range, maximum beam depth is decreased from 600mm to 500mm and beam width range is changed from 300mm-400mm to 200mm-300mm. The purpose of this reduction in beam dimension is to increase the slenderness, making the beam easier to deflect downwards. By doing this, all the deflections obtained from those range are positive (downward) and hence, this new variables will be used for all the models in double pinned support and simply supported beam for consistency purpose.

Despite having all the deflections positive, there are two different behaviour inspected in the new variables. The first one has an immediate increase in the deflection value and decreasing rate at the end (Behaviour A), and the second one has a steady but slow increase in the beginning before exponentially increasing in value and finally slowing down again (Behaviour

B). Table 6 and Figure 14 below describes the variable differences and the visualization of two different behaviours of the beam.

Table 6. Behaviour A and Behaviour B variables

Behaviour Type	f_c' (MPa)	f_y (MPa)	Depth (mm)	Width (mm)	Cover (mm)
Behaviour A	58.1	324.8	328.5	266.3	22.1
Behaviour B	75.4	545.3	497.5	244.8	31.2

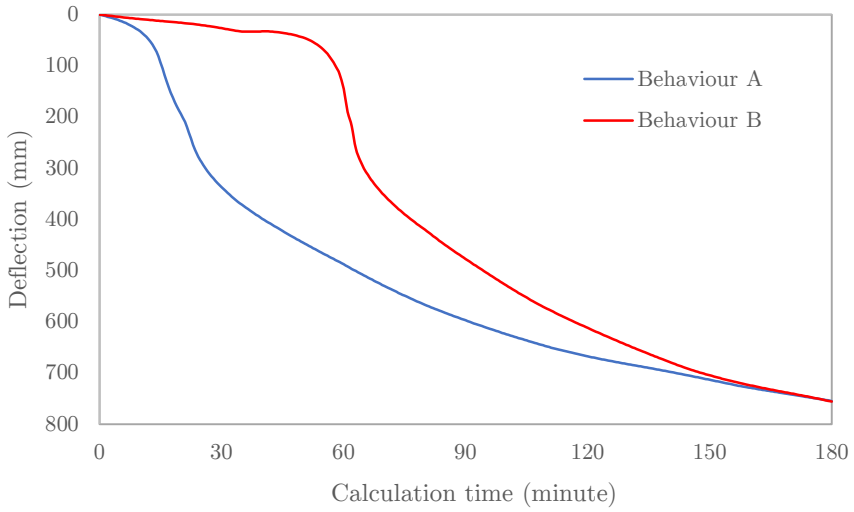

Figure 14. Different deflection behaviours from the modified variables

3.2.1.2 Regression Analysis Comparison

After the variable has been modified to a new one, the performance of the two machine learning methods are compared. In this section, the beam configuration used is double pinned support and the output compared is deflection.

3.2.1.2.1 Polynomial Regression

As discussed before in Section 3.1.4.1, the polynomial degree used in this regression is 2nd degree polynomial with 600 simulations. Figure 15 below shows the comparison between the actual and predicted data.

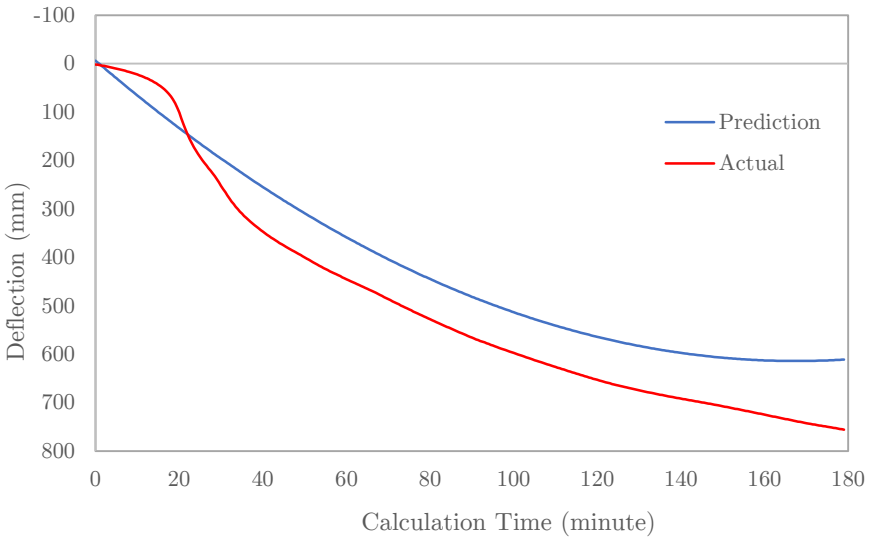

Figure 15. Prediction for initial model of polynomial regression

The comparison above shows that the regression model is not accurate enough to predict all the data with average MAPE value of 117.8% and RMSE of 80.4 mm. Using a higher polynomial degree will not improve the model considerably because as shown in Figure 7 above, the improvement by increasing the polynomial degree is not significant. So, the depth range shown in Table 5 will be divided into 4 groups – 300 to 350mm, 350 to 400mm, 400 to 450mm, and 450 to 500mm.

The purpose of dividing the depth is because it affects the stiffness of the beam, hence it is assumed to have more impact in beam deflection. Besides, in Table 6 above, the clear difference of the two behaviours is in the depth of the beam. Behaviour A has a depth value close to the minimum range, making it easier to deflect (Figure 14), while the depth of Behaviour B is close to the maximum range, making it harder to deflect. However, since the behaviour of the beam under thermal load is very non-linear, the other variables also have an impact in the deflection.

Figure 16 below shows the envelope value of the first two categories in the division – 300 to 350mm and 350 to 400mm. It can be seen that even with the division, there is still an overlapping between the two envelopes. So, dividing the beam depth does not mean that it will give two entirely different values, but the aim is to make the deflection range smaller and making the model easier to predict.

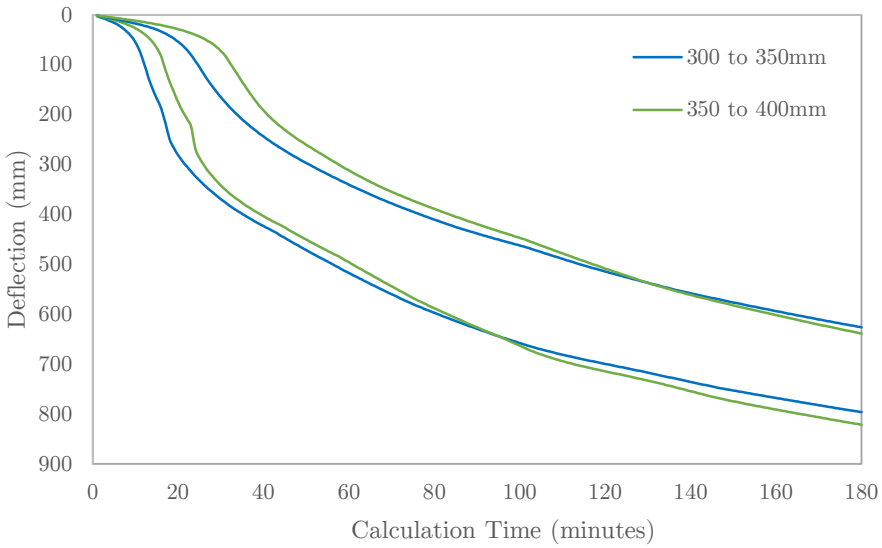

Figure 16. Max and min envelopes for beam deflection with 300 to 350mm and 350 to 400mm depth

Figure 17 below shows the comparison of the predicted and actual values for beam with 300 to 350 mm depth and when compared to Figure 15, visually, both seem show similar error. But, if calculated using the error metrics, prediction in Figure 17 has a much better accuracy with MAPE value of 48.3% and RMSE value of 68.6 mm.

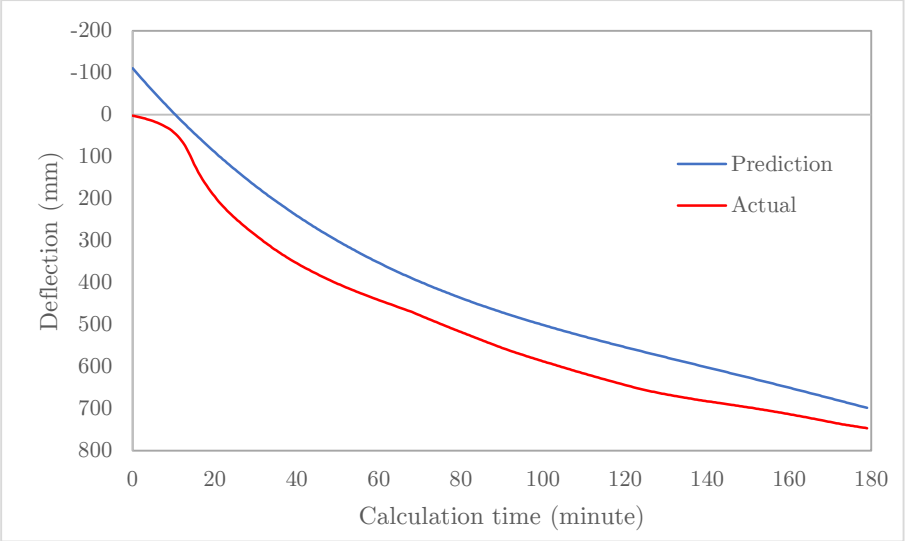

Figure 17. Comparison between predicted and actual values of beam with 300 to 350mm depth

So, the next step is to divide the calculation time into part to improve the prediction further. The timestep division, used polynomial degree, and error metrics value can be seen in Table 7 while the visualization of the prediction is displayed in Figure 18.

Table 7. Timestep division for polynomial regression

Timestep Range	Polynomial Degree	MAPE (%)	RMSE (mm)
1-5	4	6.4	0.2
6-10	2	4.8	0.8
11-15	3	9.4	3.4
16-20	3	7.5	5.1
21-25	2	3.8	5.3
26-80	3	7.2	6.7
81-180	3	1.85	4.8

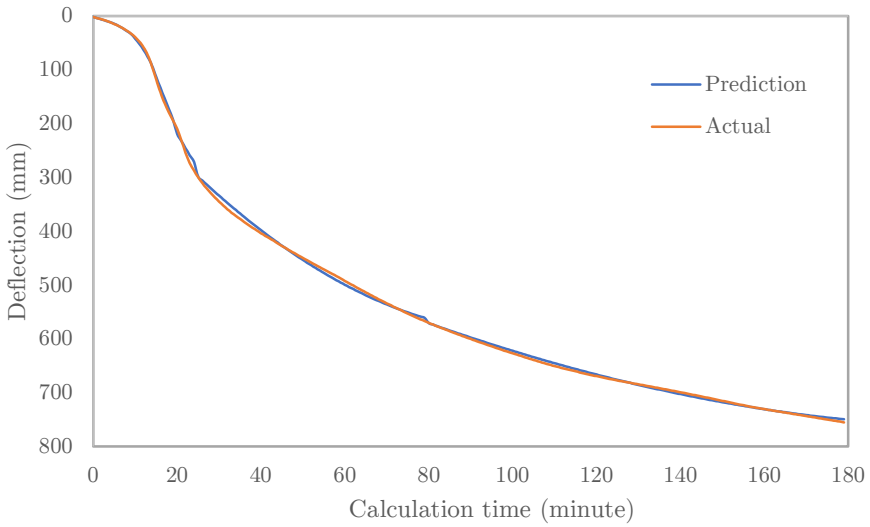

Figure 18. Comparison between predicted and actual values after timestep division

From Figure 18 above, it can be seen that the prediction matches perfectly with the actual value. However, with that amount of models, the continuity of the predicted line cannot be guaranteed, meaning that there will be a big value jump at the intersection of one model to another (Figure 19). Moreover, if this model were to be used, the value at 80 minutes would be bigger than the value at 81 minutes which will make the result questionable. Therefore, the regression used in this research will be gradient boosting on decision trees which will be explained in the following section.

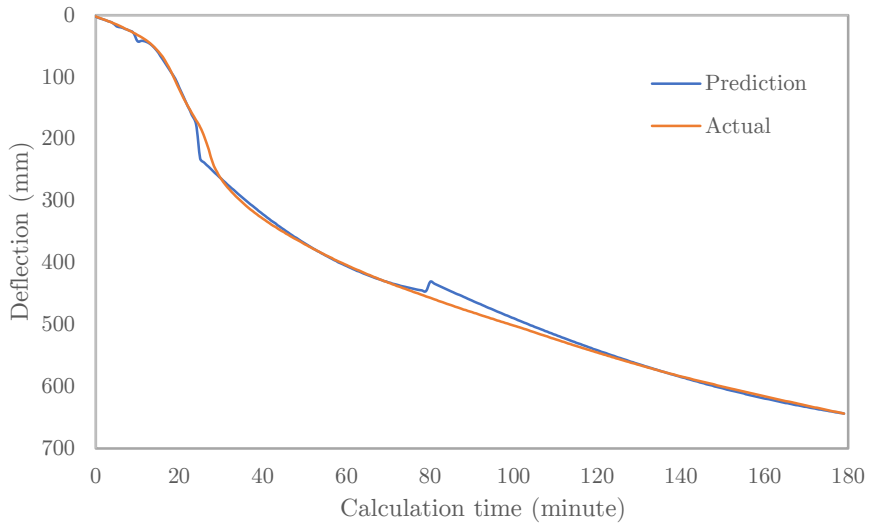

Figure 19. Comparison between predicted and actual values with jagged predicted line

3.2.1.2.2 Gradient Boosting on Decision Trees

Since the result of polynomial regression was not satisfactory, this method will be used for this research. Assuming that the number of simulations used is the same as the one used in polynomial regression, the same simulation will be predicted with this method. Figure 20 below shows the same simulation predicted by this method.

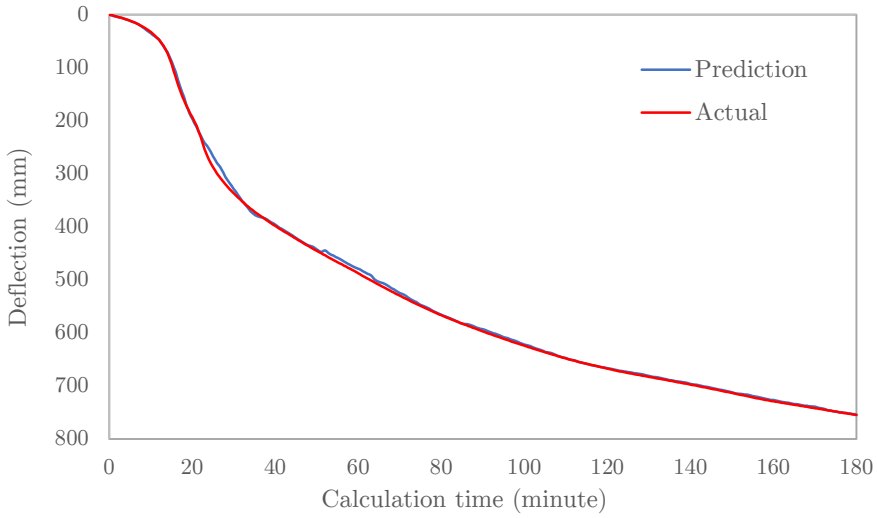

Figure 20. Deflection prediction by using gradient boosting on decision trees

It is obvious from both results that, by using this method, the variables are not needed to be split into groups (simpler), and the continuity of the line of the predicted value is guaranteed. Therefore, for the sake of accuracy and simplicity, gradient boosting on decision trees is more preferable in this research.

3.2.1.3 Double Pinned Support Beam

Beams with double pinned support means that there will be no translation in the beam either in lateral or longitudinal direction. So, when subjected to thermal load, the thermal elongation of the beams with double pinned support will be restrained by the supports and cause mechanical stress which produces axial force in the beam. If thermal bowing is more dominant tension force will occur along the beam but if thermal elongation is more dominant, compression force will occur [4].

3.2.1.3.1.1 Deflection Model

With the new variables, the deflection prediction results for all the simulations are almost identical to the actual ones, with a MAPE value of 2.6% and an RMSE value of 9.2 mm. For the two behaviour, the MAPE values are 1% and 6.5% and the RMSE values are 4.8 mm and 14.8 mm for Behaviour A and Behaviour B respectively. The visual and tabular comparison of the prediction and actual results for both behaviours are shown in Figure 21 and Table A. 1.

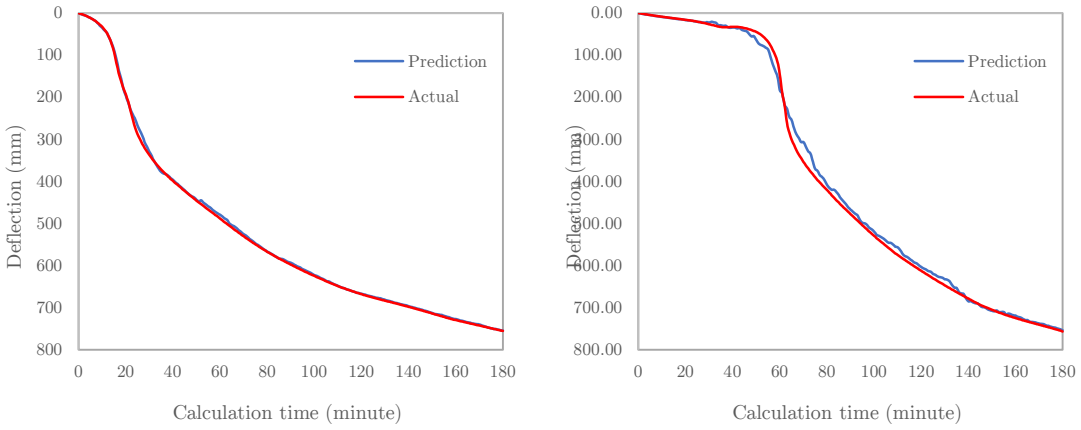

Figure 21. Deflection model prediction vs actual results for Behaviour A (left) and Behaviour B (right)

From the regression model, the importance of each variable can also be seen based on the number of times each variable is used when splitting the decision tree (Figure 22). Among the other five variables, concrete cover, beam depth, and concrete strength are the most deciding variables when it comes to beam deflection.

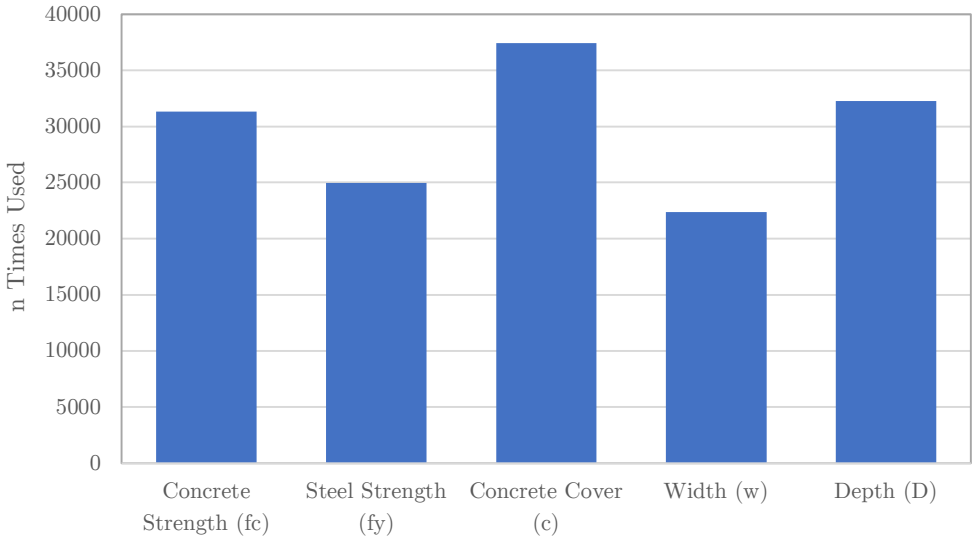

Figure 22. Deflection model variable importance

3.2.1.3.1.2 Moment Model

The second predicted result is moment value on the beam. Since the moment value is interconnected with the deflection value, due to it being a second order effect, the two different behaviours in deflection also occur in this section with the same sets of variables (Table 6). Figure 23 visualizes both differences in moment values (positive value in the diagram means sagging moment).

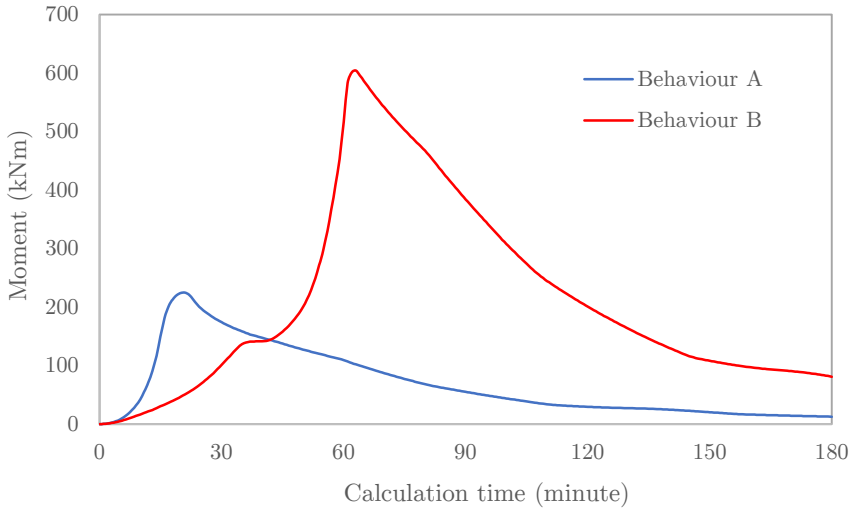

Figure 23. Different moment behaviours from the modified variables

From the regression model, the predicted values are then compared with MAPE and RMSE calculation method to the actual values. The prediction error for both behaviours are 4.5% and 4.2 kNm (Behaviour A) and 8.4% and 23.9 kNm (Behaviour B). Tabular comparison for the actual and predicted moment value is shown in Table A. 2. The prediction for this model is not as good as the deflection model but it is still considered acceptable as the comparison

graph (Figure 39) shows a strong resemblance between the predicted and actual values. The whole simulations are calculated to have an error of 5.1% and 11.7 kNm with this model.

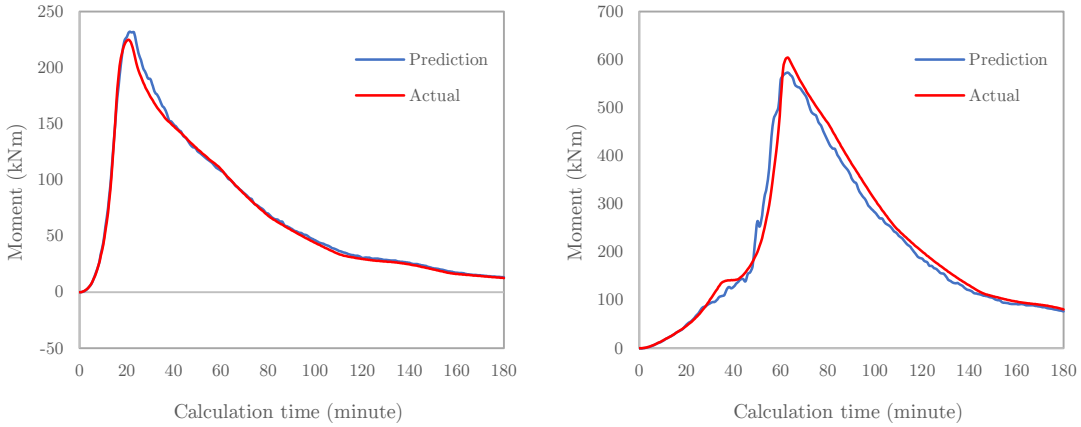

Figure 24. Moment model prediction vs actual results for Behaviour A (left) and Behaviour B (right)

The graph for the importance of the variables (Figure 25) shows similar results to the deflection model with concrete cover, beam depth, and concrete strength being the variables with the most effect on the beam bending moment.

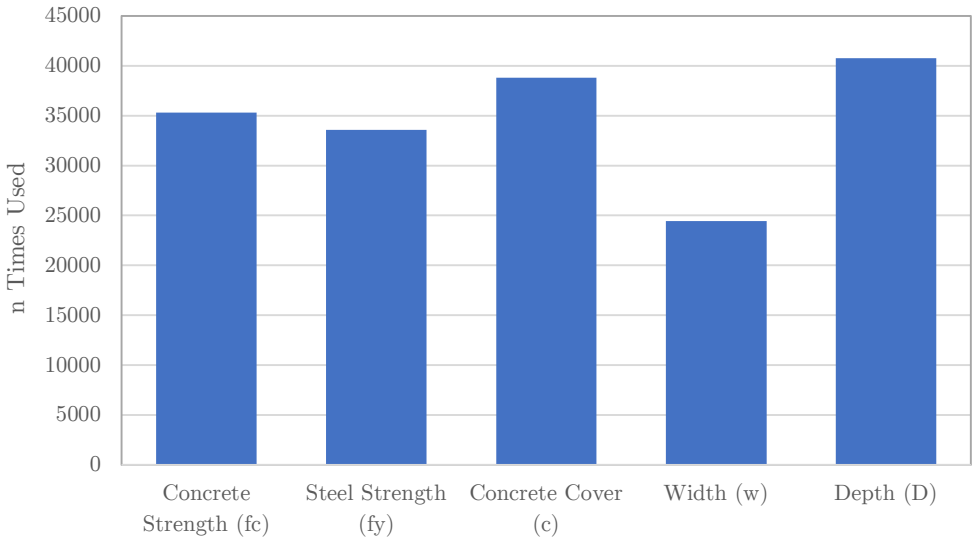

Figure 25. Moment model variable importance

3.2.1.3.1.3 Axial Model

Similar to the previous model, axial models also have correlation with moment and deflection models because of the second order effect of moment. So, the two behaviour discussed in the two sections earlier also appear in this model. Figure 26 below displays the difference between the two behaviours.

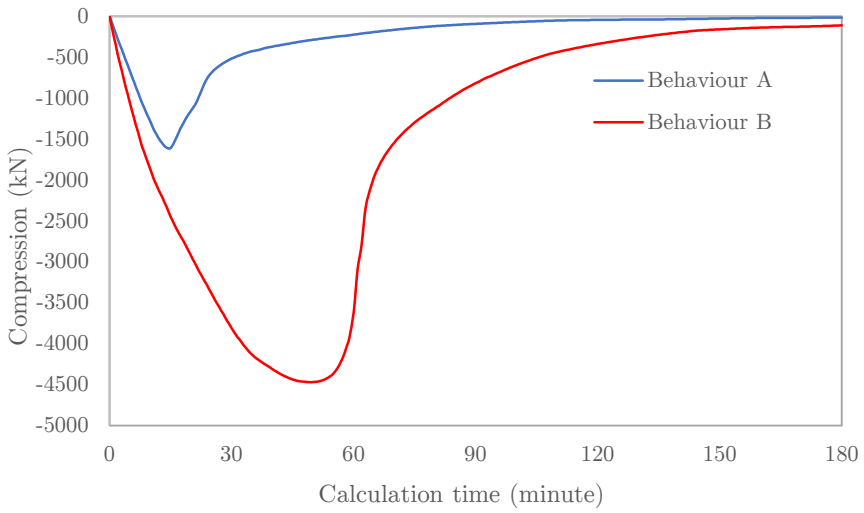

Figure 26. Different compression behaviours from the modified variables

The prediction from the regression model shows good resemblance to the actual value with the MAPE and RMSE values being 7% and 13.9 kN for Behaviour A and 4.5% and 161.6 kN for Behaviour B. The value comparison each minute for both behaviour is listed in Table A. 3. From Figure 27 below, it looks as if Behaviour A is predicted better than Behaviour B yet the MAPE value is bigger. This is because, as mentioned in Section 3.1.4.3.1, MAPE value has a tendency to give a very big number when calculating error with small actual values in Behaviour A while RMSE value penalizes more for errors at higher values which is clearly shown in Behaviour B and thus, giving it a much bigger RMSE value. For this model in average, it manages to predict excellently with 4.2% and 77.4 kN error.

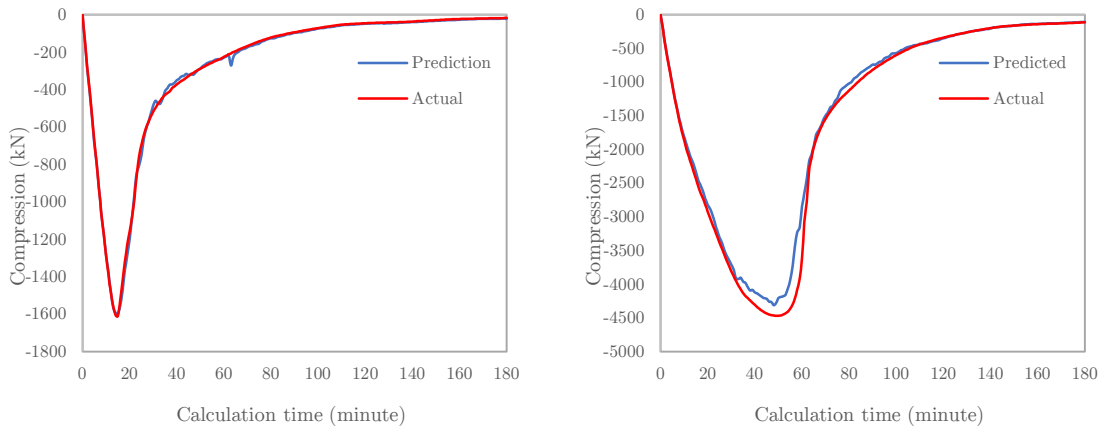

Figure 27. Compression model prediction vs actual results for Behaviour A (left) and Behaviour B (right)

From the variable importance graph (Figure 28) below, it can be seen that the depth of the beam is still the variable that affects the behaviour most with the concrete cover and the concrete strength being the second and third affecting variable.

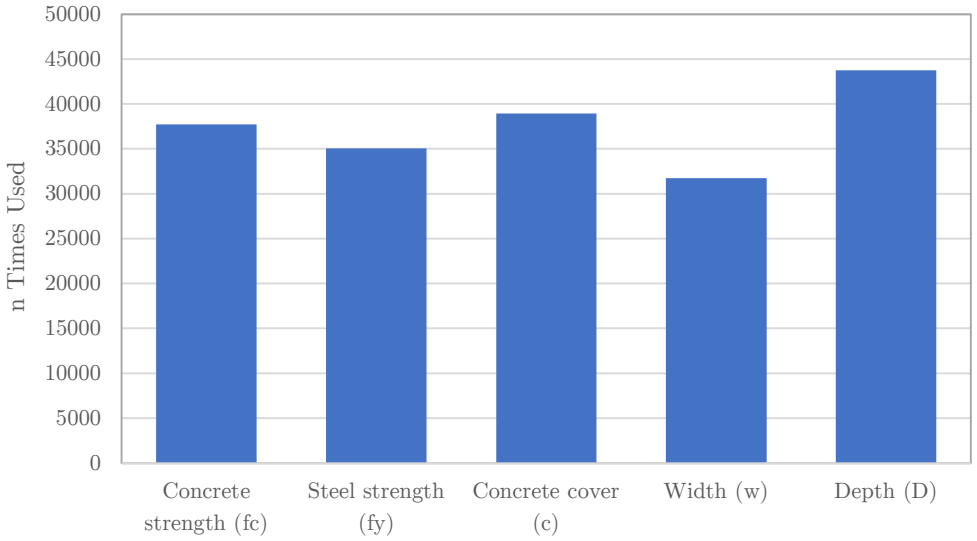

Figure 28. Compression model variable importance

3.2.1.3.1.4 Shear Model

In this model, according to the fact that it is still related to the second order effect of moment, it also exhibits two different behaviours. The compression observed in the previous section is aligned with the initial beam axis (X-axis) and when the beam is deformed, it will create an angle to the X-axis. This angle will create the shear force in the beam. Since the shear force also contributes a small portion of moment along the beam, the shape of the diagram is similar to that of moment (Figure 29).

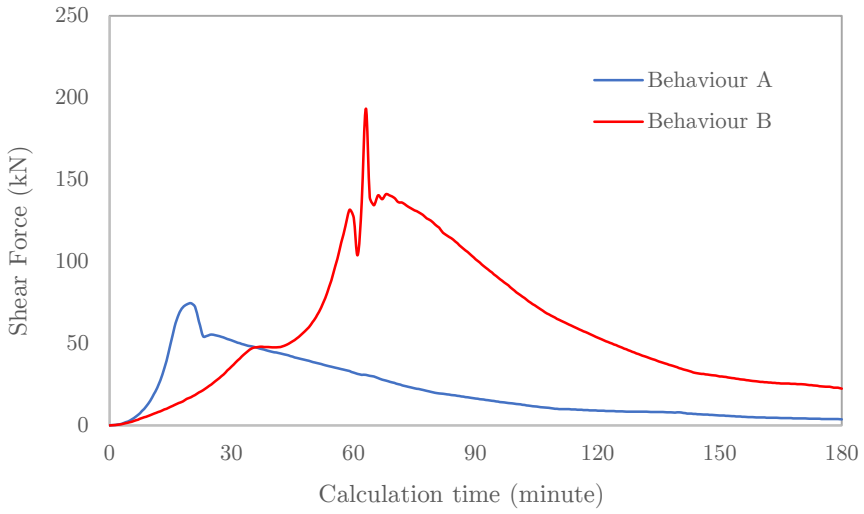

Figure 29. Different shear force behaviours from the modified variables

It can be seen from Figure 29 above that the actual value sometimes has a spike and therefore the prediction for this model has difficulties in predicting the spike. The error values for this model are considered high which are 15.3% and 10.1 kN for Behaviour A and 12.2% and 2.6 kN for Behaviour B (calculation for both error metrics is shown in Table A. 4). The big error

in this model is caused by the numerical spike in the actual model. So, the prediction sometimes cannot predict the sudden jump and the other way around – sometimes a smooth actual value is predicted to be a sudden jump (shown in Figure 30 for Behaviour B). On average, the error values for this model are 10.5% (MAPE) and 13.7 kN (RMSE).

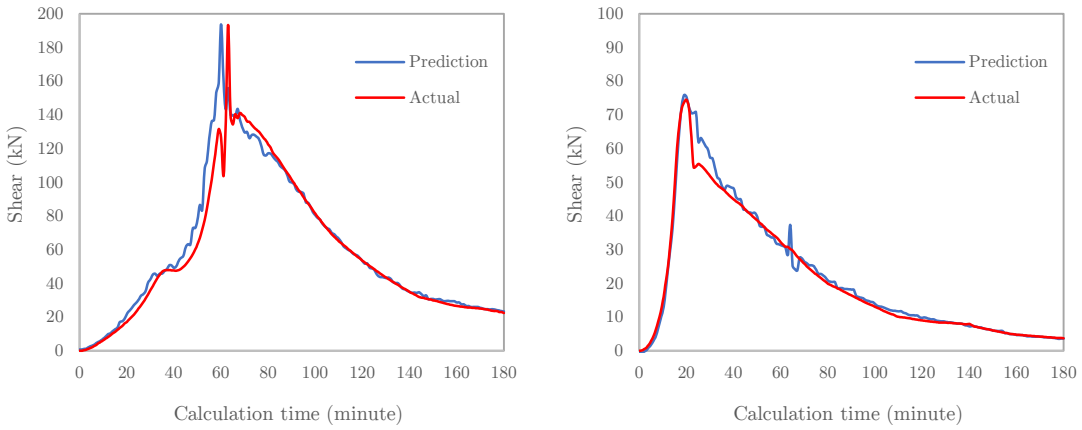

Figure 30. Shear model prediction vs actual results for Behaviour A (left) and Behaviour B (right)

Since this model is closely related to moment and compression values, the importance for each variable for this model follows the same trend of that in moment and compression models. Figure 31 below shows that depth still has the most influence in this model followed by concrete cover and strength.

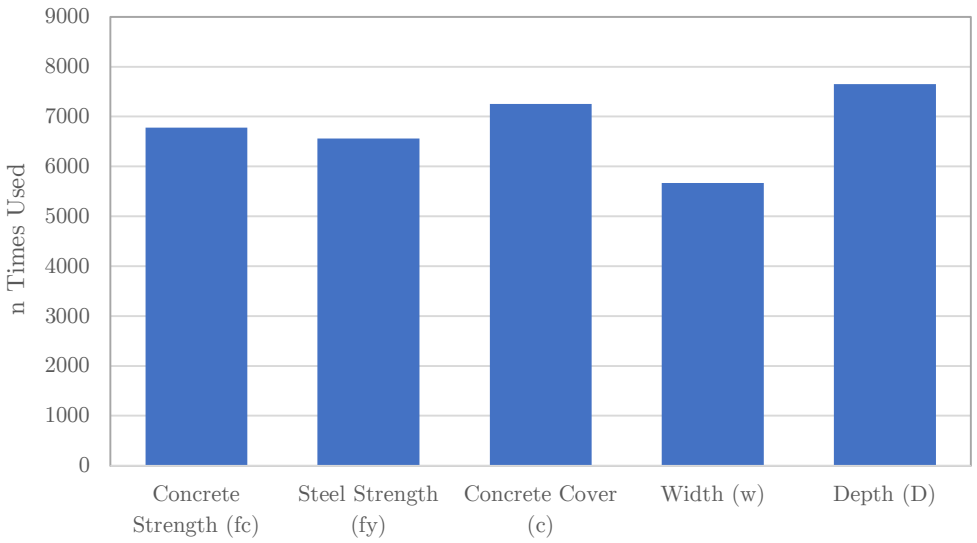

Figure 31. Shear model variable importance

3.2.1.3.2 Discussions

From the four models above it can be seen that all of them exhibit the same behaviour when the supports are pinned supports. This is because when the beam expansion is restricted by the support, it produces axial force, in this case compression force, which also results in the development of moment and shear force.

From the variable importance graphs, it is also obvious that the depth of the beam is the variable that has the most influence in the model. This can also be seen from Table 6 that the two different behaviours are resulted from the minimum and maximum values of the range – 328.5mm for Behaviour A and 497.5 for Behaviour B. Concrete cover is also an important variable in this analysis which is shown in Figure 22 as the variable of most importance for deflection model. It works as a protection to the steel reinforcement bar as the rebar will rapidly lose its strength when exposed to high temperature.

All of the four regression models in this beam configuration can also predict the result with high accuracy. However, on shear model, the prediction results show the biggest error among all models due to the numerical noises in the actual values. A much better regression result can be obtained from shear model if the model is trained when the values have been smoothened.

3.2.1.4 Simply Supported Beam (Pinned and Roller Support)

The second beam configuration that is analysed in this research is pinned and roller support. The difference between this and the previous configuration is that, in this configuration, the thermal elongation of the beam will not be restrained by the roller support. Therefore, the roller support will move according to the elongation of the beam and will not create a compression force along the beam. That being said, the second order moment effect does not occur in this configuration and the moment, shear, and axial forces are zero.

The regression models that will be created in this configuration is deflections in X direction (horizontal) and Y direction (vertical). The variables that are used to create the models are listed in Table 5.

3.2.1.4.1 Regression Model

3.2.1.4.1.1 Vertical Deflection Model

In this model, in spite of not having second order moment effect, there are also two behaviours observed. In order to avoid confusion with the previous model, the naming is changed in this model into Behaviour C and Behaviour D. Figure 32 shows the shape of each behaviour where Behaviour C has a maximum deflection and a decreasing vertical deflection; and Behaviour D just increases until the calculation ends. Table 8 shows the value of each variable for the two behaviours.

Table 8. Variables for the two different behaviours

Behaviour Type	f'_c (MPa)	f_y (MPa)	Depth (mm)	Width (mm)	Cover (mm)
Behaviour C	60.4	312.5	395	202.5	20.2
Behaviour D	65.4	327.5	325	299.2	39.8

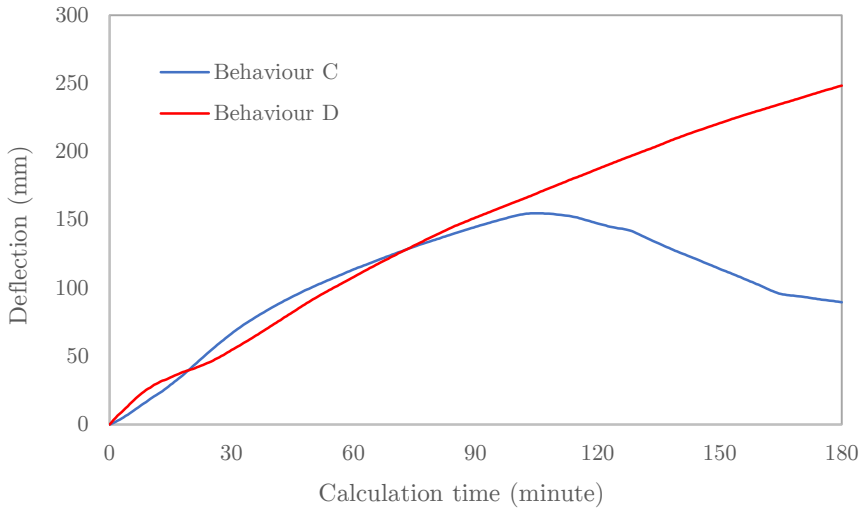

Figure 32. Different vertical deflection behaviours in simply supported beam configuration

The regression model prediction indicates a strong similarity to the actual value with error values of 6.2% and 8.9 mm for Behaviour C; and 3.2% and 4.2 mm for Behaviour D. The comparison between the prediction and actual values for both behaviour in Figure 33 and Table A. 5 shows that the model manages to predict the maximum value in Behaviour C but is having difficulties in predicting the deflection value after the maximum point where in Behaviour D, the model has succeeded in predicting the deflection value. The average value of both error metrics are 3.1% for MAPE and 5.1 mm for RMSE.

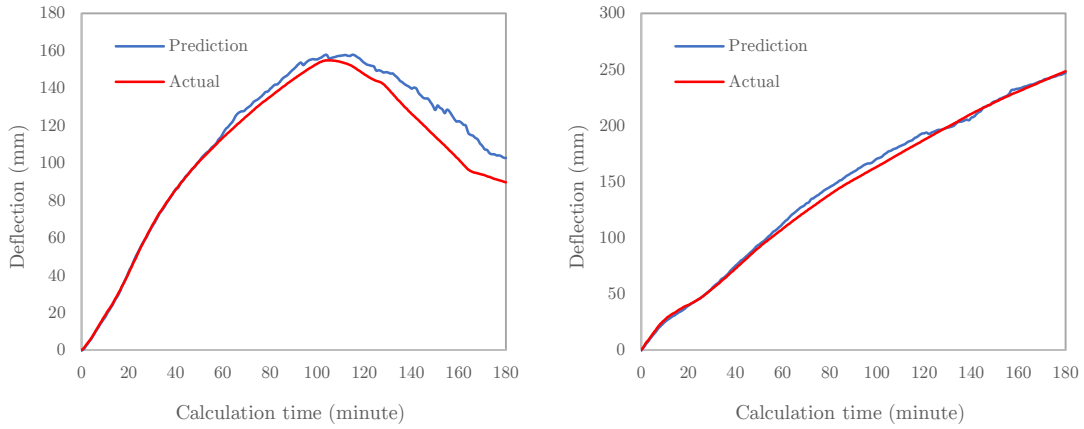

Figure 33. Vertical deflection model prediction vs actual results for Behaviour C (left) and Behaviour D (right)

The importance factor for this model (Figure 34) indicates that concrete cover is the most used variable when training the model with depth as the second most used variable. The difference in the importance factors is due to the fact that beam with pinned and roller support does not have second order of moment effect and therefore, the behaviour is also different.

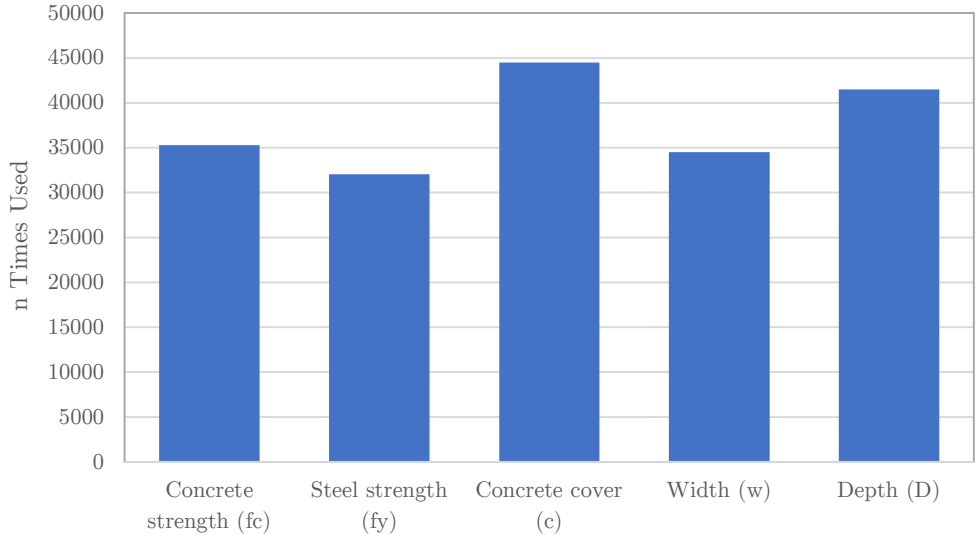

Figure 34. Vertical deflection model variable importance

3.2.1.4.1.2 Horizontal Deflection Model

Among all models built in this research, the model for horizontal deflection in a simply supported beam does not show two different behaviours. The horizontal deflection of the beam just keeps increasing due to thermal elongation of the beam. However, the main difference in this model is only in the value. Figure 35 below shows Behaviour C and Behaviour D which are also the maximum and minimum range of the horizontal deflection.

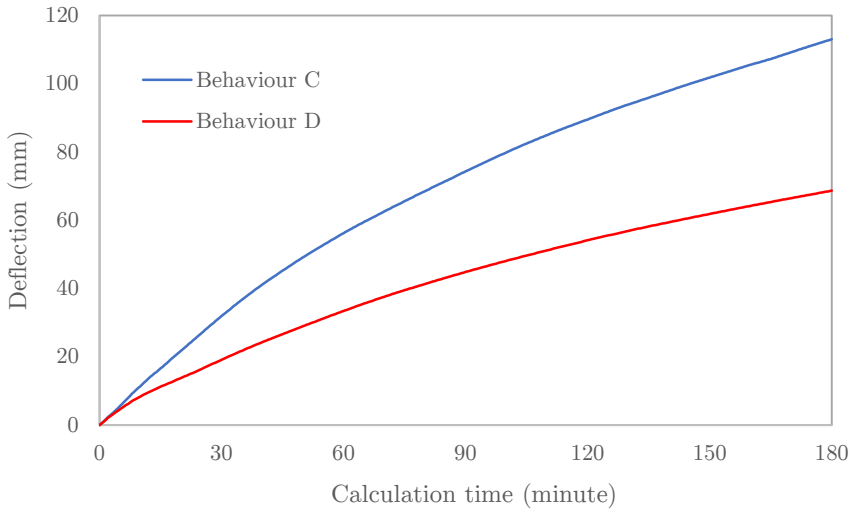

Figure 35. Minimum and maximum range of horizontal deflection in simply supported beam configuration

Since there is only one behaviour for horizontal deflection in simply supported beam configuration, the prediction for this model shows a strong resemblance to the actual value with average error of 1.4% for MAPE and 0.9 mm for RMSE, while for each case, 2.1% and 1.8 mm for Behaviour C; and 0.8% and 0.43 mm for Behaviour C. Figure 36 and Table A. 6 show the comparison of the forecast values for Behaviour C and D for horizontal deflection.

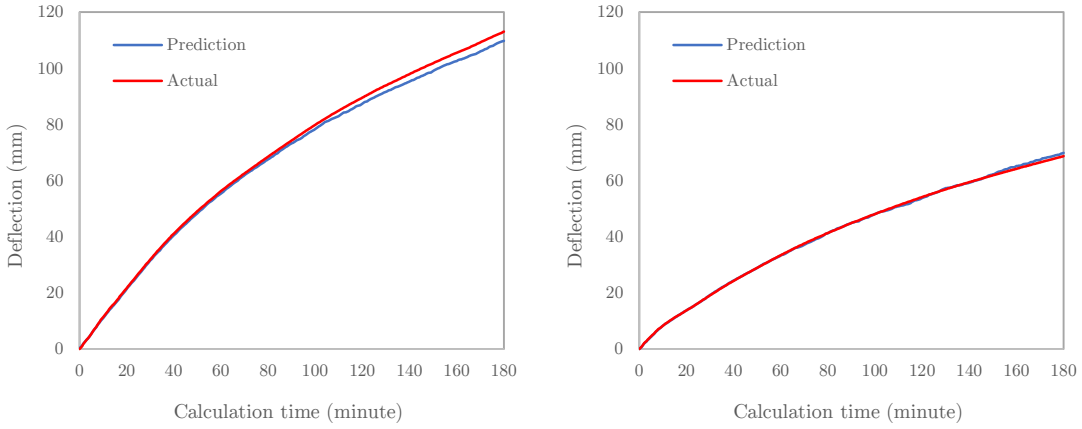

Figure 36. Horizontal deflection model prediction vs actual results for Behaviour C (left) and Behaviour D (right) value

Similar to the vertical deflection model in the previous section, the variable that is of most importance is the concrete cover. Steel strength however, still affects the deflection but with less significance. Figure 37 below shows the importance of each variable for horizontal deflection model.

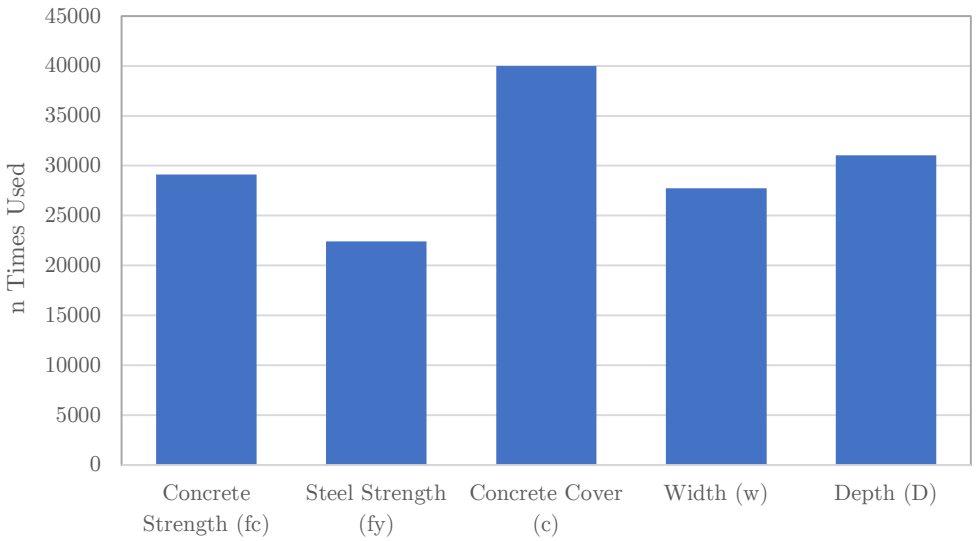

Figure 37. Horizontal deflection model variable importance

3.2.1.4.2 Discussions

For a simply supported beam, since the beam does not experience a second order moment effect, there is no internal forces in the beam. So, in this configuration, only models for vertical deflection and horizontal deflection are built.

In Figure 32, where the two behaviours of the beam is displayed, there are one main difference from the two behaviours. One with lower concrete cover and width (Behaviour C) will experience maximum moment before the deflection decreases while Behaviour D only increases until the calculation ends.

It is observed that the concrete cover will affect such behaviour. The maximum point in the deflection is dependent on the concrete cover – the bigger the concrete cover, the later this maximum point will be reached, and on the opposite, the smaller the concrete cover, the faster this maximum point will be reached. This is because the concrete cover protects the reinforcement bar from the heat and evidently, the maximum point will be reached when the top reinforcement bar has reached 500°C. Additionally, with regards to horizontal deflection, concrete cover will have a negative effect. The bigger the concrete cover, the smaller the horizontal deflection and the other way around.

A simply supported beam under thermal load will experience two types of deformation. The first is curvature deformation where the beam will bend towards the fire and pull the roller support inward, and the second is thermal elongation where the beam will push the roller support outward and "pull" the beam back to the initial X axis. When the deflection decreases after reaching the maximum point, the beam deformation is dominated by the thermal elongation and it caused the beam deflect back to the original X axis. This can be seen in Figure 35 where the horizontal deflection is still increasing when the vertical deflection is decreasing.

The depth of the beam, which is the second most important variable in vertical deflection model, affects the behaviour the same way as it does in double-pinned beam configuration. The bigger the depth of the beam is, the bigger the moment inertia of the beam, hence making the deflection value smaller. Each of these two variables with the most effect affects the vertical deflection behaviour in a different way.

3.2.2 Calculation Tool Interface

The regression models obtained from the previous section are then integrated to the calculation tool. It is observed that by using the regression models, it only needs 2 milliseconds to calculate the wanted output. Figure 38 shows the interface of the tool and the descriptions of each part.

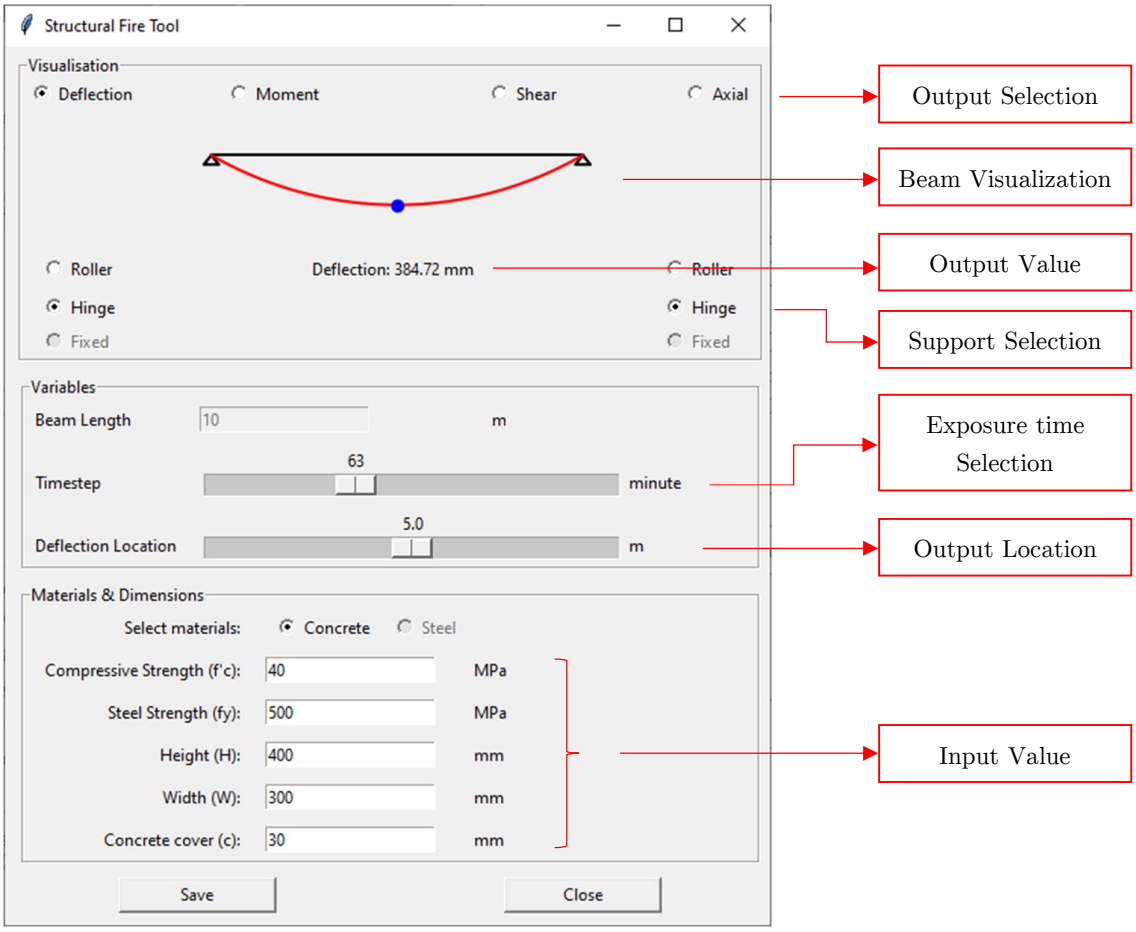

Figure 38. Structural fire tool interface

The tool user interface was designed to be able to show the deflection at each point and users can change the inspected output location by moving the slider. However, due to time constraint, the regression model can only predict the output in the mid span of the beam. It is also important to note that this tool can only predict the output for a given range of inputs listed in Table 5. If the value inputted is bigger than the maximum value, it will only calculate the maximum value itself and if the value inputted is smaller, it will only calculate the minimum value.

4 Structural Fire Analysis

4.1 Methodology

This section discusses the beam behaviour anomaly that happened during the regression research. It was observed that a beam, which was deflecting downwards at first might, at some point, have a negative bending effect that caused the beam deflection direction to change to the opposite way, in this case, upwards.

This analysis started off with selecting the beam to be analysed. In this study, the behaviour of two beams will be analysed. The first one is the beam with the downward deflection, and the second one is the beam with upward deflection (Figure 13). In order to see the beam behaviour under certain thermal load, a moment-curvature diagram of the beams will need to be observed. After which, the deflection is calculated again using the calculated moment-curvature diagram and virtual work method as a way of validation.

4.1.1 Moment-Curvature Diagram

Moment-Curvature diagram is a diagram that shows a beam strength and deflection under thermal load; and it is dependent on the fire exposure, axial force, material specifications, and beam dimension [21]. Figure 39 below shows the examples of moment-curvature diagrams every 15-minute interval of fire exposure with and without axial load.

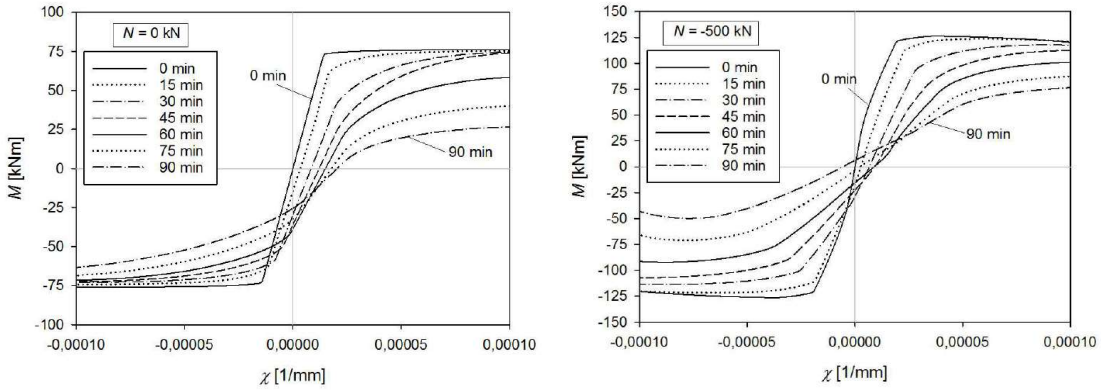

Figure 39. Moment-curvature diagrams without axial load (left) and with 500kN compression load (right) [22]

A section analysis needs to be conducted to generate a moment-curvature diagram. The overview of the analysis process is described in a flowchart in Figure 40 below.

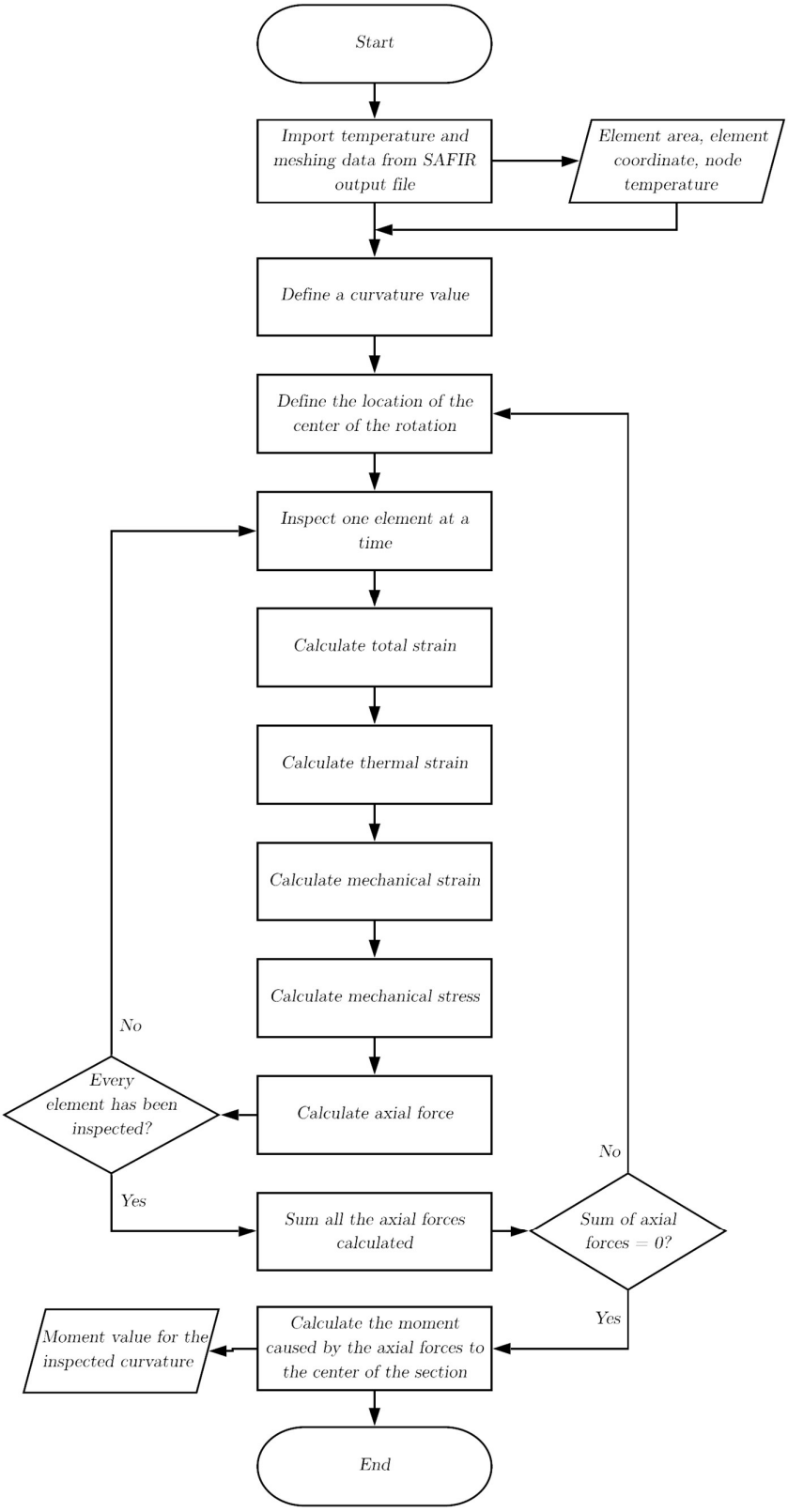

Figure 40. Moment-curvature diagram calculation flowchart

In Usmani's paper [4], the relationship between the total strain (ε_{tot}), thermal strain (ε_{th}) and mechanical strain (ε_{mech}) is addressed in the following equation (4.1). The illustration of the strain relationship is shown in Figure 41 below.

$$\varepsilon_{tot} = \varepsilon_{th} + \varepsilon_{mech} \tag{4.1}$$

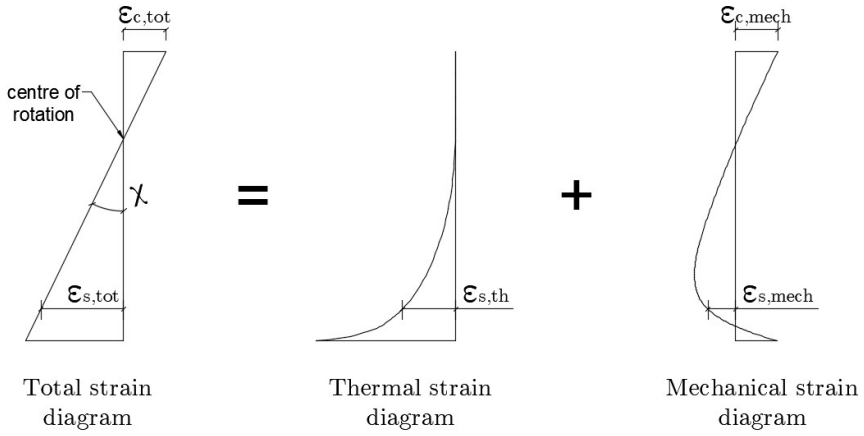

Figure 41. Strain relationship illustration (Reproduced from [21])

As this is a finite element based calculation, each element generated in SAFIR thermal calculation will be analysed. For each element, a curvature (χ) which will be calculated and the distance to the centre of rotation of the beam are selected. After that the total strain can be calculated by multiplying the selected curvature with the distance from the element to the assumed centre of rotation.

After getting the total strain value, thermal strain can be calculated with the temperature values obtained from SAFIR thermal analysis. Since the temperature values listed in thermal analysis output file are the temperatures on the element nodes ($\theta_i, \theta_j, \theta_k$), the calculation starts with averaging the three temperatures. Figure 42 and Equation (4.2) below show the visualization of the beam temperature using Diamond, SAFIR post-processor GUI software, and the standard averaging equation to calculate average temperature ($\bar{\theta}$) in the centre of the element.

$$\bar{\theta} = \frac{(\theta_i + \theta_j + \theta_k)}{3} \tag{4.2}$$

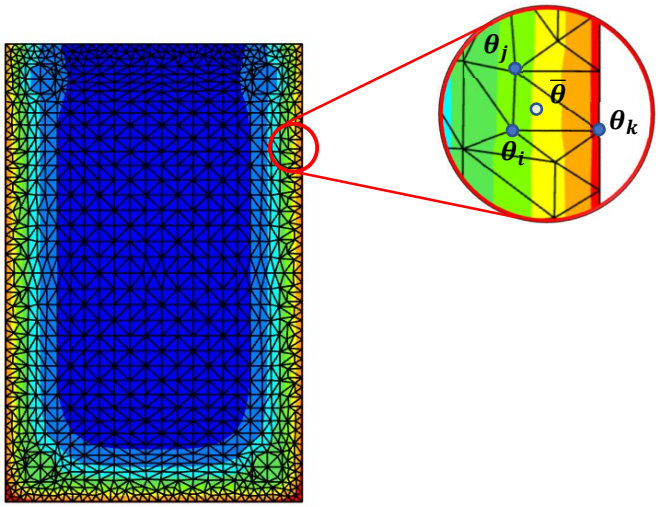

Figure 42. Visualization of beam temperature with meshes using Diamond

After the average temperature per mesh is obtained, the next step is to calculate the thermal strain (ε_{th}) depending on the material of the element observed. Equation 4.3 to 4.7 below are obtained from Eurocode EN1992-1-2 Section 3.3 (concrete) and Section 3.4 (steel) [9].

for concrete:

$$\varepsilon_c(\theta) = -1.8 \times 10^{-4} + 9 \times 10^{-6}.\theta + 2.3 \times 10^{-11}.\theta^3 \quad (20°C \leq \theta \leq 700°C) \quad (4.3)$$

$$\varepsilon_c(\theta) = 14 \times 10^{-3} \quad (700°C \leq \theta \leq 1200°C) \quad (4.4)$$

for reinforcing steel:

$$\varepsilon_s(\theta) = -2.416 \times 10^{-4} + 1.2 \times 10^{-5}.\theta + 0.4 \times 10^{-8}.\theta^2 \quad (20°C \leq \theta \leq 750°C) \quad (4.5)$$

$$\varepsilon_s(\theta) = 11 \times 10^{-3} \quad (750°C \leq \theta \leq 860°C) \quad (4.6)$$

$$\varepsilon_s(\theta) = -6.2 \times 10^{-3} + 2 \times 10^{-5}.\theta \quad (860°C \leq \theta \leq 1200°C) \quad (4.7)$$

Since we already have the values of the total strain and thermal strain, by using Equation 4.1, the value of mechanical strain can be calculated. Afterwards, stress-strain relationship from Eurocode EN1992-1-2 Section 3.2.2 (for concrete) and Section 3.2.3 (for reinforcing steel) [9] are used to calculate the mechanical stress of the element which will then be multiplied by the element area (from SAFIR structural output) to get the axial force per element (F_i). Figure 43 below visualizes the mechanical strain and stress in the beam section.

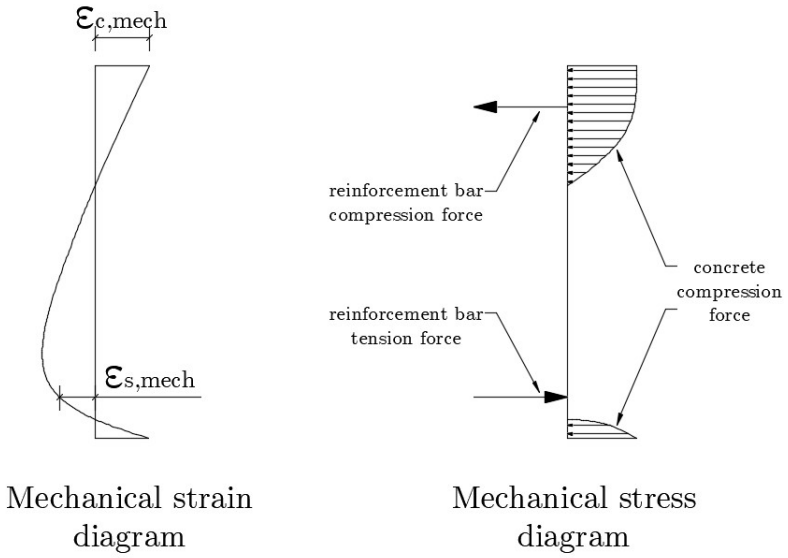

Figure 43. Mechanical strain and stress visualization (Reproduced from [21])

Subsequently, the sum of all the axial forces needs to be equal to the external axial load (N). If there is no axial load imposed on the beam, then the sum of the axial forces need to be equal to 0 as shown in Equation 4.8 where N is negative if compression and positive if tension. Otherwise, the assumed location of the centre of rotation needs to be changed and the calculation is restarted until Equation 4.8 is achieved.

$$\sum_{i=0}^{n} F_i = N \tag{4.8}$$

After Equation 4.8 is achieved, the axial forces (F_i) are multiplied by the distance from the element to the centre of the beam (y_i) to get the moment for the selected curvature (Equation 4.9). Repeat this step until all the curvatures have been analysed. In this research, the analysed curvature range is from -5×10^{-5} to 5×10^{-5} mm^{-1}.

$$M = \sum_{i=0}^{n} F_i . y_i \tag{4.9}$$

As this analysis requires a solver function to achieve Equation 4.8, Python will be used to develop a calculation tool. This tool will be discussed in the following section.

4.1.1.1 Moment-Curvature Diagram Tool

Moment-curvature diagram tool is a Python program created to help to calculate moment-curvature diagrams of a beam with different exposure times. There are basic assumptions that are used in this tool which are:

1. Plane sections remain plane
2. Zero tensile strength for concrete
3. No bond-slip between the concrete and the reinforcement bar

This tool uses a solver function to solve an iterative calculation described in the previous section. In Python library, there are many solver algorithm available but for this tool, the solver used is broyden1.

Broyden1 is a root-finding algorithm which is able to calculate the value of a variable with a given result in a non-linear problem. For example in this case, Equation 4.8 will be set to be the wanted result, and the distance to the centre of rotation (Figure 41) will be the variable.

4.1.1.2 M-χ Diagram Tool Validation

Due to the time limitation of the research, the moment-curvature diagram calculation and tool are validated by comparing the result with another result from a published and more functional report by Van Coile [22]. From his research, the moment-curvature diagrams that will be recalculated are for beam type B without axial load (Figure 44) and with 500kN compression load (Figure 45).

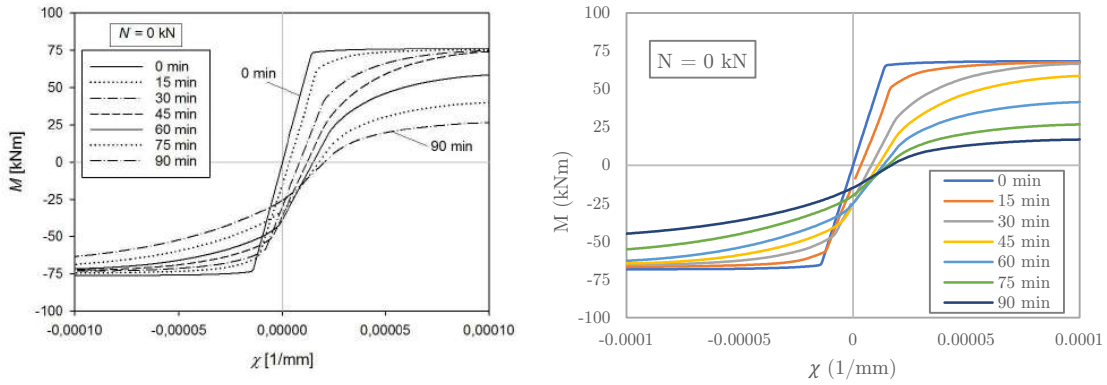

Figure 44. Comparison of the result from the developed M-χ diagram tool (right) to Van Coile's M-χ diagram calculation result without axial load (left) [22]

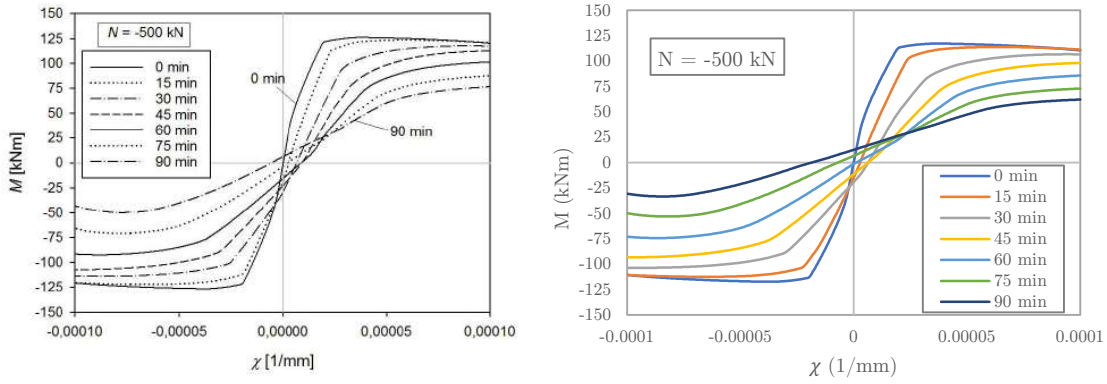

Figure 45. Comparison of the result from the developed M-χ diagram tool (right) to Van Coile's M-χ diagram calculation result with 500kN compression load (left) [22]

It can be observed from the comparisons above that the tool produces a remarkably similar diagram shape to Van Coile's results despite having lower absolute moment value. This difference could happen as the assumptions used in his calculation and this calculation might be different.

4.1.2 Validation by Deflection Calculation with Virtual Work Method

After the moment-curvature diagrams for Beam A and Beam B are obtained, by using virtual work method, the deflection of the beam can be recalculated based on the calculated moment curvature diagram. The equation is shown in Equation 4.10 below:

$$v = \int_0^L m.\chi \, dx \tag{4.10}$$

with L as beam length, m as virtual moment, and χ as the curvature. However, as this is a double pinned support, there will be an additional second order moment effect from the compression caused by the thermal elongation of the beam. Thus, the beam needs to be divided into smaller segments and the deflection of each segment will be calculated as it will also contribute to the second order effect. [23]

In the beginning, the beam will be calculated without the moment effect since in this research, it is assumed that there will be no load on the beam. With zero moment, the curvature value at each point will be obtained from the M-χ diagram and Equation 4.10 will be used to calculate the deflection at each point. The calculated deflection will then be multiplied by the axial load to calculate the first moment. After that, the moment will affect the curvature which will also affect the deflection at that point. This iterative calculation will continue until the deflection converges.

A calculation tool will also be developed in this research to help calculating the iteration. It will calculate all the deflections at every point on the beam depending on the M-χ relationship for certain exposure time.

4.1.2.1 Virtual Work Deflection Tool Validation

A similar calculation was conducted by Van Coile [22] calculating a column deflection due to thermal load and an eccentric load. His calculation was based on Wang's research [23] for his doctoral dissertation. For the purpose of validating this tool, one of his column specimens is recalculated. The specimen used is a 300 mm by 300 mm column with 4D32 bars with the configuration shown in Figure 46 below.

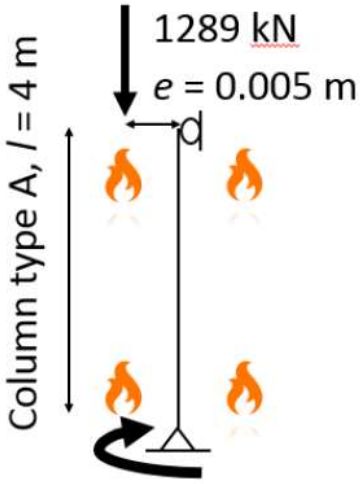

Figure 46. Column configuration taken from [22]

The comparison between Van Coile's result and the developed tool results are shown in Figure 47. It can be seen that the similarity between both graphs is uncanny and hence, the tool can be considered well functional.

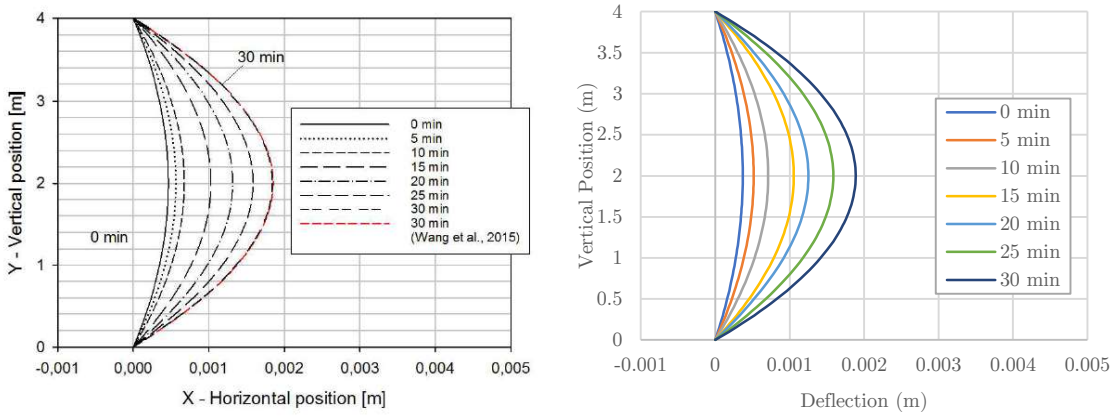

Figure 47. Comparison between Van Coile's result (left) [22] and the developed tool result (right)

4.2 Results and Discussions

4.2.1 Moment-Curvature Diagram

Using the tool above, M-χ diagrams for both beams can be generated for each minute depending on the compression load at that time. Figure 48 and Figure 49 below show the M-χ diagrams per 15 minutes for Beam A and Beam B respectively. The value of each point is presented in Table B. 1 (Beam A) and Table B. 2 (Beam B).

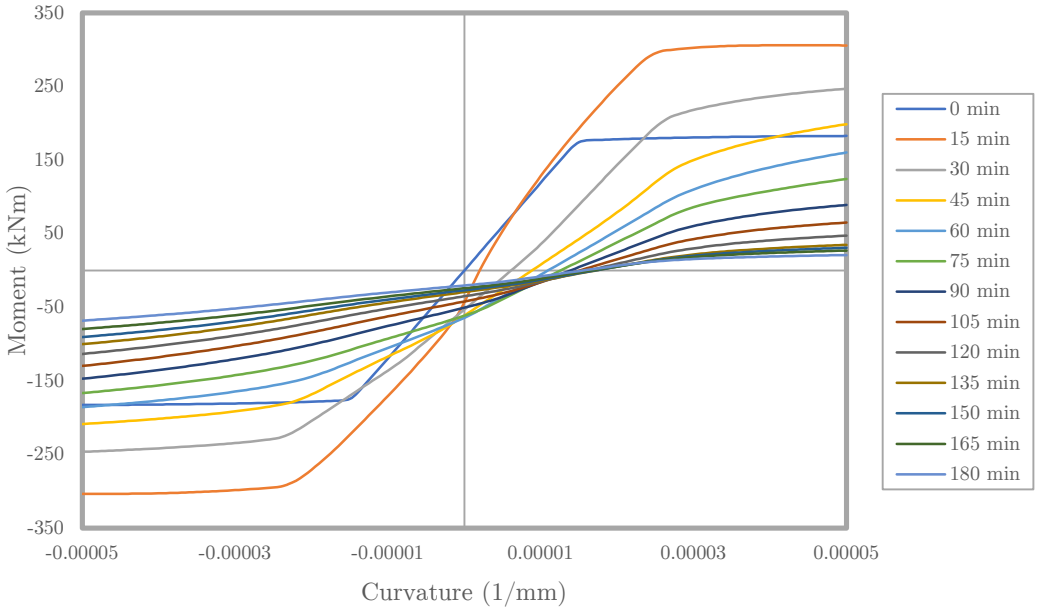

Figure 48. M-χ diagram for Beam A

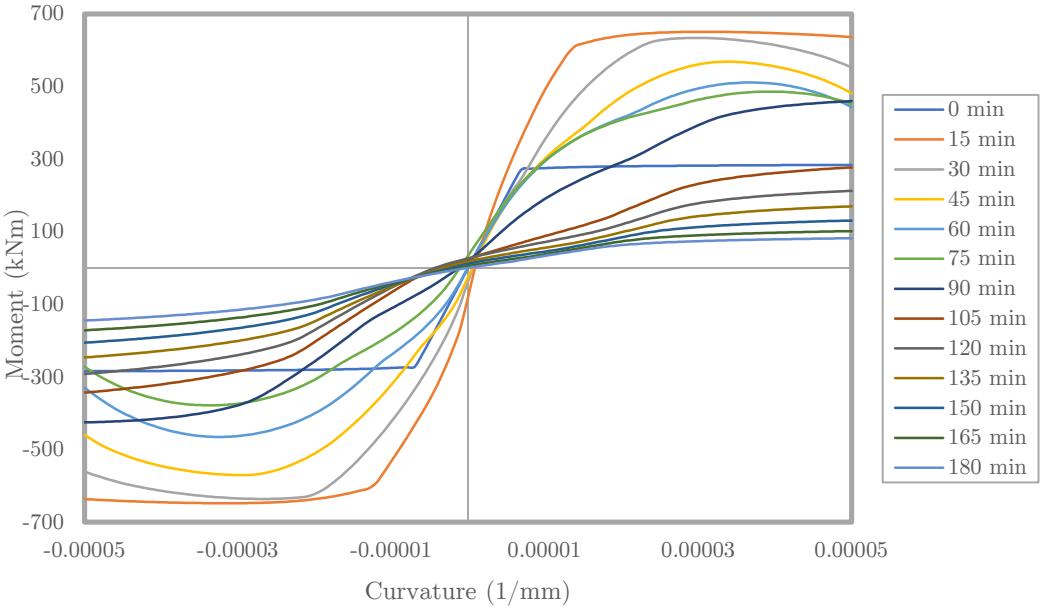

Figure 49. M-χ diagram from Beam B

In order to check the deflection behaviour for each beam, the curvature for each timestep needs to be obtained from the moment-curvature diagram with the moment values. Table 9 below shows moment values for Beam A and Beam B taken from SAFIR.

Table 9. Moment values for Beam A and Beam B per 15 minutes (from SAFIR)

Timestep (minute)	Beam A moment (kNm)	Beam B moment (kNm)
0	0	0
15	103.70	40.46
30	203.50	77.32
45	171.60	104.00
60	144.30	94.21
75	121.00	-10.84
90	92.33	-367.50
105	70.36	-309.30
120	52.97	-266.00
135	40.12	-227.10
150	35.96	-190.10
165	31.77	-159.20
180	24.58	-136.40

Both beams start with 0 moment at 0 minute because in this research, it is assumed that there is no external load working on the beam including the self-weight of the beam. Therefore, the moment values listed in Table 9 are the moments due to second order effects which are caused by compression forces multiplied by the deflections. By plotting these moment values in the moment curvature diagrams from Figure 48 and Figure 49, we can find the curvatures for each timestep.

Figure 50 plots the Beam A moment values in the M-χ diagrams. It shows that the curvature for each moment value is increasing for each timestep. However, the opposite is shown in Figure 51 where the curvature is increasing until 45 minutes before it goes to a negative curvature at around 75 minutes, hence making the the second order effects of bending moment negative as well.

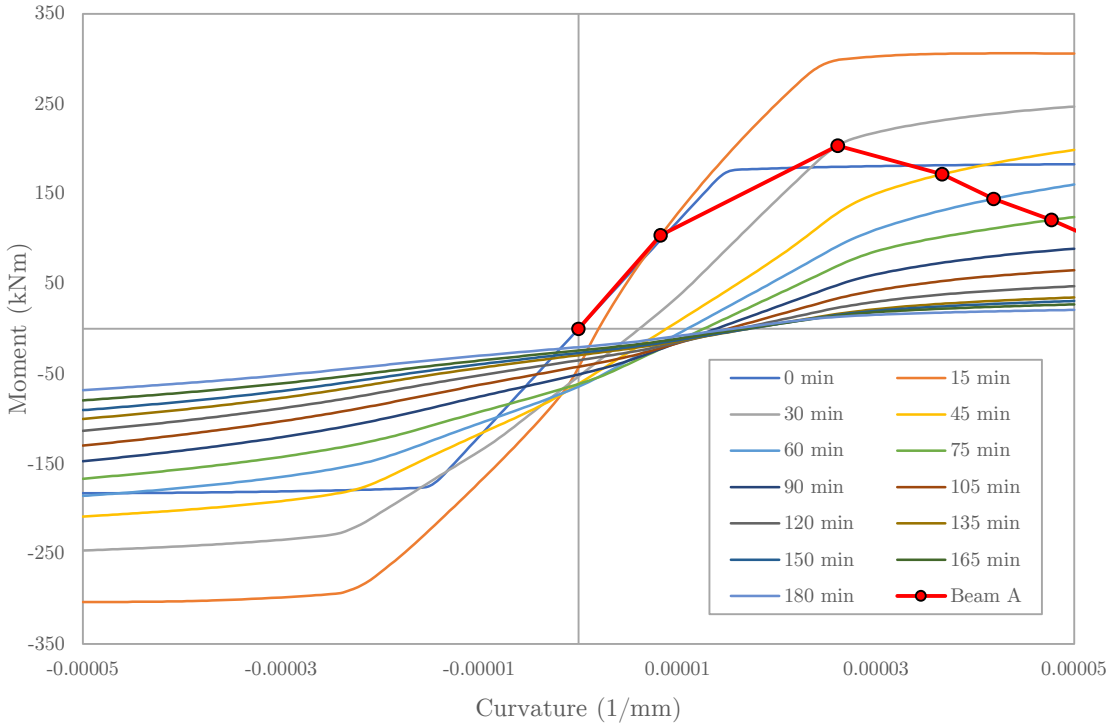

Figure 50. Beam A plotted M-χ diagrams

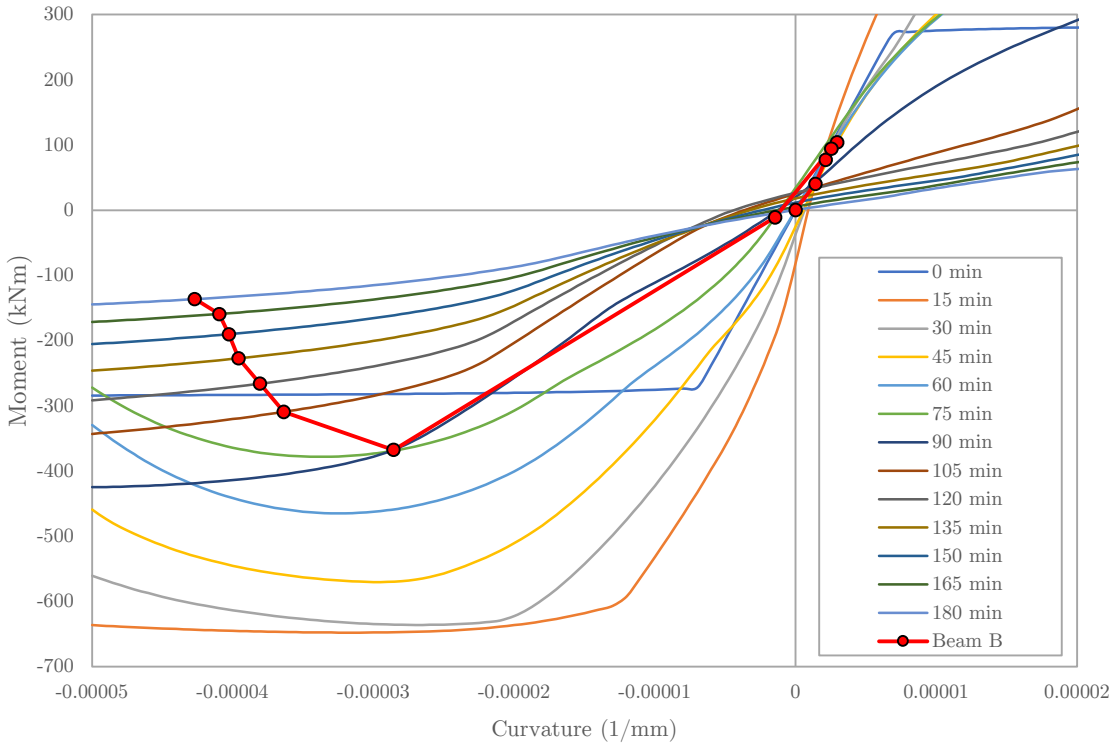

Figure 51. Beam B plotted M-χ diagrams

4.2.2 Validation by Deflection Calculation with Virtual Work Method

In order to validate the calculation in the previous section, the deflections from SAFIR are then recalculated using the M-χ diagrams and virtual moment. Using the tool developed in this research, the deflection values calculated are shown in Figure 52 and Figure 53.

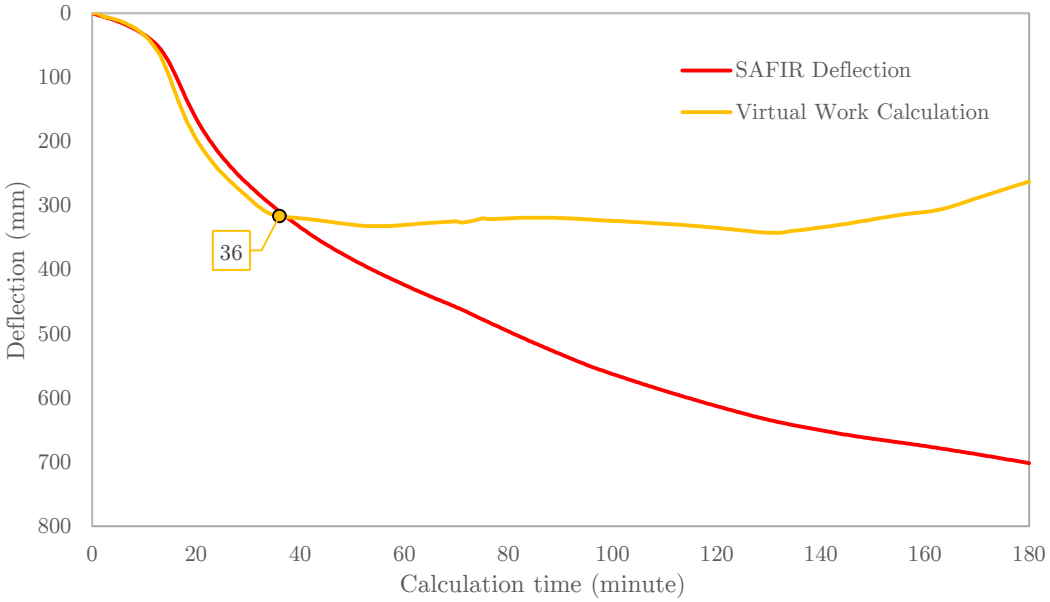

Figure 52. Comparison between deflection from SAFIR and virtual work method for Beam A

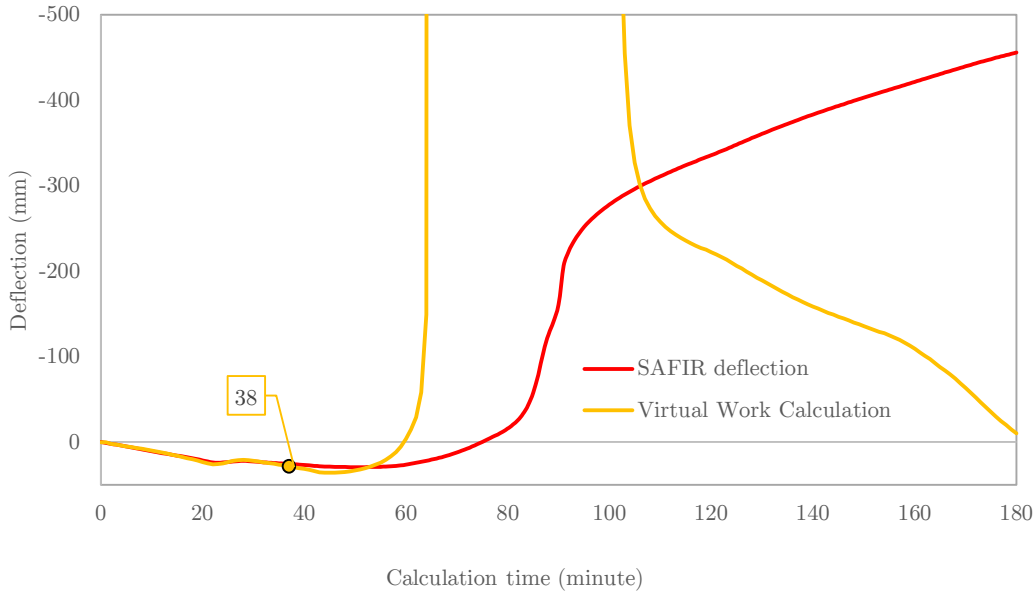

Figure 53. Comparison between deflection from SAFIR and virtual work method for Beam B

4.2.3 Discussions

From Figure 50 and Figure 51 above it can be seen that the curvature for Beam A is moving to the positive curvature and the one for Beam B is moving to positive curvature at first and then it goes to the opposite direction. This behaviour shows that Beam B, given the moment values from SAFIR, will deflect downward until around 60-75 minutes before finally experience negative bending and starts bending upwards.

The moment curvature diagrams in Figure 48 and Figure 49 show that for Beam A, with any moment, the curvature value will go to the positive side over the exposure time. However, for Beam B, a positive curvature can be achieved if the moment is retained at around 100 kNm at 90 minutes exposure time. This implies that Beam B needs more load to deflect downwards since from Table 9, the maximum moment for Beam B is 104 kNm at 45 minutes and then it starts decreasing.

The validation using the virtual work calculation shows a good resemblance to SAFIR calculation until around 35 to 40 minutes, after which, the calculation results start to deviate from the SAFIR deflection. Since the beam used in this research is slender ($\lambda \geq 70$), this might be the effect of slenderness mentioned in Wang's research which results in the iteration not capable of converging at one point.

5 Conclusions and Future Research

The aim of this research is to build an interactive tool for structural fire engineering awareness. This tool is built with the help of machine learning algorithm to create a prediction model so that the calculation does not need a huge calculation effort, hence making the calculation almost instantaneous.

In this research, the performance of polynomial degree is not satisfactory as the variables and timesteps need to be divided into parts, making it complex to integrate into the tool. On the other hand, gradient boosting method displays higher simplicity as it only needs one model per output. Additionally, it also shows better performance with all the models having less than 10% error with MAPE calculation except for shear force. This is due to the fact that the actual model has some numerical noises and it makes the prediction not as accurate as the other models. Smoothening the actual graph should improve this prediction further. By using these models, the tool also proves to be able to predict the necessary output within a split of second and, together with the interface, it can be used and learned more easily to increase the users awareness, in this case, structural and fire engineers.

As this research only includes deflection, moment, shear, and axial force as outputs with a limited range of variables, a broader research can be done with more variables, such as putting natural fire as a selection apart from ISO fire or adding the effect of the beam self-weight. Furthermore, there is also a possibility that both of the beam behaviours (upward and downward deflections) could be modelled in one regression model.

However when validating with the virtual work method, due to time constraint, the deviation in the calculation results when compared to SAFIR results cannot be explored further. This also opens an opportunity for future researches to explore the limitation of virtual work calculation method for a beam exposed to fire for a longer period of time since it is dependent on the exposure time (M-χ diagram) and compression load.

6 References

[1] G. Rein, "Introduction to Fire Dynamics for Structural Engineers.," in *Training School for Young Researchers Integrated Fire Engineering and Response*, [Online]. Available: http://people.fsv.cvut.cz/~wald/fire/ifer/2012-Training_school/Lectures/03_Rein.pdf.

[2] T. Gernay, "Fire Resistance and Burnout Resistance of Reinforced Concrete Columns," *Fire Safety Journal,* vol. 104, pp. 67-78, 2019.

[3] A. Law, N. Butterworth and J. Stern-Gottfried, "A risk based framework for time equivalence and fire resistance," *Fire Technology,* vol. 51(4), pp. 771-784, 2015.

[4] A. Usmani, J. Rotter, S. Lamont, A. Sanad and M. Gillie, "Fundamental Principles of Structural Behaviour Under Thermal Effects," *Fire Safety Journal,* vol. 36, pp. 721-744, 2001.

[5] V. Kodur and M. Dwaikat, "A Numerical Model for Predicting the Fire Resistance of Reinforced Concrete Beams," *Cement & Concrete Composites,* vol. 30, pp. 431-443, 2008.

[6] C. S. Lin and M. E. Wu, "A Study of Evaluating an Evacuation," *Advances in Mechanical Engineering,* vol. 10, no. 4, pp. 1-11, 2018.

[7] W. Kenton, "Multiple Linear Regression – MLR Definition," Investopedia, 14 April 2019. [Online]. Available: https://www.investopedia.com/terms/m/mlr.asp. [Accessed 15 April 2020].

[8] N. Johansson and P. van Hees, "A Correlation for Predicting Smoke Layer Temperature In a Room Adjacent to a Room Involved in a Pre-flashover Fire," *Fire and Materials,* vol. 38(2), 2014.

[9] European Comission, EN 1992-1-2: Eurocode 2: Design of Concrete Structures - Part 1-2: General Rules - Structural Fire Design, Brussels: European Committee for Standardization, 2004.

[10] Stephanie, "Latin Hypercube Sampling: Simple Definition," Statistics How To, 5 January 2018. [Online]. Available: https://www.statisticshowto.com/latin-hypercube-sampling/. [Accessed 15 April 2020].

[11] RiskAMP, "Latin Hypercube Sampling," RiskAMP, [Online]. Available: https://www.riskamp.com/latin-hypercube-sampling. [Accessed 15 April 2020].

[12] J.-M. Franssen and T. Gernay, "Modeling Structures in Fire with SAFIR®: Theoretical Background and Capabilities," *Journal of Structural Fire Engineering,* vol. 8, no. 3, pp. 300-323, 2017.

[13] S. Ioffe and C. Szegedy, "Batch Normalization: Accelerating Deep Network Training by Reducing Internal Covariate Shift," 1502.03167, 2015.

[14] L. Breiman, J. Friedman, R. Olshen and C. Stone, Classification and Regression Trees, Monterey, CA: Wadsworth and Brooks, 1984.

[15] M. Gashler, C. Giraud-Carrier and T. Martinez, "Decision Tree Ensemble: Small Heterogeneous Is Better Than Large Homogenous," *2008 Seventh International Conference on Machine Learning and Applications,* pp. 900-905, 2008.

[16] G. Ke, Q. Meng, T. Finley, T. Wang, W. Chen, W. Ma, Q. Ye and T. Liu, "LightGBM: A Highly Efficient Gradient Boosting Decision Tree," *Advances in Neural Information Processing Systems,* pp. 3146-3154, 2017.

[17] Microsoft Corporation, "LightGBM Parameters," Microsoft Corporation, [Online]. Available: https://lightgbm.readthedocs.io/en/latest/Parameters.html. [Accessed 28 April 2020].

[18] J. Bergstra, D. Yamins and D. D. Cox, "Hyperopt: A Python Library for Optimizing the Hyperparameters of Machine Learning Algorithms," in *Proceedings of the 12th Python in Science Conference*, 2013.

[19] S. Kim and H. Kim, "A New Metric of Absolute Percentage Error for Intermittent Demand Forecasts," *International Journal of Forecasting,* vol. 32, no. 3, pp. 669-679, 2016.

[20] N. Gayatari, S. Nickolas and A. Reddy, "Feature Selection Using Decision Tree Induction in Class level Metrics Dataset for Software Defect Predictions," in *World Congress on Engineering and Computer Science 2010 Vol I*, San Francisco, USA, 2010.

[21] R. Van Coile, "Reliability-Based Decision Making for Concrete Elements Exposed to Fire," Ghent University, Ghent, 2015.

[22] R. Van Coile, "Towards Reliability-based Structural Fire Safety: Development and Probabilistic Applications of a Direct Stiffness Method for Concrete Frames Exposed to Fire," Ghent University, Ghent, 2016.

[23] L. Wang, "Second-order Effects in Reinforced Concrete Columns Exposed to Fire (Doctoral Dissertation)," Ghent University, Ghent, 2017.

[24] University of Liege, September 2015. [Online]. Available: http://orbi.ulg.ac.be/bitstream/2268/186186/1/SAFIR-presentation_Sep2015.pdf. [Accessed 2020 March 26].

[25] B. Karlsson and J. G. Quintiere, Enclosure Fire, CRC Press LLC, 2000.

[26] T. Thienpont, R. Van Coile, R. Caspeele and W. De Corte, "Comparison of Fire Resistance and Burnout Resistance of Simply Supported Reinforced Concrete Slabs Exposed to Parametric Fires," in *CONFAB 2019, 3rd International Conference on Structural Safety under Fire and Blast Loading, Proceedings*, London, 2019.

[27] British Constructional Steelwork Association Limited, "SteelConstruction.info," [Online]. Available: https://www.steelconstruction.info/Structural_fire_engineering. [Accessed 25 March 2020].

[28] European Commission, EN 1991-1-2: Eurocode 1: Actions on Structures - Part 1-2: General Actions - Actions on Structures Exposed to Fire, Brussels: European Committee for Standardization, 2002.

[29] B. Foley, "What is Regression Analysis and Why Should I Use It?," Surveygizmo, 14 February 2018. [Online]. Available: https://www.surveygizmo.com/resources/blog/regression-analysis/. [Accessed 15 April 2020].

[30] X. Li, "18-660: Numerical Methods for Engineering Design and Optimization," Department of Electrical and Computer Engineering, Carnegie Mellon University, [Online]. Available: https://users.ece.cmu.edu/~xinli/classes/cmu_18660/Lec25.pdf. [Accessed 15 April 2020].

Appendix A

Table A. 1. Tabular comparison for Behaviour A and Behaviour B deflection (Figure 21)

Time (min)	Behaviour A				Behaviour B			
	Predicted (mm)	Actual (mm)	MAPE (%)	RMSE (mm)	Predicted (mm)	Actual (mm)	MAPE (%)	RMSE (mm)
0	0.23	0	-	0.05	0.32	0	-	0.10
1	2.30	2.03	13.17	0.07	1.17	0.97	20.74	0.04
2	4.36	4.28	1.79	0.01	2.08	1.96	6.33	0.02
3	6.21	6.45	3.71	0.06	3.17	2.85	11.20	0.10
4	8.98	8.87	1.18	0.01	4.01	3.74	7.34	0.08
5	11.58	11.68	0.85	0.01	4.90	4.64	5.63	0.07
6	14.85	14.84	0.05	0.00	5.72	5.54	3.34	0.03
7	18.07	18.55	2.61	0.23	6.66	6.43	3.64	0.05
8	23.66	22.7	4.25	0.93	7.55	7.28	3.72	0.07
9	29.52	27.4	7.74	4.50	8.35	8.04	3.87	0.10
10	35.33	32.88	7.44	5.99	9.19	8.79	4.58	0.16
11	41.37	39.75	4.07	2.62	9.85	9.53	3.37	0.10
12	47.39	47.84	0.93	0.20	10.40	10.22	1.74	0.03
13	59.53	58.34	2.05	1.43	11.30	10.95	3.16	0.12
14	70.78	72.74	2.69	3.83	11.95	11.72	2.00	0.05
15	88.43	93.03	4.94	21.14	12.86	12.43	3.50	0.19
16	108.67	118.5	8.30	96.66	13.47	13.12	2.70	0.13
17	134.79	141.95	5.05	51.33	14.55	13.81	5.36	0.55
18	155.57	161.92	3.92	40.32	14.85	14.53	2.21	0.10
19	180.00	179.01	0.55	0.98	15.69	15.27	2.76	0.18
20	197.10	194.03	1.58	9.44	16.56	16.04	3.26	0.27
21	212.18	209.76	1.16	5.88	17.35	16.82	3.16	0.28
22	228.53	230.85	1.01	5.40	17.93	17.61	1.80	0.10
23	242.06	254.23	4.79	148.07	18.71	18.48	1.25	0.05
24	252.42	273.09	7.57	427.11	19.82	19.42	2.04	0.16
25	267.05	287.55	7.13	420.24	20.98	20.48	2.45	0.25
26	279.87	299.85	6.66	399.15	21.58	21.55	0.16	0.00
27	290.88	310.59	6.34	388.32	21.92	22.7	3.43	0.61
28	306.38	320.22	4.32	191.54	23.23	23.93	2.91	0.48
29	317.71	328.99	3.43	127.31	21.74	25.23	13.85	12.21
30	328.88	337.1	2.44	67.55	22.66	26.59	14.77	15.42
31	339.65	344.84	1.51	26.94	20.99	27.96	24.91	48.52
32	351.36	352.19	0.24	0.70	21.81	29.34	25.66	56.70
33	360.29	359.11	0.33	1.40	23.78	30.75	22.66	48.53
34	370.44	365.6	1.32	23.45	29.24	32.08	8.85	8.06
35	377.06	371.59	1.47	29.98	28.77	33.06	12.98	18.41
36	381.20	377.27	1.04	15.47	30.68	33.43	8.24	7.58
37	382.73	382.81	0.02	0.01	29.93	33.46	10.54	12.44
38	386.44	388.28	0.47	3.38	33.53	33.32	0.63	0.04
39	391.55	393.55	0.51	3.98	35.14	33.12	6.11	4.10
40	395.90	398.69	0.70	7.76	34.10	32.9	3.64	1.44
41	401.74	403.65	0.47	3.65	34.47	32.81	5.07	2.76
42	406.23	408.44	0.54	4.86	36.68	33.04	11.02	13.26
43	411.01	413.1	0.51	4.37	35.76	33.64	6.30	4.49
44	415.74	417.82	0.50	4.33	40.42	34.54	17.01	34.53
45	421.50	422.68	0.28	1.40	41.88	35.66	17.44	38.69
46	426.28	427.47	0.28	1.41	43.58	36.98	17.86	43.61
47	431.02	432.1	0.25	1.17	49.91	38.51	29.61	130.07

48	435.46	436.64	0.27	1.39	55.48	40.28	37.75	231.18
49	437.81	441.05	0.73	10.47	55.13	42.31	30.29	164.29
50	442.92	445.43	0.56	6.28	64.14	44.72	43.43	377.27
51	447.35	449.79	0.54	5.98	72.24	47.75	51.28	599.54
52	444.73	454.12	2.07	88.13	76.00	51.5	47.56	600.05
53	450.95	458.45	1.64	56.31	78.25	56.17	39.31	487.65
54	454.78	462.7	1.71	62.78	82.01	61.68	32.96	413.17
55	458.82	466.94	1.74	65.90	86.80	68.21	27.26	345.72
56	462.83	471.1	1.75	68.32	103.15	76.68	34.52	700.75
57	467.96	475.26	1.54	53.31	120.85	87.15	38.67	1135.94
58	471.76	479.36	1.59	57.78	136.67	100.23	36.35	1327.74
59	476.27	483.49	1.49	52.16	151.14	116.08	30.20	1228.87
60	478.96	487.85	1.82	79.02	182.44	145.3	25.56	1379.30
61	483.29	492.35	1.84	82.10	191.96	190.29	0.88	2.78
62	487.88	496.81	1.80	79.67	217.49	218.29	0.37	0.64
63	491.38	501.03	1.93	93.19	227.22	261.75	13.19	1192.20
64	499.83	505.32	1.09	30.14	246.43	283.32	13.02	1360.96
65	503.95	509.55	1.10	31.40	253.87	300.56	15.54	2180.20
66	506.66	513.75	1.38	50.32	273.87	313.54	12.65	1573.51
67	510.83	517.93	1.37	50.35	287.27	325.47	11.74	1459.21
68	515.96	522.03	1.16	36.90	295.97	335.38	11.75	1552.94
69	520.33	526.08	1.09	33.10	306.50	344.75	11.10	1463.09
70	525.24	530.09	0.91	23.51	306.66	353.31	13.20	2176.08
71	528.38	534.03	1.06	31.87	316.38	361.5	12.48	2036.15
72	533.68	537.94	0.79	18.17	328.31	369.08	11.05	1661.93
73	538.55	541.79	0.60	10.47	333.55	376.42	11.39	1837.47
74	542.09	545.56	0.64	12.05	353.64	383.45	7.78	888.88
75	547.54	549.29	0.32	3.07	370.30	390.17	5.09	394.95
76	550.52	552.94	0.44	5.85	374.72	396.53	5.50	475.75
77	554.27	556.51	0.40	5.00	385.40	402.64	4.28	297.31
78	558.76	560.04	0.23	1.65	389.94	408.67	4.58	350.78
79	562.59	563.54	0.17	0.90	396.54	414.51	4.34	322.92
80	565.98	566.99	0.18	1.02	408.06	420.33	2.92	150.48
81	569.38	570.31	0.16	0.87	414.99	426.32	2.66	128.46
82	572.45	573.53	0.19	1.16	419.54	432.47	2.99	167.09
83	575.95	576.63	0.12	0.46	419.87	438.6	4.27	350.70
84	579.30	579.69	0.07	0.15	424.61	444.46	4.47	394.21
85	583.01	582.73	0.05	0.08	432.71	450.21	3.89	306.17
86	583.48	585.74	0.39	5.09	440.83	455.82	3.29	224.61
87	585.39	588.72	0.57	11.10	446.79	461.36	3.16	212.25
88	588.54	591.65	0.53	9.69	453.81	466.79	2.78	168.50
89	591.61	594.56	0.50	8.68	461.55	472.17	2.25	112.75
90	593.27	597.43	0.70	17.30	466.45	477.53	2.32	122.76
91	596.26	600.29	0.67	16.27	471.74	482.79	2.29	122.12
92	599.36	603.11	0.62	14.06	476.59	488.06	2.35	131.45
93	602.00	605.89	0.64	15.16	480.83	493.3	2.53	155.42
94	604.68	608.65	0.65	15.79	491.80	498.53	1.35	45.32
95	608.22	611.37	0.51	9.91	497.94	503.76	1.16	33.90
96	610.28	614.03	0.61	14.07	499.60	508.96	1.84	87.64
97	613.26	616.66	0.55	11.53	503.43	514.1	2.08	113.91
98	615.59	619.26	0.59	13.45	509.97	519.2	1.78	85.11
99	619.03	621.83	0.45	7.85	513.95	524.21	1.96	105.35
100	622.27	624.37	0.34	4.41	518.87	529.16	1.95	105.95
101	624.08	626.89	0.45	7.91	526.39	534.05	1.43	58.70
102	627.19	629.39	0.35	4.84	529.08	538.89	1.82	96.24

103	630.31	631.86	0.25	2.40	532.34	543.68	2.09	128.64
104	632.23	634.31	0.33	4.33	535.86	548.37	2.28	156.55
105	635.88	636.73	0.13	0.73	540.14	552.99	2.32	165.21
106	637.29	639.14	0.29	3.44	545.23	557.55	2.21	151.89
107	639.71	641.5	0.28	3.19	546.08	562.06	2.84	255.50
108	643.40	643.85	0.07	0.20	549.23	566.43	3.04	295.84
109	645.67	646.18	0.08	0.26	554.87	570.63	2.76	248.44
110	647.60	648.45	0.13	0.72	556.34	574.66	3.19	335.70
111	650.52	650.59	0.01	0.01	562.72	578.58	2.74	251.47
112	651.96	652.66	0.11	0.49	571.05	582.46	1.96	130.08
113	654.67	654.64	0.00	0.00	577.30	586.31	1.54	81.23
114	656.49	656.57	0.01	0.01	579.15	590.12	1.86	120.30
115	658.56	658.47	0.01	0.01	583.83	593.88	1.69	100.94
116	660.62	660.36	0.04	0.07	587.85	597.61	1.63	95.22
117	662.15	662.23	0.01	0.01	592.13	601.31	1.53	84.23
118	664.05	664.06	0.00	0.00	594.57	604.98	1.72	108.44
119	665.29	665.87	0.09	0.34	598.95	608.63	1.59	93.76
120	666.83	667.64	0.12	0.65	603.12	612.23	1.49	82.92
121	668.02	669.35	0.20	1.77	606.73	615.8	1.47	82.23
122	669.79	671.04	0.19	1.56	609.16	619.36	1.65	104.02
123	671.53	672.67	0.17	1.30	612.74	622.87	1.63	102.56
124	672.70	674.25	0.23	2.39	614.19	626.37	1.95	148.44
125	673.91	675.79	0.28	3.52	619.24	629.81	1.68	111.64
126	675.42	677.3	0.28	3.53	622.18	633.25	1.75	122.65
127	676.75	678.78	0.30	4.12	625.36	636.67	1.78	127.87
128	677.48	680.24	0.41	7.61	627.43	640.05	1.97	159.20
129	679.32	681.69	0.35	5.63	628.71	643.39	2.28	215.42
130	681.13	683.13	0.29	4.00	632.10	646.72	2.26	213.75
131	682.92	684.55	0.24	2.66	632.97	650	2.62	289.95
132	684.09	685.97	0.27	3.54	637.34	653.26	2.44	253.55
133	685.50	687.37	0.27	3.51	645.32	656.48	1.70	124.56
134	687.69	688.8	0.16	1.22	651.90	659.68	1.18	60.56
135	689.03	690.23	0.17	1.43	652.94	662.86	1.50	98.48
136	690.36	691.68	0.19	1.74	662.59	666.01	0.51	11.68
137	691.94	693.17	0.18	1.50	666.26	669.15	0.43	8.36
138	692.89	694.66	0.26	3.14	667.20	672.25	0.75	25.52
139	694.25	696.16	0.27	3.65	677.51	675.31	0.33	4.85
140	696.25	697.67	0.20	2.01	684.68	678.36	0.93	39.88
141	697.48	699.18	0.24	2.90	684.10	681.38	0.40	7.39
142	699.13	700.73	0.23	2.57	687.23	684.37	0.42	8.17
143	700.83	702.29	0.21	2.13	689.21	687.32	0.28	3.59
144	702.16	703.86	0.24	2.89	689.76	690.25	0.07	0.24
145	703.72	705.44	0.24	2.95	695.66	693	0.38	7.10
146	705.43	707.03	0.23	2.55	698.19	695.58	0.38	6.84
147	707.05	708.63	0.22	2.51	699.10	698	0.16	1.21
148	708.39	710.24	0.26	3.44	703.01	700.28	0.39	7.48
149	710.47	711.87	0.20	1.97	705.75	702.52	0.46	10.44
150	712.35	713.5	0.16	1.31	707.16	704.73	0.34	5.90
151	714.69	715.15	0.06	0.21	708.18	706.91	0.18	1.60
152	714.98	716.79	0.25	3.26	706.43	709.07	0.37	6.96
153	716.34	718.43	0.29	4.35	710.21	711.22	0.14	1.02
154	716.99	720.07	0.43	9.51	709.66	713.28	0.51	13.09
155	719.29	721.73	0.34	5.97	709.86	715.28	0.76	29.39
156	720.55	723.38	0.39	8.01	715.82	717.22	0.19	1.95
157	722.42	724.99	0.35	6.61	713.95	719.07	0.71	26.22

158	724.25	726.47	0.31	4.92	715.11	720.87	0.80	33.22
159	725.98	727.88	0.26	3.61	717.94	722.64	0.65	22.12
160	726.84	729.22	0.33	5.68	718.71	724.38	0.78	32.16
161	728.29	730.54	0.31	5.06	721.74	726.08	0.60	18.84
162	730.22	731.85	0.22	2.65	723.00	727.75	0.65	22.56
163	731.25	733.15	0.26	3.59	725.75	729.37	0.50	13.09
164	732.64	734.44	0.24	3.23	729.13	730.99	0.25	3.47
165	734.36	735.74	0.19	1.91	729.32	732.56	0.44	10.48
166	735.19	737.03	0.25	3.39	732.84	734.11	0.17	1.61
167	737.03	738.3	0.17	1.62	733.77	735.62	0.25	3.41
168	737.74	739.58	0.25	3.40	733.97	737.12	0.43	9.94
169	738.89	740.85	0.27	3.86	735.57	738.61	0.41	9.24
170	739.46	742.13	0.36	7.11	737.59	740.1	0.34	6.29
171	741.90	743.42	0.20	2.32	738.26	741.58	0.45	11.04
172	743.21	744.71	0.20	2.24	739.00	743.1	0.55	16.82
173	745.68	746.01	0.04	0.11	741.75	744.62	0.39	8.26
174	747.16	747.3	0.02	0.02	743.02	746.18	0.42	10.02
175	748.63	748.6	0.00	0.00	745.10	747.78	0.36	7.18
176	749.89	749.89	0.00	0.00	746.31	749.39	0.41	9.51
177	750.53	751.18	0.09	0.42	747.57	751.04	0.46	12.01
178	751.81	752.45	0.08	0.41	749.72	752.69	0.40	8.84
179	753.05	753.71	0.09	0.44	751.15	754.36	0.43	10.34
180	754.27	754.98	0.09	0.50	753.32	756.04	0.36	7.39
Avg.			**1.07**	**4.79**			**6.46**	**14.83**

Table A. 2. Tabular comparison for Behaviour A and Behaviour B moment (Figure 24)

Time (min)	Behaviour A				Behaviour B			
	Predicted (mm)	Actual (mm)	MAPE (%)	RMSE (mm)	Predicted (mm)	Actual (mm)	MAPE (%)	RMSE (mm)
0	-0.11	0.00	-	0.01	-0.26	0.00	-	0.07
1	0.20	0.27	25.08	0.00	-0.06	0.20	131.41	0.07
2	0.95	1.18	19.47	0.05	0.57	0.91	37.36	0.11
3	2.21	2.60	15.01	0.15	1.51	1.88	19.93	0.14
4	4.74	4.74	0.10	0.00	2.75	3.23	14.69	0.22
5	7.44	7.80	4.57	0.13	4.06	4.89	16.98	0.69
6	12.07	11.85	1.88	0.05	6.39	6.87	6.87	0.22
7	18.19	17.27	5.30	0.84	8.69	9.11	4.66	0.18
8	23.92	24.03	0.45	0.01	10.92	11.56	5.50	0.40
9	33.88	32.14	5.42	3.04	12.98	13.91	6.66	0.86
10	44.14	42.25	4.47	3.56	15.65	16.39	4.51	0.55
11	58.85	55.27	6.48	12.83	18.59	19.05	2.43	0.22
12	75.17	70.83	6.12	18.80	21.63	21.60	0.13	0.00
13	94.51	90.64	4.27	14.96	24.49	24.25	0.97	0.06
14	119.95	116.70	2.79	10.59	26.78	27.26	1.75	0.23
15	148.88	149.70	0.55	0.68	30.17	30.35	0.58	0.03
16	173.84	181.40	4.17	57.15	33.68	33.48	0.60	0.04
17	192.67	201.50	4.38	77.91	36.37	36.54	0.47	0.03
18	212.14	213.50	0.64	1.86	38.67	39.66	2.49	0.97
19	223.61	220.40	1.46	10.29	43.46	43.11	0.81	0.12
20	227.48	224.10	1.51	11.41	49.27	46.84	5.18	5.89
21	231.84	224.60	3.22	52.42	53.19	50.75	4.81	5.95
22	231.28	221.20	4.55	101.52	56.99	54.79	4.02	4.85
23	231.36	213.30	8.46	325.99	61.31	59.15	3.65	4.67
24	222.44	204.30	8.88	328.89	67.40	63.87	5.52	12.44
25	212.80	197.40	7.80	237.07	72.88	69.25	5.24	13.16
26	206.55	191.80	7.69	217.57	80.24	74.78	7.31	29.85
27	199.10	186.80	6.59	151.35	85.53	80.67	6.03	23.62
28	195.64	182.10	7.44	183.34	86.98	87.11	0.15	0.02
29	190.28	178.10	6.84	148.47	90.93	93.96	3.23	9.20
30	189.80	174.20	8.96	243.46	93.70	101.20	7.41	56.24
31	183.55	170.60	7.59	167.65	96.16	108.60	11.45	154.75
32	177.75	167.30	6.24	109.14	96.46	116.00	16.84	381.62
33	175.52	164.20	6.89	128.05	101.56	123.50	17.77	481.54
34	171.02	161.40	5.96	92.57	107.09	130.80	18.13	562.24
35	166.20	158.80	4.66	54.73	108.53	136.50	20.49	782.44
36	163.85	156.00	5.03	61.55	110.78	139.50	20.59	824.95
37	158.88	153.30	3.64	31.14	121.90	140.80	13.43	357.34
38	152.80	151.60	0.79	1.45	127.59	141.30	9.70	187.83
39	151.80	149.50	1.54	5.29	124.92	141.60	11.78	278.07
40	149.05	147.50	1.05	2.39	127.89	141.70	9.75	190.83
41	147.35	145.60	1.20	3.06	133.64	142.30	6.08	74.92
42	144.47	143.70	0.53	0.59	138.88	144.20	3.69	28.34
43	143.07	141.80	0.89	1.60	143.43	147.80	2.96	19.09
44	139.07	139.80	0.52	0.53	144.13	152.50	5.49	70.13
45	137.49	137.60	0.08	0.01	139.18	158.10	11.97	358.07
46	134.60	135.40	0.59	0.64	154.47	164.50	6.10	100.54
47	131.48	133.40	1.44	3.68	158.45	171.70	7.72	175.54
48	129.24	131.40	1.65	4.68	170.14	179.80	5.37	93.24
49	128.52	129.40	0.68	0.78	216.75	189.00	14.68	769.90

50	125.67	127.50	1.44	3.35	263.47	199.80	31.86	4053.39
51	123.91	125.60	1.34	2.84	252.82	213.00	18.70	1585.74
52	122.23	123.80	1.27	2.45	276.52	229.20	20.65	2239.65
53	120.34	121.90	1.28	2.43	313.37	249.00	25.85	4143.37
54	118.56	120.20	1.36	2.67	334.36	271.60	23.11	3939.01
55	117.21	118.40	1.00	1.41	373.97	297.40	25.75	5862.70
56	115.44	116.70	1.08	1.60	438.95	329.60	33.18	11957.03
57	113.13	115.00	1.63	3.50	476.20	366.70	29.86	11990.22
58	110.97	113.30	2.06	5.43	488.82	408.80	19.57	6402.71
59	109.58	111.60	1.81	4.09	502.40	453.10	10.88	2430.35
60	108.14	109.50	1.24	1.85	559.01	516.80	8.17	1781.77
61	106.67	107.00	0.31	0.11	567.26	583.20	2.73	254.05
62	104.50	104.30	0.19	0.04	571.26	601.10	4.96	890.67
63	101.09	102.30	1.18	1.46	573.08	604.20	5.15	968.22
64	99.69	100.00	0.31	0.09	568.40	596.40	4.69	784.02
65	97.62	97.83	0.21	0.04	562.94	586.50	4.02	555.07
66	95.20	95.60	0.42	0.16	547.86	577.10	5.07	855.09
67	93.25	93.41	0.17	0.03	543.30	567.20	4.21	571.15
68	91.49	91.25	0.26	0.06	541.45	558.50	3.05	290.59
69	89.80	89.15	0.72	0.42	535.14	549.50	2.61	206.26
70	87.84	87.07	0.88	0.59	528.16	541.40	2.45	175.35
71	86.04	85.05	1.17	0.98	520.53	533.10	2.36	158.02
72	83.68	83.05	0.76	0.40	503.74	525.30	4.10	464.99
73	82.79	81.06	2.14	3.00	491.07	517.60	5.13	704.00
74	78.89	79.12	0.29	0.05	486.32	509.90	4.62	555.89
75	77.78	77.22	0.72	0.31	483.24	502.60	3.85	374.66
76	76.38	75.34	1.38	1.09	469.97	495.40	5.13	646.69
77	74.85	73.50	1.84	1.83	462.87	488.40	5.23	651.74
78	73.34	71.68	2.32	2.76	451.27	481.20	6.22	895.58
79	70.63	69.88	1.07	0.56	441.14	474.50	7.03	1112.58
80	70.05	68.09	2.87	3.82	429.64	467.50	8.10	1433.20
81	67.78	66.50	1.92	1.63	420.72	459.60	8.46	1511.95
82	66.05	65.07	1.51	0.96	415.56	451.00	7.86	1256.27
83	64.84	63.77	1.68	1.14	413.60	442.20	6.47	817.97
84	64.76	62.49	3.63	5.14	401.81	433.60	7.33	1010.43
85	63.02	61.24	2.91	3.18	394.28	425.00	7.23	943.96
86	62.59	59.99	4.34	6.78	385.14	416.60	7.55	989.50
87	59.23	58.75	0.81	0.23	378.56	408.30	7.28	884.47
88	58.67	57.53	1.98	1.30	372.64	400.10	6.86	753.98
89	57.46	56.32	2.02	1.29	365.56	392.10	6.77	704.11
90	56.35	55.12	2.22	1.50	354.21	384.10	7.78	893.14
91	54.81	53.93	1.63	0.77	345.82	376.30	8.10	928.85
92	54.24	52.76	2.80	2.18	342.58	368.60	7.06	676.98
93	53.10	51.59	2.92	2.28	328.67	360.80	8.91	1032.66
94	52.66	50.44	4.41	4.94	320.91	353.10	9.12	1036.13
95	51.38	49.30	4.21	4.31	314.03	345.50	9.11	990.12
96	51.03	48.19	5.89	8.05	307.79	337.70	8.86	894.67
97	49.53	47.10	5.15	5.89	297.35	330.20	9.95	1079.29
98	48.09	46.02	4.49	4.27	292.17	322.80	9.49	938.33
99	47.18	44.94	4.98	5.01	286.68	315.10	9.02	807.60
100	46.04	43.87	4.95	4.72	282.16	308.00	8.39	667.52
101	44.91	42.82	4.89	4.38	276.32	301.00	8.20	609.24
102	43.75	41.77	4.75	3.94	270.01	294.10	8.19	580.22
103	43.39	40.74	6.52	7.05	269.42	287.20	6.19	316.20
104	42.60	39.71	7.28	8.36	261.88	280.40	6.60	342.90

105	41.53	38.70	7.30	7.98	257.61	274.00	5.98	268.70
106	40.88	37.70	8.44	10.13	254.94	267.50	4.69	157.72
107	39.46	36.72	7.47	7.53	249.51	261.10	4.44	134.39
108	38.67	35.74	8.19	8.57	243.32	255.10	4.62	138.65
109	37.92	34.80	8.97	9.75	240.39	249.70	3.73	86.74
110	36.82	33.91	8.58	8.46	234.02	244.70	4.37	114.13
111	36.14	33.20	8.85	8.63	230.29	240.00	4.05	94.27
112	35.42	32.60	8.65	7.95	225.84	235.40	4.06	91.42
113	34.90	32.12	8.65	7.72	219.05	230.90	5.13	140.42
114	34.05	31.71	7.38	5.48	214.31	226.30	5.30	143.65
115	33.21	31.32	6.05	3.59	210.50	222.00	5.18	132.14
116	33.02	30.94	6.73	4.33	203.49	217.60	6.48	198.95
117	32.51	30.56	6.39	3.81	197.88	213.30	7.23	237.65
118	32.47	30.21	7.47	5.09	190.75	209.10	8.78	336.68
119	31.69	29.86	6.14	3.36	187.57	205.00	8.50	303.95
120	30.39	29.53	2.91	0.74	186.37	200.80	7.18	208.15
121	30.78	29.22	5.36	2.45	180.92	196.80	8.07	252.08
122	30.91	28.93	6.86	3.94	179.11	192.80	7.10	187.52
123	30.66	28.65	7.02	4.04	171.90	188.90	9.00	289.08
124	29.84	28.40	5.09	2.09	171.07	185.00	7.53	193.94
125	30.02	28.17	6.55	3.41	166.80	181.30	8.00	210.28
126	29.90	27.98	6.88	3.70	164.43	177.50	7.36	170.85
127	29.77	27.79	7.11	3.90	159.60	173.80	8.17	201.67
128	29.26	27.61	5.99	2.74	156.12	170.20	8.27	198.30
129	28.86	27.44	5.18	2.02	155.07	166.60	6.92	132.85
130	28.74	27.27	5.40	2.17	149.69	163.00	8.16	177.06
131	28.51	27.10	5.19	1.98	142.73	159.50	10.52	281.34
132	28.30	26.93	5.11	1.89	139.71	156.00	10.44	265.38
133	28.32	26.74	5.92	2.51	136.79	152.60	10.36	249.90
134	28.19	26.54	6.23	2.74	134.96	149.20	9.54	202.78
135	27.38	26.32	4.04	1.13	135.69	146.00	7.06	106.32
136	27.20	26.06	4.38	1.30	132.57	142.70	7.10	102.67
137	26.93	25.76	4.55	1.38	129.85	139.50	6.92	93.07
138	26.71	25.44	5.00	1.62	125.20	136.40	8.21	125.44
139	26.38	25.09	5.13	1.66	122.30	133.40	8.32	123.13
140	26.09	24.72	5.53	1.87	120.37	130.30	7.62	98.51
141	25.27	24.33	3.87	0.88	118.50	127.40	6.99	79.26
142	25.07	23.94	4.72	1.28	114.78	124.40	7.73	92.51
143	25.02	23.52	6.40	2.26	113.88	121.40	6.20	56.62
144	24.65	23.09	6.74	2.42	112.50	118.60	5.14	37.21
145	24.03	22.64	6.16	1.95	111.40	116.10	4.05	22.14
146	23.73	22.18	7.00	2.41	109.65	114.00	3.82	18.96
147	23.24	21.72	7.02	2.32	108.98	112.20	2.87	10.34
148	22.40	21.25	5.42	1.33	107.36	110.90	3.20	12.56
149	21.95	20.77	5.67	1.39	105.84	109.50	3.34	13.42
150	21.24	20.30	4.63	0.88	104.99	108.20	2.96	10.29
151	21.12	19.82	6.54	1.68	101.53	106.90	5.02	28.81
152	20.71	19.34	7.08	1.88	100.27	105.70	5.13	29.45
153	20.25	18.87	7.31	1.90	99.52	104.50	4.77	24.82
154	19.82	18.39	7.75	2.03	95.40	103.20	7.56	60.90
155	19.42	17.92	8.37	2.25	94.78	102.10	7.17	53.57
156	18.75	17.46	7.38	1.66	94.03	101.00	6.90	48.56
157	18.42	17.04	8.10	1.90	92.98	99.93	6.96	48.36
158	18.11	16.70	8.47	2.00	92.04	98.94	6.97	47.55
159	17.55	16.45	6.69	1.21	91.89	97.96	6.20	36.90

160	17.35	16.26	6.70	1.19	91.76	97.07	5.47	28.21
161	17.16	16.07	6.76	1.18	91.35	96.20	5.04	23.52
162	17.10	15.87	7.75	1.51	92.03	95.45	3.58	11.68
163	16.71	15.69	6.47	1.03	91.19	94.71	3.71	12.36
164	16.14	15.50	4.14	0.41	89.49	94.09	4.89	21.14
165	15.87	15.31	3.64	0.31	89.11	93.41	4.60	18.49
166	15.60	15.13	3.10	0.22	89.20	92.92	4.00	13.84
167	15.45	14.94	3.41	0.26	89.15	92.34	3.45	10.15
168	15.32	14.76	3.78	0.31	88.39	91.75	3.66	11.30
169	15.05	14.57	3.30	0.23	87.42	91.15	4.09	13.88
170	14.98	14.39	4.11	0.35	86.43	90.52	4.52	16.75
171	14.77	14.22	3.87	0.30	85.59	89.89	4.78	18.45
172	14.53	14.03	3.56	0.25	85.24	89.16	4.40	15.38
173	14.37	13.85	3.77	0.27	83.70	88.40	5.31	22.05
174	14.14	13.68	3.35	0.21	82.74	87.55	5.49	23.09
175	13.97	13.50	3.48	0.22	81.84	86.61	5.51	22.79
176	13.85	13.33	3.93	0.27	80.90	85.64	5.53	22.46
177	13.79	13.17	4.68	0.38	80.01	84.56	5.38	20.72
178	13.66	13.00	5.10	0.44	79.00	83.41	5.29	19.47
179	13.39	12.83	4.40	0.32	77.88	82.26	5.32	19.19
180	13.35	12.66	5.48	0.48	76.75	80.98	5.22	17.87
Avg.			4.49	4.22			8.39	23.88

Table A. 3. Tabular comparison for Behaviour A and Behaviour B compression force (Figure 27)

Time (min)	Behaviour A				Behaviour B			
	Predicted (mm)	Actual (mm)	MAPE (%)	RMSE (mm)	Predicted (mm)	Actual (mm)	MAPE (%)	RMSE (mm)
0	-4.26	0.00	-	18.15	2.70	0.00	-	7.28
1	-138.48	-134.30	3.12	17.50	-219.65	-227.00	3.24	54.06
2	-283.65	-276.10	2.74	57.05	-449.62	-462.50	2.79	165.93
3	-414.44	-403.70	2.66	115.42	-643.68	-662.20	2.80	343.04
4	-541.73	-534.20	1.41	56.75	-851.16	-862.10	1.27	119.74
5	-681.80	-667.30	2.17	210.14	-1036.15	-1054.00	1.69	318.70
6	-797.62	-798.80	0.15	1.40	-1219.26	-1239.00	1.59	389.84
7	-927.72	-931.10	0.36	11.46	-1396.83	-1416.00	1.35	367.63
8	-1061.17	-1058.00	0.30	10.02	-1552.94	-1586.00	2.08	1093.04
9	-1170.60	-1173.00	0.20	5.75	-1687.45	-1730.00	2.46	1810.40
10	-1279.86	-1285.00	0.40	26.46	-1812.41	-1865.00	2.82	2765.72
11	-1377.95	-1391.00	0.94	170.35	-1923.02	-1999.00	3.80	5773.49
12	-1477.33	-1481.00	0.25	13.49	-2042.62	-2113.00	3.33	4953.06
13	-1559.17	-1554.00	0.33	26.77	-2137.03	-2215.00	3.52	6079.41
14	-1592.06	-1605.00	0.81	167.43	-2219.00	-2327.00	4.64	11664.43
15	-1598.40	-1610.00	0.72	134.54	-2340.75	-2442.00	4.15	10250.73
16	-1557.97	-1531.00	1.76	727.65	-2459.80	-2551.00	3.58	8317.42
17	-1473.04	-1420.00	3.74	2813.19	-2530.41	-2646.00	4.37	13361.88
18	-1363.55	-1319.00	3.38	1984.47	-2627.65	-2731.00	3.78	10681.90
19	-1290.04	-1232.00	4.71	3368.76	-2733.73	-2823.00	3.16	7968.32
20	-1197.84	-1157.00	3.53	1667.59	-2819.41	-2920.00	3.44	10118.42
21	-1089.46	-1085.00	0.41	19.88	-2881.00	-3018.00	4.54	18768.86
22	-954.88	-982.30	2.79	751.95	-2969.72	-3111.00	4.54	19960.63
23	-846.58	-859.70	1.53	172.26	-3088.88	-3201.00	3.50	12570.33
24	-807.78	-759.80	6.31	2301.68	-3201.76	-3289.00	2.65	7611.46
25	-750.26	-694.00	8.11	3165.31	-3304.59	-3382.00	2.29	5991.65
26	-664.66	-644.80	3.08	394.31	-3385.18	-3470.00	2.44	7193.81
27	-612.78	-605.70	1.17	50.08	-3491.20	-3555.00	1.79	4070.54
28	-570.63	-573.10	0.43	6.08	-3569.73	-3641.00	1.96	5079.19
29	-528.61	-544.10	2.85	239.79	-3642.00	-3726.00	2.25	7056.64
30	-486.42	-519.20	6.31	1074.29	-3707.47	-3808.00	2.64	10105.41
31	-459.92	-496.90	7.44	1367.53	-3790.32	-3885.00	2.44	8964.09
32	-474.74	-477.00	0.47	5.13	-3912.97	-3953.00	1.01	1602.79
33	-474.16	-459.10	3.28	226.74	-3921.30	-4017.00	2.38	9157.79
34	-449.66	-443.00	1.50	44.35	-3905.49	-4077.00	4.21	29415.85
35	-409.65	-428.90	4.49	370.66	-3961.47	-4131.00	4.10	28741.11
36	-392.32	-419.00	6.37	711.56	-3978.95	-4173.00	4.65	37654.12
37	-373.88	-409.20	8.63	1247.52	-4045.85	-4209.00	3.88	26618.49
38	-371.65	-392.80	5.38	447.17	-4093.90	-4243.00	3.51	22231.02
39	-363.80	-382.00	4.76	331.12	-4084.30	-4275.00	4.46	36367.61
40	-350.13	-371.70	5.80	465.19	-4120.86	-4307.00	4.32	34647.61
41	-342.22	-362.30	5.54	403.35	-4137.05	-4339.00	4.65	40784.65
42	-329.29	-353.80	6.93	600.91	-4163.05	-4368.00	4.69	42002.82
43	-327.02	-346.00	5.49	360.36	-4188.50	-4394.00	4.68	42232.16
44	-316.03	-336.30	6.03	410.73	-4208.56	-4416.00	4.70	43030.14
45	-323.14	-327.30	1.27	17.28	-4217.80	-4435.00	4.90	47176.36
46	-316.62	-318.80	0.68	4.75	-4257.79	-4450.00	4.32	36945.01
47	-320.42	-310.50	3.19	98.35	-4264.10	-4459.00	4.37	37984.49
48	-309.15	-302.80	2.10	40.34	-4310.57	-4465.00	3.46	23848.78
49	-295.88	-295.40	0.16	0.23	-4279.19	-4469.00	4.25	36029.54

50	-286.85	-288.20	0.47	1.83	-4206.02	-4468.00	5.86	68633.07
51	-275.15	-281.10	2.11	35.35	-4189.26	-4462.00	6.11	74389.34
52	-266.31	-274.40	2.95	65.43	-4181.26	-4452.00	6.08	73299.90
53	-257.83	-267.90	3.76	101.42	-4155.59	-4433.00	6.26	76956.14
54	-253.02	-261.50	3.24	71.85	-4061.12	-4405.00	7.81	118252.16
55	-249.48	-255.50	2.36	36.29	-3942.80	-4365.00	9.67	178253.15
56	-243.24	-249.60	2.55	40.42	-3723.55	-4300.00	13.41	332289.80
57	-238.51	-243.90	2.21	29.08	-3431.13	-4209.00	18.48	605083.48
58	-237.44	-238.40	0.40	0.91	-3228.97	-4081.00	20.88	725960.95
59	-236.94	-232.90	1.74	16.36	-3154.28	-3913.00	19.39	575663.10
60	-228.80	-226.10	1.19	7.29	-2844.69	-3612.00	21.24	588767.75
61	-223.94	-218.70	2.40	27.49	-2656.17	-3088.00	13.98	186476.73
62	-215.47	-212.20	1.54	10.69	-2436.02	-2775.00	12.22	114910.52
63	-270.99	-205.70	31.74	4262.94	-2183.51	-2320.00	5.88	18628.31
64	-226.18	-200.00	13.09	685.51	-2075.55	-2126.00	2.37	2545.09
65	-207.62	-194.20	6.91	180.05	-1945.61	-1967.00	1.09	457.47
66	-199.13	-188.40	5.69	115.10	-1781.97	-1854.00	3.89	5188.43
67	-190.03	-182.60	4.07	55.22	-1716.06	-1755.00	2.22	1516.25
68	-184.99	-177.00	4.51	63.85	-1650.38	-1677.00	1.59	708.52
69	-180.44	-171.70	5.09	76.40	-1564.07	-1606.00	2.61	1758.40
70	-174.11	-166.40	4.63	59.46	-1495.06	-1543.00	3.11	2298.43
71	-167.71	-161.30	3.97	41.09	-1449.62	-1485.00	2.38	1251.41
72	-166.04	-156.30	6.23	94.79	-1373.21	-1434.00	4.24	3694.84
73	-160.32	-151.50	5.82	77.79	-1358.79	-1386.00	1.96	740.62
74	-157.52	-146.70	7.38	117.12	-1281.12	-1341.00	4.47	3585.95
75	-154.15	-142.30	8.33	140.42	-1237.07	-1298.00	4.69	3713.01
76	-144.08	-137.80	4.56	39.47	-1148.44	-1260.00	8.85	12446.08
77	-139.73	-133.60	4.59	37.54	-1099.10	-1223.00	10.13	15351.59
78	-132.49	-129.50	2.31	8.96	-1071.60	-1189.00	9.87	13782.91
79	-129.70	-125.40	3.43	18.52	-1044.05	-1156.00	9.68	12531.69
80	-126.01	-121.40	3.80	21.25	-1019.23	-1123.00	9.24	10767.72
81	-125.90	-118.00	6.70	62.46	-998.31	-1090.00	8.41	8406.95
82	-122.52	-114.90	6.63	58.05	-947.13	-1056.00	10.31	11852.78
83	-118.36	-112.10	5.59	39.22	-926.97	-1022.00	9.30	9030.01
84	-115.34	-109.30	5.52	36.43	-893.77	-989.40	9.67	9144.54
85	-112.39	-106.60	5.43	33.50	-856.95	-957.70	10.52	10149.79
86	-108.91	-103.90	4.82	25.11	-835.86	-927.60	9.89	8416.73
87	-104.37	-101.20	3.13	10.05	-809.17	-898.10	9.90	7908.10
88	-103.17	-98.64	4.60	20.55	-789.72	-870.10	9.24	6461.45
89	-99.98	-96.11	4.02	14.95	-764.67	-843.70	9.37	6245.24
90	-95.98	-93.67	2.47	5.34	-740.17	-817.70	9.48	6011.27
91	-95.85	-91.21	5.09	21.54	-742.48	-792.80	6.35	2532.56
92	-92.84	-88.81	4.54	16.26	-719.90	-768.80	6.36	2391.22
93	-93.09	-86.43	7.71	44.38	-697.39	-745.90	6.50	2352.76
94	-88.75	-84.10	5.53	21.61	-686.80	-723.30	5.05	1332.43
95	-87.22	-81.80	6.63	29.37	-647.05	-701.80	7.80	2997.74
96	-84.82	-79.60	6.56	27.27	-631.42	-680.20	7.17	2379.23
97	-81.04	-77.48	4.59	12.66	-616.72	-658.20	6.30	1720.45
98	-79.88	-75.41	5.93	19.97	-578.65	-638.90	9.43	3629.73
99	-76.58	-73.40	4.33	10.09	-573.53	-617.50	7.12	1933.03
100	-73.74	-71.35	3.35	5.71	-567.88	-598.40	5.10	931.68
101	-71.77	-69.34	3.51	5.92	-550.52	-579.60	5.02	845.92
102	-71.52	-67.34	6.20	17.44	-527.77	-561.80	6.06	1158.26
103	-68.95	-65.37	5.47	12.79	-514.81	-543.60	5.30	829.03
104	-67.10	-63.45	5.76	13.36	-492.85	-526.30	6.36	1118.78

105	-66.15	-61.59	7.41	20.81	-476.90	-509.90	6.47	1088.73
106	-64.56	-59.76	8.03	23.03	-470.20	-494.10	4.84	571.26
107	-62.26	-57.98	7.38	18.33	-459.51	-478.40	3.95	356.86
108	-60.28	-56.23	7.20	16.39	-450.70	-463.80	2.82	171.57
109	-58.88	-54.54	7.96	18.86	-448.68	-451.00	0.51	5.36
110	-56.81	-52.98	7.23	14.66	-433.10	-439.30	1.41	38.42
111	-54.73	-51.88	5.49	8.11	-435.17	-428.10	1.65	50.03
112	-53.99	-50.91	6.06	9.51	-424.96	-417.10	1.88	61.80
113	-54.22	-50.14	8.14	16.64	-422.06	-406.70	3.78	235.83
114	-53.17	-49.45	7.52	13.83	-409.68	-396.00	3.45	187.13
115	-52.49	-48.72	7.73	14.19	-398.00	-386.10	3.08	141.52
116	-51.72	-47.99	7.77	13.89	-389.93	-376.20	3.65	188.38
117	-50.49	-47.29	6.76	10.22	-384.13	-366.60	4.78	307.14
118	-49.33	-46.64	5.77	7.24	-376.55	-357.40	5.36	366.89
119	-49.00	-45.95	6.64	9.30	-359.48	-348.30	3.21	124.97
120	-47.76	-45.35	5.31	5.80	-348.69	-339.20	2.80	90.12
121	-46.82	-44.77	4.57	4.18	-340.50	-330.70	2.96	95.98
122	-46.77	-44.20	5.81	6.59	-325.69	-322.10	1.11	12.86
123	-45.82	-43.71	4.82	4.44	-319.33	-313.90	1.73	29.51
124	-46.42	-43.24	7.34	10.09	-313.87	-305.80	2.64	65.17
125	-46.48	-42.79	8.63	13.64	-297.03	-298.00	0.33	0.95
126	-45.83	-42.40	8.09	11.76	-292.35	-290.00	0.81	5.53
127	-44.74	-41.99	6.54	7.54	-283.75	-282.60	0.41	1.32
128	-47.28	-41.68	13.44	31.38	-277.91	-275.10	1.02	7.92
129	-45.88	-41.40	10.82	20.07	-272.86	-267.70	1.93	26.66
130	-45.57	-41.11	10.85	19.88	-260.25	-260.50	0.10	0.06
131	-45.17	-40.79	10.74	19.20	-251.13	-253.60	0.97	6.10
132	-43.92	-40.47	8.52	11.88	-246.24	-246.90	0.27	0.44
133	-43.67	-40.11	8.88	12.69	-240.22	-240.40	0.07	0.03
134	-43.38	-39.76	9.10	13.08	-235.35	-234.00	0.58	1.81
135	-42.30	-39.33	7.56	8.84	-232.88	-227.80	2.23	25.78
136	-41.53	-38.91	6.73	6.87	-226.57	-221.60	2.24	24.71
137	-41.30	-38.39	7.58	8.48	-222.01	-215.60	2.97	41.08
138	-40.66	-37.88	7.35	7.75	-212.02	-209.70	1.11	5.40
139	-39.90	-37.26	7.09	6.97	-211.59	-204.00	3.72	57.62
140	-39.01	-36.79	6.04	4.95	-204.44	-198.50	2.99	35.28
141	-38.82	-35.99	7.86	8.00	-190.97	-192.90	1.00	3.71
142	-38.37	-34.56	11.02	14.51	-187.66	-187.60	0.03	0.00
143	-37.88	-33.91	11.71	15.76	-183.00	-182.40	0.33	0.36
144	-37.21	-33.21	12.06	16.03	-180.86	-177.30	2.01	12.66
145	-36.02	-32.50	10.84	12.40	-176.80	-173.60	1.84	10.22
146	-34.74	-31.82	9.19	8.55	-174.91	-170.60	2.53	18.61
147	-34.43	-31.08	10.78	11.22	-171.14	-167.80	1.99	11.13
148	-33.38	-30.34	10.02	9.25	-169.59	-165.70	2.35	15.11
149	-32.99	-29.60	11.44	11.46	-163.17	-163.20	0.02	0.00
150	-32.26	-28.87	11.75	11.51	-158.50	-160.80	1.43	5.28
151	-32.16	-28.14	14.29	16.18	-155.79	-158.40	1.65	6.82
152	-31.45	-27.38	14.85	16.52	-154.51	-156.00	0.96	2.23
153	-30.64	-26.71	14.71	15.43	-146.48	-153.80	4.76	53.64
154	-29.88	-26.01	14.87	14.95	-144.09	-151.30	4.77	52.04
155	-29.21	-25.27	15.60	15.55	-142.92	-149.00	4.08	36.99
156	-28.13	-24.62	14.26	12.32	-141.17	-146.80	3.84	31.75
157	-28.46	-23.96	18.78	20.24	-137.08	-144.60	5.20	56.52
158	-28.16	-23.41	20.30	22.59	-136.68	-142.70	4.22	36.21
159	-26.89	-23.03	16.78	14.93	-135.86	-140.90	3.57	25.36

160	-26.60	-22.72	17.08	15.07	-135.55	-139.30	2.69	14.05
161	-25.63	-22.43	14.25	10.21	-134.81	-137.70	2.10	8.35
162	-25.09	-22.09	13.56	8.98	-133.32	-136.40	2.25	9.46
163	-24.55	-21.83	12.46	7.40	-131.52	-135.00	2.58	12.13
164	-24.30	-21.52	12.91	7.71	-129.43	-133.90	3.34	19.99
165	-24.05	-21.23	13.29	7.96	-129.23	-132.50	2.47	10.69
166	-23.58	-20.99	12.32	6.69	-128.44	-131.80	2.55	11.26
167	-22.69	-20.66	9.85	4.14	-127.59	-131.20	2.75	13.01
168	-22.48	-20.41	10.16	4.30	-125.55	-130.20	3.57	21.60
169	-22.29	-20.11	10.82	4.74	-125.55	-129.10	2.75	12.58
170	-22.41	-19.84	12.96	6.61	-122.24	-127.90	4.43	32.08
171	-21.81	-19.65	10.99	4.66	-120.09	-126.70	5.22	43.66
172	-21.80	-19.33	12.79	6.11	-119.34	-125.40	4.83	36.66
173	-21.57	-19.06	13.16	6.29	-117.90	-124.10	5.00	38.50
174	-21.63	-18.80	15.03	7.98	-115.91	-122.50	5.38	43.37
175	-21.49	-18.52	16.03	8.82	-114.78	-121.00	5.14	38.69
176	-21.61	-18.29	18.16	11.03	-112.90	-119.30	5.36	40.90
177	-21.42	-18.03	18.79	11.48	-111.47	-117.60	5.21	37.60
178	-20.86	-17.77	17.41	9.57	-109.22	-115.60	5.52	40.71
179	-20.96	-17.52	19.66	11.86	-108.05	-114.00	5.22	35.35
180	-21.43	-17.32	23.71	16.86	-104.96	-111.60	5.95	44.09
Avg.			6.96	13.89			4.52	161.58

Table A. 4. Tabular comparison for Behaviour A and Behaviour B shear force (Figure 30)

Time (min)	Behaviour A				Behaviour B			
	Predicted (mm)	Actual (mm)	MAPE (%)	RMSE (mm)	Predicted (mm)	Actual (mm)	MAPE (%)	RMSE (mm)
0	0.72	0.00	-	0.51	-0.71	0.00	-	0.51
1	0.82	0.08	878.85	0.54	-0.71	0.10	781.84	0.67
2	1.07	0.35	203.72	0.52	-0.27	0.45	160.01	0.53
3	1.41	0.73	93.54	0.47	0.20	0.99	79.83	0.63
4	2.32	1.25	86.37	1.16	1.02	1.79	43.33	0.60
5	2.89	1.86	55.27	1.06	1.78	2.92	39.09	1.30
6	3.43	2.63	30.25	0.63	3.07	4.43	30.68	1.85
7	4.50	3.48	29.23	1.03	4.33	6.33	31.62	4.01
8	5.32	4.48	18.99	0.72	6.68	8.68	22.96	3.97
9	6.03	5.27	14.38	0.57	9.52	11.52	17.38	4.01
10	7.29	6.20	17.70	1.20	12.02	14.97	19.69	8.69
11	8.30	7.18	15.62	1.26	16.53	19.34	14.52	7.89
12	9.79	8.11	20.83	2.85	23.63	24.42	3.24	0.62
13	10.30	9.08	13.42	1.48	29.47	30.92	4.69	2.10
14	11.56	10.18	13.54	1.90	36.31	39.40	7.84	9.55
15	12.68	11.29	12.33	1.94	45.69	49.42	7.55	13.92
16	13.66	12.42	10.00	1.54	56.23	60.14	6.51	15.31
17	16.88	13.52	24.85	11.29	66.32	67.73	2.09	2.00
18	17.56	14.63	20.05	8.60	72.99	72.00	1.37	0.97
19	18.80	16.08	16.90	7.39	75.89	73.73	2.93	4.68
20	21.79	17.18	26.81	21.21	75.26	74.52	1.00	0.55
21	23.64	18.55	27.42	25.87	72.41	72.33	0.11	0.01
22	25.06	19.97	25.47	25.86	70.62	63.46	11.29	51.29
23	27.25	21.49	26.80	33.16	70.58	54.40	29.75	261.93
24	28.51	23.13	23.26	28.94	70.83	54.72	29.45	259.63
25	30.19	24.99	20.81	27.05	61.97	55.45	11.76	42.49
26	32.59	26.89	21.20	32.49	63.15	55.05	14.72	65.67
27	33.57	28.91	16.13	21.73	62.23	54.42	14.35	60.99
28	35.35	31.00	14.03	18.92	60.82	53.58	13.52	52.46
29	40.38	33.44	20.74	48.09	59.85	52.72	13.53	50.88
30	42.33	35.88	17.98	41.61	57.38	51.87	10.61	30.31
31	45.19	38.35	17.84	46.79	57.08	50.92	12.10	37.94
32	45.71	40.79	12.05	24.16	54.41	50.06	8.68	18.88
33	44.39	43.19	2.77	1.43	51.50	49.30	4.47	4.86
34	45.88	45.18	1.55	0.49	50.91	48.65	4.65	5.11
35	45.80	46.94	2.42	1.29	48.97	48.16	1.68	0.65
36	47.27	47.66	0.83	0.16	47.83	47.55	0.58	0.08
37	48.50	47.90	1.25	0.36	48.97	46.87	4.47	4.39
38	50.76	47.88	6.00	8.27	48.80	46.18	5.68	6.87
39	50.68	47.76	6.11	8.53	48.48	45.51	6.52	8.80
40	49.22	47.60	3.39	2.61	48.14	44.89	7.23	10.54
41	50.06	47.57	5.24	6.22	45.71	44.38	2.99	1.76
42	53.45	47.88	11.63	31.02	44.93	43.87	2.43	1.13
43	55.18	48.64	13.44	42.71	44.92	43.36	3.59	2.42
44	56.27	49.80	12.99	41.88	42.03	42.65	1.46	0.39
45	61.60	51.26	20.17	106.94	41.89	41.84	0.11	0.00
46	63.31	52.99	19.48	106.53	41.18	41.21	0.08	0.00
47	62.94	54.99	14.45	63.14	41.00	40.55	1.12	0.21
48	72.78	57.32	26.97	239.01	40.81	39.94	2.19	0.77
49	72.85	59.99	21.44	165.47	40.94	39.32	4.11	2.62

50	77.26	63.14	22.36	199.29	39.69	38.68	2.61	1.02
51	86.61	67.06	29.15	382.24	37.11	38.02	2.40	0.83
52	83.47	71.86	16.16	134.83	36.80	37.40	1.60	0.36
53	108.05	77.73	39.00	919.21	36.77	36.68	0.25	0.01
54	112.70	84.51	33.36	794.86	34.55	36.04	4.12	2.21
55	125.92	92.66	35.89	1105.91	34.09	35.45	3.84	1.85
56	136.28	101.70	34.00	1195.70	33.64	34.91	3.65	1.62
57	137.04	111.60	22.80	647.20	33.56	34.28	2.10	0.52
58	153.38	121.60	26.13	1009.89	31.87	33.76	5.59	3.56
59	159.61	131.60	21.29	784.83	31.63	33.07	4.34	2.06
60	193.75	126.70	52.92	4495.96	31.36	32.16	2.49	0.64
61	160.08	103.80	54.22	3167.05	31.06	31.42	1.16	0.13
62	143.32	136.50	4.99	46.47	30.59	30.89	0.98	0.09
63	156.07	193.40	19.30	1393.43	28.60	30.81	7.18	4.89
64	140.01	139.30	0.51	0.51	37.36	30.19	23.75	51.42
65	140.01	134.30	4.25	32.58	25.24	29.76	15.20	20.47
66	138.89	140.40	1.08	2.29	24.19	28.78	15.96	21.09
67	143.60	138.10	3.98	30.22	23.83	27.91	14.62	16.64
68	137.09	141.10	2.84	16.06	27.69	27.28	1.50	0.17
69	132.85	140.10	5.17	52.49	27.36	26.49	3.29	0.76
70	129.65	138.90	6.66	85.58	26.38	25.83	2.14	0.31
71	129.87	136.20	4.65	40.11	26.04	25.10	3.76	0.89
72	126.21	135.90	7.13	93.86	25.40	24.43	3.98	0.95
73	128.11	134.20	4.54	37.10	25.41	23.83	6.61	2.48
74	128.27	132.60	3.26	18.73	25.05	23.22	7.88	3.35
75	127.05	131.20	3.16	17.20	24.04	22.66	6.08	1.90
76	125.85	130.10	3.27	18.07	22.83	22.11	3.25	0.52
77	122.10	128.50	4.98	40.96	22.82	21.55	5.88	1.61
78	116.72	126.30	7.59	91.81	22.31	21.01	6.18	1.68
79	115.91	124.90	7.19	80.75	21.77	20.51	6.15	1.59
80	117.27	122.60	4.35	28.39	20.78	19.88	4.52	0.81
81	116.98	120.60	3.00	13.12	20.47	19.54	4.78	0.87
82	115.40	117.60	1.87	4.84	20.43	19.21	6.36	1.49
83	113.39	115.80	2.08	5.80	20.29	18.90	7.33	1.92
84	112.35	114.20	1.62	3.43	18.59	18.56	0.18	0.00
85	109.89	112.30	2.15	5.83	18.59	18.21	2.11	0.15
86	108.53	109.90	1.25	1.88	18.61	17.83	4.37	0.61
87	107.33	107.80	0.43	0.22	18.35	17.46	5.11	0.80
88	104.71	105.80	1.03	1.19	18.31	17.09	7.15	1.49
89	100.55	103.70	3.04	9.92	18.25	16.72	9.13	2.33
90	99.91	101.40	1.47	2.23	18.16	16.43	10.53	2.99
91	98.72	99.31	0.60	0.35	18.00	16.04	12.24	3.86
92	95.52	97.21	1.74	2.85	16.22	15.67	3.54	0.31
93	94.48	95.18	0.73	0.49	15.99	15.34	4.24	0.42
94	94.22	93.29	1.00	0.87	15.74	15.02	4.77	0.51
95	93.23	91.16	2.27	4.30	15.56	14.61	6.52	0.91
96	88.07	89.20	1.26	1.27	14.96	14.28	4.80	0.47
97	87.80	87.22	0.67	0.34	14.86	13.98	6.32	0.78
98	85.08	85.44	0.42	0.13	14.53	13.68	6.24	0.73
99	82.21	83.33	1.34	1.25	14.41	13.37	7.80	1.09
100	80.30	81.24	1.15	0.88	13.86	13.05	6.23	0.66
101	78.79	79.36	0.71	0.32	13.31	12.74	4.47	0.32
102	77.64	77.66	0.03	0.00	13.12	12.40	5.84	0.52
103	75.37	75.78	0.54	0.17	13.02	12.02	8.30	1.00
104	73.99	74.05	0.08	0.00	12.71	11.71	8.54	1.00

105	72.73	72.45	0.39	0.08	12.46	11.44	8.92	1.04
106	72.09	70.78	1.85	1.72	12.17	11.10	9.67	1.15
107	69.96	69.11	1.22	0.72	11.93	10.87	9.76	1.13
108	69.10	67.70	2.07	1.97	11.85	10.67	11.06	1.39
109	67.66	66.36	1.97	1.70	11.80	10.28	14.81	2.32
110	66.52	65.06	2.24	2.12	11.65	10.03	16.20	2.64
111	64.45	63.87	0.91	0.34	11.76	9.96	18.15	3.26
112	61.94	62.67	1.16	0.53	11.28	9.90	13.99	1.92
113	60.87	61.49	1.02	0.39	11.12	9.82	13.25	1.69
114	59.84	60.32	0.80	0.23	10.71	9.70	10.49	1.03
115	59.14	59.19	0.09	0.00	10.53	9.59	9.88	0.90
116	57.62	57.99	0.63	0.14	10.52	9.42	11.61	1.20
117	56.96	56.89	0.12	0.00	10.49	9.35	12.21	1.30
118	56.38	55.74	1.14	0.40	10.45	9.21	13.53	1.55
119	54.79	54.64	0.27	0.02	9.87	9.09	8.63	0.62
120	53.23	53.45	0.42	0.05	9.81	9.00	9.03	0.66
121	51.63	52.43	1.52	0.64	9.92	8.91	11.28	1.01
122	51.80	51.37	0.84	0.19	9.67	8.80	9.95	0.77
123	49.37	50.37	1.98	0.99	9.46	8.72	8.57	0.56
124	48.87	49.39	1.05	0.27	9.32	8.63	7.90	0.47
125	48.08	48.41	0.67	0.11	9.31	8.55	8.81	0.57
126	45.56	47.38	3.84	3.31	8.93	8.48	5.33	0.20
127	44.02	46.34	5.00	5.36	8.87	8.39	5.70	0.23
128	43.69	45.37	3.71	2.83	8.73	8.37	4.40	0.14
129	43.60	44.41	1.83	0.66	8.73	8.35	4.63	0.15
130	43.11	43.44	0.76	0.11	8.59	8.33	3.15	0.07
131	43.44	42.59	2.00	0.72	8.48	8.29	2.18	0.03
132	42.63	41.68	2.27	0.90	8.42	8.31	1.36	0.01
133	40.69	40.81	0.31	0.02	8.31	8.21	1.27	0.01
134	40.20	39.96	0.61	0.06	8.13	8.17	0.47	0.00
135	40.14	39.09	2.70	1.11	8.08	8.10	0.26	0.00
136	38.52	38.22	0.78	0.09	8.10	8.07	0.37	0.00
137	36.77	37.37	1.61	0.36	7.94	7.96	0.17	0.00
138	36.40	36.63	0.62	0.05	7.58	7.87	3.69	0.08
139	35.56	35.88	0.90	0.10	7.47	7.84	4.73	0.14
140	34.89	34.95	0.16	0.00	7.25	7.94	8.71	0.48
141	34.42	34.17	0.72	0.06	7.27	7.61	4.55	0.12
142	34.58	33.48	3.29	1.21	7.30	7.25	0.72	0.00
143	34.30	32.71	4.86	2.52	7.08	7.08	0.07	0.00
144	34.67	31.95	8.53	7.42	6.96	6.91	0.66	0.00
145	33.67	31.58	6.60	4.35	6.92	6.75	2.45	0.03
146	32.37	31.29	3.44	1.16	6.60	6.61	0.23	0.00
147	32.95	30.95	6.48	4.02	6.44	6.48	0.63	0.00
148	30.56	30.68	0.41	0.02	6.38	6.34	0.61	0.00
149	30.72	30.32	1.32	0.16	6.28	6.18	1.64	0.01
150	30.72	29.91	2.71	0.66	5.98	6.03	0.85	0.00
151	30.43	29.70	2.44	0.53	5.92	5.89	0.56	0.00
152	30.62	29.24	4.72	1.90	5.85	5.74	1.90	0.01
153	30.62	28.88	6.02	3.03	5.85	5.61	4.18	0.06
154	29.61	28.51	3.86	1.21	5.85	5.46	7.20	0.15
155	29.53	28.13	4.99	1.97	5.27	5.32	1.00	0.00
156	29.59	27.79	6.47	3.24	5.25	5.19	1.21	0.00
157	29.53	27.39	7.83	4.59	4.96	5.05	1.67	0.01
158	29.40	27.12	8.42	5.22	4.90	4.95	1.09	0.00
159	29.40	26.87	9.43	6.42	4.88	4.86	0.36	0.00

160	28.65	26.59	7.74	4.23	4.69	4.78	1.88	0.01
161	28.65	26.35	8.72	5.28	4.64	4.72	1.70	0.01
162	27.59	26.19	5.35	1.96	4.64	4.65	0.20	0.00
163	27.59	25.96	6.28	2.66	4.57	4.61	0.80	0.00
164	26.57	25.76	3.13	0.65	4.33	4.55	4.89	0.05
165	26.56	25.61	3.72	0.91	4.29	4.47	4.10	0.03
166	26.01	25.58	1.67	0.18	4.29	4.42	2.93	0.02
167	25.98	25.44	2.12	0.29	4.18	4.36	4.11	0.03
168	25.98	25.36	2.44	0.38	4.18	4.32	3.06	0.02
169	25.98	25.21	3.05	0.59	4.20	4.28	1.91	0.01
170	25.55	25.10	1.79	0.20	4.21	4.19	0.34	0.00
171	25.05	24.84	0.83	0.04	4.07	4.15	2.04	0.01
172	24.74	24.64	0.40	0.01	3.96	4.10	3.37	0.02
173	24.69	24.42	1.09	0.07	3.96	4.03	1.80	0.01
174	24.44	24.11	1.39	0.11	3.92	3.98	1.61	0.00
175	24.66	23.75	3.81	0.82	3.87	3.93	1.53	0.00
176	24.48	23.61	3.67	0.75	3.75	3.89	3.45	0.02
177	24.17	23.56	2.59	0.37	3.67	3.83	4.15	0.03
178	23.92	23.03	3.85	0.79	3.51	3.80	7.47	0.08
179	23.52	22.94	2.51	0.33	3.58	3.78	5.20	0.04
180	23.39	22.45	4.21	0.89	3.58	3.68	2.70	0.01
Avg.			15.25	10.08			12.20	2.65

Table A. 5. Tabular comparison for Behaviour C and Behaviour D vertical deflection (Figure 33)

Time (min)	Behaviour A				Behaviour B			
	Predicted (mm)	Actual (mm)	MAPE (%)	RMSE (mm)	Predicted (mm)	Actual (mm)	MAPE (%)	RMSE (mm)
0	-0.32	0.00	-	0.10	-0.52	0.00	-	0.27
1	0.69	1.30	46.91	0.37	2.51	3.30	23.87	0.62
2	2.44	2.88	15.44	0.20	5.44	6.62	17.78	1.39
3	4.09	4.51	9.40	0.18	8.18	9.26	11.71	1.18
4	5.92	6.33	6.45	0.17	10.95	12.01	8.82	1.12
5	7.88	8.30	5.04	0.17	13.47	14.97	10.01	2.25
6	9.89	10.35	4.41	0.21	16.08	17.83	9.81	3.06
7	12.10	12.51	3.28	0.17	18.86	20.61	8.48	3.05
8	14.01	14.60	4.04	0.35	20.96	23.04	9.03	4.33
9	15.82	16.59	4.65	0.60	23.24	25.37	8.38	4.52
10	17.67	18.74	5.70	1.14	25.10	27.06	7.24	3.84
11	19.83	20.72	4.31	0.80	26.75	29.05	7.92	5.30
12	21.89	22.55	2.94	0.44	28.21	30.66	8.01	6.03
13	23.80	24.55	3.05	0.56	29.80	32.10	7.16	5.29
14	26.36	26.77	1.53	0.17	30.90	33.16	6.81	5.09
15	28.42	29.04	2.14	0.39	32.42	34.60	6.30	4.74
16	30.71	31.41	2.22	0.48	33.69	35.93	6.24	5.03
17	33.56	33.76	0.60	0.04	34.99	37.18	5.89	4.79
18	36.40	36.17	0.63	0.05	36.19	38.47	5.93	5.20
19	38.84	38.72	0.31	0.01	37.99	39.34	3.43	1.82
20	42.16	41.37	1.90	0.62	39.67	40.30	1.57	0.40
21	44.39	44.04	0.78	0.12	41.14	41.35	0.51	0.04
22	47.29	46.69	1.27	0.35	42.34	42.56	0.53	0.05
23	50.32	49.38	1.90	0.88	43.60	43.79	0.43	0.04
24	52.49	52.05	0.85	0.19	45.01	44.97	0.10	0.00
25	54.97	54.63	0.62	0.12	46.30	46.31	0.03	0.00
26	57.50	57.14	0.64	0.13	47.98	47.80	0.37	0.03
27	59.38	59.62	0.40	0.06	49.52	49.36	0.32	0.02
28	61.46	62.00	0.87	0.29	51.38	51.04	0.67	0.12
29	64.15	64.40	0.39	0.06	53.16	52.80	0.67	0.13
30	66.24	66.71	0.71	0.22	55.23	54.60	1.16	0.40
31	68.25	68.96	1.03	0.51	57.34	56.32	1.80	1.03
32	70.45	71.11	0.93	0.43	58.96	58.04	1.58	0.84
33	72.82	73.16	0.47	0.12	60.66	59.75	1.52	0.83
34	74.64	75.08	0.58	0.19	63.38	61.53	3.01	3.44
35	76.36	76.97	0.79	0.37	64.40	63.36	1.64	1.09
36	78.31	78.83	0.66	0.27	66.60	65.20	2.14	1.95
37	80.44	80.66	0.27	0.05	68.47	67.10	2.04	1.87
38	82.20	82.47	0.33	0.07	71.14	68.99	3.12	4.62
39	84.24	84.19	0.06	0.00	73.24	70.89	3.32	5.54
40	86.23	85.87	0.42	0.13	75.20	72.79	3.31	5.80
41	86.77	87.51	0.84	0.54	77.04	74.67	3.18	5.63
42	89.52	89.12	0.45	0.16	79.44	76.59	3.72	8.12
43	90.56	90.70	0.16	0.02	80.72	78.50	2.83	4.92
44	92.54	92.24	0.33	0.09	82.62	80.41	2.75	4.87
45	94.02	93.80	0.23	0.05	84.38	82.29	2.54	4.37
46	95.27	95.32	0.05	0.00	86.42	84.24	2.59	4.77
47	96.82	96.76	0.06	0.00	88.40	86.18	2.58	4.93
48	97.99	98.18	0.19	0.03	90.46	88.07	2.71	5.70
49	99.88	99.57	0.31	0.09	92.62	89.89	3.04	7.46

50	101.11	100.94	0.17	0.03	94.09	91.69	2.61	5.74
51	102.98	102.29	0.67	0.47	95.95	93.44	2.69	6.32
52	104.20	103.57	0.61	0.40	97.31	95.14	2.29	4.73
53	105.54	104.87	0.64	0.45	99.41	96.84	2.65	6.59
54	106.47	106.13	0.32	0.12	101.23	98.44	2.84	7.79
55	107.94	107.34	0.56	0.37	103.30	100.07	3.23	10.45
56	109.14	108.58	0.52	0.32	105.45	101.68	3.70	14.19
57	110.29	109.89	0.37	0.16	106.62	103.28	3.23	11.16
58	112.35	111.18	1.05	1.37	108.80	104.89	3.73	15.29
59	113.77	112.45	1.18	1.75	110.51	106.51	3.76	16.00
60	115.84	113.67	1.91	4.73	112.63	108.12	4.17	20.36
61	118.07	114.84	2.82	10.46	114.83	109.80	4.58	25.30
62	119.15	115.95	2.76	10.23	116.49	111.44	4.53	25.53
63	120.64	117.09	3.03	12.62	118.82	113.04	5.12	33.44
64	122.10	118.22	3.28	15.04	120.90	114.63	5.47	39.38
65	124.38	119.39	4.18	24.95	122.48	116.19	5.42	39.62
66	126.15	120.54	4.66	31.52	124.37	117.79	5.59	43.34
67	127.17	121.67	4.52	30.21	125.98	119.34	5.57	44.13
68	127.58	122.82	3.88	22.66	127.57	120.85	5.56	45.17
69	127.86	123.94	3.16	15.39	128.60	122.36	5.10	38.90
70	129.11	125.05	3.24	16.45	130.70	123.87	5.52	46.70
71	130.04	126.13	3.10	15.31	131.56	125.38	4.93	38.22
72	131.18	127.23	3.10	15.61	134.44	126.85	5.98	57.58
73	132.67	128.33	3.38	18.87	135.29	128.31	5.44	48.67
74	133.38	129.44	3.04	15.49	136.95	129.81	5.50	51.05
75	134.25	130.52	2.86	13.93	138.14	131.30	5.21	46.76
76	135.26	131.55	2.82	13.77	139.61	132.81	5.12	46.30
77	136.47	132.52	2.98	15.64	141.37	134.27	5.29	50.39
78	137.93	133.48	3.33	19.81	142.92	135.75	5.28	51.40
79	138.23	134.44	2.82	14.35	143.88	137.20	4.87	44.61
80	139.57	135.40	3.08	17.41	145.39	138.64	4.87	45.60
81	140.71	136.36	3.19	18.94	146.49	140.07	4.58	41.16
82	141.78	137.33	3.24	19.83	147.71	141.48	4.41	38.84
83	141.99	138.32	2.65	13.49	149.27	142.87	4.48	41.00
84	143.24	139.29	2.83	15.57	150.71	144.24	4.49	41.91
85	144.72	140.25	3.18	19.95	151.72	145.55	4.24	38.10
86	145.90	141.19	3.33	22.14	153.28	146.81	4.41	41.87
87	146.56	142.14	3.11	19.55	155.03	148.05	4.71	48.70
88	147.73	143.08	3.25	21.66	156.39	149.27	4.77	50.62
89	149.19	143.97	3.62	27.23	157.66	150.48	4.77	51.59
90	150.18	144.89	3.65	27.98	158.76	151.67	4.68	50.29
91	151.58	145.79	3.97	33.52	159.86	152.85	4.58	49.09
92	152.71	146.65	4.13	36.73	161.56	154.02	4.89	56.78
93	153.64	147.50	4.16	37.70	162.76	155.18	4.88	57.41
94	152.32	148.37	2.66	15.59	164.17	156.39	4.98	60.58
95	153.38	149.23	2.78	17.25	165.31	157.59	4.90	59.67
96	154.46	150.06	2.94	19.40	166.22	158.76	4.70	55.59
97	155.21	150.86	2.88	18.91	166.34	159.95	3.99	40.80
98	155.41	151.63	2.49	14.28	167.23	161.11	3.80	37.41
99	155.36	152.35	1.98	9.07	168.98	162.28	4.13	44.90
100	155.41	153.06	1.53	5.50	170.62	163.43	4.40	51.67
101	156.00	153.74	1.47	5.10	171.20	164.58	4.02	43.79
102	156.64	154.30	1.52	5.48	172.35	165.73	3.99	43.83
103	157.48	154.65	1.83	8.01	174.25	166.91	4.40	53.88
104	157.73	154.80	1.89	8.56	175.67	168.14	4.48	56.70

105	155.78	154.81	0.63	0.94	177.07	169.39	4.54	59.02
106	156.10	154.78	0.85	1.74	177.77	170.66	4.17	50.57
107	156.45	154.65	1.17	3.26	179.12	171.90	4.20	52.07
108	156.88	154.51	1.54	5.63	179.54	173.10	3.72	41.49
109	157.15	154.25	1.88	8.41	180.91	174.27	3.81	44.05
110	157.33	153.95	2.20	11.44	182.02	175.46	3.74	42.98
111	157.51	153.58	2.56	15.44	182.72	176.66	3.43	36.78
112	157.67	153.22	2.90	19.79	183.75	177.86	3.31	34.68
113	157.23	152.82	2.89	19.48	185.38	179.06	3.53	40.00
114	157.23	152.28	3.25	24.55	186.13	180.25	3.26	34.59
115	157.87	151.63	4.12	38.96	187.18	181.40	3.19	33.43
116	157.36	150.79	4.36	43.16	188.95	182.56	3.50	40.81
117	156.49	149.90	4.39	43.38	189.89	183.71	3.37	38.25
118	155.79	149.09	4.49	44.91	191.57	184.89	3.61	44.64
119	154.40	148.22	4.17	38.24	192.86	186.11	3.63	45.52
120	153.50	147.37	4.16	37.63	193.10	187.27	3.11	33.96
121	152.63	146.59	4.12	36.52	193.64	188.46	2.75	26.85
122	152.28	145.79	4.45	42.06	192.36	189.63	1.44	7.43
123	151.92	145.05	4.73	47.16	193.63	190.82	1.47	7.90
124	151.55	144.41	4.94	50.91	194.49	191.99	1.30	6.27
125	149.40	143.89	3.83	30.33	195.40	193.18	1.15	4.93
126	149.52	143.45	4.23	36.86	196.18	194.33	0.95	3.42
127	149.13	142.94	4.33	38.28	196.13	195.48	0.33	0.42
128	148.39	142.12	4.41	39.36	196.61	196.63	0.01	0.00
129	148.49	141.01	5.30	55.93	197.53	197.74	0.10	0.04
130	148.38	139.64	6.26	76.45	198.05	198.87	0.41	0.67
131	147.73	138.19	6.91	91.07	198.65	199.99	0.67	1.80
132	147.77	136.81	8.01	120.16	199.24	201.12	0.94	3.55
133	146.67	135.42	8.31	126.61	200.60	202.26	0.82	2.74
134	145.64	134.02	8.67	135.05	202.77	203.42	0.32	0.42
135	143.94	132.68	8.48	126.70	203.24	204.59	0.66	1.83
136	143.16	131.36	8.99	139.35	203.68	205.76	1.01	4.33
137	142.12	130.05	9.28	145.70	204.42	206.97	1.23	6.53
138	141.38	128.74	9.81	159.66	205.36	208.18	1.36	7.97
139	140.66	127.45	10.37	174.52	204.58	209.35	2.28	22.73
140	139.71	126.23	10.68	181.80	207.04	210.47	1.63	11.75
141	140.28	125.07	12.16	231.22	207.76	211.56	1.80	14.46
142	139.74	123.87	12.81	251.76	209.71	212.61	1.36	8.40
143	137.28	122.70	11.88	212.49	211.73	213.68	0.91	3.80
144	136.02	121.48	11.97	211.32	212.87	214.72	0.86	3.42
145	134.79	120.28	12.06	210.44	216.07	215.75	0.15	0.10
146	134.46	118.99	13.00	239.41	216.73	216.77	0.02	0.00
147	134.31	117.74	14.08	274.64	217.72	217.81	0.04	0.01
148	132.53	116.56	13.70	255.14	218.42	218.82	0.18	0.16
149	130.60	115.31	13.26	233.81	220.82	219.83	0.45	0.97
150	128.29	114.04	12.50	203.15	221.57	220.85	0.32	0.51
151	130.74	112.90	15.80	318.19	222.31	221.82	0.22	0.24
152	129.43	111.74	15.83	313.00	223.69	222.85	0.38	0.70
153	128.73	110.51	16.48	331.80	224.52	223.84	0.31	0.47
154	126.64	109.28	15.89	301.45	225.62	224.84	0.35	0.61
155	128.47	108.05	18.90	416.89	226.48	225.79	0.31	0.48
156	127.57	106.78	19.47	432.08	228.24	226.76	0.65	2.18
157	125.54	105.54	18.95	400.19	231.41	227.68	1.64	13.94
158	123.74	104.29	18.65	378.47	231.85	228.57	1.44	10.78
159	122.17	103.05	18.55	365.40	232.54	229.49	1.33	9.33

160	122.31	101.81	20.14	420.34	232.87	230.39	1.07	6.13
161	121.63	100.40	21.14	450.62	233.32	231.31	0.87	4.04
162	120.43	99.08	21.55	455.81	234.30	232.22	0.90	4.32
163	119.93	97.75	22.69	491.79	234.96	233.11	0.79	3.42
164	116.09	96.55	20.23	381.63	235.48	234.05	0.61	2.05
165	115.05	95.71	20.21	373.99	236.50	234.93	0.67	2.45
166	114.60	95.15	20.44	378.43	236.58	235.80	0.33	0.62
167	113.49	94.73	19.81	352.08	237.39	236.71	0.29	0.46
168	112.54	94.45	19.16	327.32	238.33	237.60	0.31	0.53
169	110.39	94.12	17.28	264.59	239.16	238.52	0.27	0.41
170	109.14	93.80	16.35	235.27	239.83	239.45	0.16	0.14
171	107.33	93.41	14.90	193.69	241.07	240.39	0.28	0.47
172	106.92	92.94	15.04	195.44	241.56	241.30	0.11	0.07
173	105.20	92.49	13.74	161.61	241.90	242.21	0.13	0.10
174	104.65	92.01	13.74	159.71	242.78	243.13	0.14	0.12
175	104.66	91.58	14.29	171.16	243.41	244.05	0.26	0.41
176	104.03	91.16	14.12	165.62	244.00	244.95	0.39	0.91
177	104.06	90.81	14.60	175.66	245.03	245.78	0.31	0.56
178	103.60	90.46	14.53	172.73	245.18	246.63	0.59	2.12
179	102.86	90.02	14.27	164.98	246.00	247.54	0.62	2.37
180	102.60	89.64	14.46	168.00	246.87	248.45	0.63	2.49
Avg.			6.19	8.94			3.21	4.19

Table A. 6. Tabular comparison for Behaviour C and Behaviour D horizontal deflection (Figure 36)

Time (min)	Behaviour A				Behaviour B			
	Predicted (mm)	Actual (mm)	MAPE (%)	RMSE (mm)	Predicted (mm)	Actual (mm)	MAPE (%)	RMSE (mm)
0	0.26	0.00	-	0.07	-0.07	0.00	-	0.00
1	1.18	1.03	14.48	0.02	0.74	0.89	16.75	0.02
2	2.34	2.26	3.33	0.01	1.86	2.02	7.87	0.03
3	3.24	3.24	0.04	0.00	2.72	2.86	4.83	0.02
4	4.26	4.31	1.12	0.00	3.54	3.70	4.30	0.03
5	5.48	5.48	0.07	0.00	4.34	4.54	4.37	0.04
6	6.62	6.68	0.94	0.00	5.21	5.38	3.13	0.03
7	7.78	7.89	1.43	0.01	6.09	6.20	1.85	0.01
8	8.93	9.11	1.97	0.03	6.84	6.99	2.18	0.02
9	9.95	10.30	3.36	0.12	7.61	7.66	0.66	0.00
10	10.99	11.34	3.05	0.12	8.31	8.33	0.23	0.00
11	12.11	12.43	2.56	0.10	8.88	8.95	0.82	0.01
12	13.22	13.55	2.42	0.11	9.39	9.53	1.46	0.02
13	14.18	14.64	3.12	0.21	10.01	10.10	0.87	0.01
14	15.09	15.55	2.93	0.21	10.56	10.69	1.22	0.02
15	16.12	16.53	2.46	0.16	11.14	11.22	0.75	0.01
16	17.12	17.56	2.52	0.20	11.63	11.73	0.85	0.01
17	18.15	18.63	2.56	0.23	12.26	12.22	0.33	0.00
18	19.31	19.73	2.11	0.17	12.73	12.73	0.00	0.00
19	20.27	20.73	2.24	0.21	13.27	13.25	0.12	0.00
20	21.47	21.71	1.11	0.06	13.73	13.77	0.27	0.00
21	22.40	22.72	1.42	0.10	14.34	14.27	0.52	0.01
22	23.42	23.75	1.39	0.11	14.74	14.77	0.23	0.00
23	24.38	24.79	1.66	0.17	15.27	15.29	0.13	0.00
24	25.35	25.82	1.84	0.23	15.82	15.84	0.10	0.00
25	26.41	26.84	1.59	0.18	16.36	16.39	0.19	0.00
26	27.49	27.87	1.35	0.14	16.89	16.94	0.32	0.00
27	28.47	28.92	1.55	0.20	17.36	17.48	0.67	0.01
28	29.54	29.92	1.27	0.14	17.99	18.02	0.17	0.00
29	30.54	30.92	1.23	0.14	18.72	18.57	0.81	0.02
30	31.50	31.90	1.27	0.16	19.21	19.11	0.52	0.01
31	32.49	32.88	1.20	0.16	19.76	19.65	0.57	0.01
32	33.44	33.85	1.21	0.17	20.33	20.19	0.69	0.02
33	34.29	34.81	1.49	0.27	20.88	20.72	0.79	0.03
34	35.14	35.76	1.74	0.39	21.35	21.24	0.53	0.01
35	36.17	36.69	1.41	0.27	21.93	21.76	0.76	0.03
36	37.02	37.60	1.54	0.34	22.40	22.28	0.55	0.02
37	37.93	38.51	1.52	0.34	22.86	22.79	0.29	0.00
38	38.80	39.40	1.52	0.36	23.40	23.30	0.43	0.01
39	39.67	40.28	1.52	0.38	23.94	23.79	0.62	0.02
40	40.50	41.13	1.52	0.39	24.38	24.27	0.43	0.01
41	41.27	41.96	1.65	0.48	24.85	24.75	0.39	0.01
42	42.21	42.79	1.35	0.33	25.28	25.23	0.20	0.00
43	43.02	43.60	1.33	0.34	25.78	25.70	0.32	0.01
44	43.80	44.42	1.41	0.39	26.25	26.17	0.29	0.01
45	44.60	45.22	1.37	0.38	26.68	26.64	0.14	0.00
46	45.30	46.01	1.55	0.51	27.12	27.10	0.08	0.00
47	46.09	46.80	1.51	0.50	27.51	27.55	0.16	0.00
48	46.96	47.58	1.30	0.38	28.00	28.01	0.05	0.00
49	47.68	48.35	1.39	0.45	28.39	28.47	0.30	0.01

50	48.36	49.11	1.53	0.57	28.92	28.93	0.03	0.00
51	49.17	49.85	1.37	0.47	29.41	29.39	0.06	0.00
52	49.84	50.58	1.47	0.55	29.97	29.84	0.42	0.02
53	50.66	51.31	1.26	0.42	30.40	30.30	0.32	0.01
54	51.48	52.03	1.06	0.30	30.68	30.76	0.24	0.01
55	52.18	52.74	1.06	0.31	31.18	31.21	0.11	0.00
56	52.79	53.45	1.23	0.43	31.65	31.66	0.02	0.00
57	53.49	54.15	1.22	0.44	32.03	32.11	0.25	0.01
58	54.21	54.86	1.18	0.42	32.50	32.55	0.14	0.00
59	54.81	55.55	1.33	0.55	32.83	32.99	0.49	0.03
60	55.37	56.24	1.55	0.76	33.32	33.42	0.30	0.01
61	56.07	56.92	1.49	0.72	33.60	33.86	0.77	0.07
62	56.84	57.58	1.29	0.55	33.99	34.28	0.85	0.09
63	57.48	58.22	1.26	0.54	34.56	34.71	0.43	0.02
64	58.10	58.86	1.28	0.57	35.03	35.14	0.32	0.01
65	58.80	59.48	1.14	0.46	35.39	35.56	0.47	0.03
66	59.38	60.10	1.19	0.51	35.97	35.97	0.01	0.00
67	59.96	60.72	1.25	0.57	36.11	36.39	0.78	0.08
68	60.74	61.34	0.98	0.36	36.35	36.80	1.23	0.21
69	61.27	61.96	1.11	0.48	36.70	37.19	1.33	0.24
70	61.95	62.57	0.98	0.38	37.15	37.59	1.17	0.19
71	62.55	63.18	0.99	0.39	37.59	37.98	1.02	0.15
72	63.13	63.78	1.01	0.42	37.89	38.37	1.26	0.23
73	63.64	64.38	1.15	0.55	38.32	38.75	1.11	0.19
74	64.21	64.98	1.18	0.59	38.71	39.13	1.06	0.17
75	64.73	65.58	1.29	0.72	39.14	39.50	0.90	0.13
76	65.28	66.18	1.36	0.80	39.45	39.87	1.06	0.18
77	65.90	66.77	1.30	0.76	39.92	40.24	0.80	0.10
78	66.41	67.36	1.42	0.91	40.33	40.60	0.66	0.07
79	67.10	67.95	1.26	0.73	40.97	40.96	0.02	0.00
80	67.56	68.53	1.42	0.95	41.20	41.33	0.31	0.02
81	68.14	69.12	1.41	0.95	41.78	41.69	0.21	0.01
82	68.66	69.70	1.50	1.09	42.13	42.05	0.20	0.01
83	69.36	70.28	1.30	0.84	42.43	42.40	0.08	0.00
84	69.76	70.86	1.56	1.22	42.91	42.75	0.38	0.03
85	70.58	71.44	1.20	0.74	43.19	43.11	0.19	0.01
86	71.10	72.02	1.28	0.85	43.54	43.46	0.19	0.01
87	71.67	72.59	1.26	0.84	43.77	43.81	0.10	0.00
88	72.19	73.16	1.33	0.94	44.28	44.15	0.30	0.02
89	72.81	73.73	1.24	0.84	44.54	44.50	0.09	0.00
90	73.25	74.30	1.41	1.11	44.86	44.84	0.05	0.00
91	73.72	74.87	1.54	1.33	45.17	45.18	0.02	0.00
92	74.27	75.43	1.54	1.35	45.43	45.51	0.17	0.01
93	74.66	76.00	1.77	1.80	45.50	45.84	0.75	0.12
94	75.07	76.57	1.96	2.26	46.02	46.17	0.33	0.02
95	75.77	77.13	1.76	1.85	46.38	46.50	0.27	0.02
96	76.23	77.69	1.87	2.12	46.76	46.83	0.16	0.01
97	76.94	78.24	1.66	1.69	46.83	47.15	0.67	0.10
98	77.42	78.80	1.75	1.89	47.29	47.47	0.38	0.03
99	77.85	79.34	1.88	2.23	47.76	47.79	0.06	0.00
100	78.38	79.88	1.88	2.25	48.12	48.11	0.02	0.00
101	79.01	80.42	1.75	1.99	48.47	48.43	0.09	0.00
102	79.59	80.95	1.68	1.85	48.76	48.74	0.03	0.00
103	80.11	81.47	1.67	1.85	48.94	49.05	0.22	0.01
104	80.76	81.99	1.50	1.52	49.15	49.36	0.42	0.04

105	81.09	82.49	1.70	1.97	49.35	49.67	0.65	0.10
106	81.44	82.99	1.87	2.40	49.54	49.97	0.85	0.18
107	81.92	83.49	1.89	2.48	49.93	50.27	0.68	0.12
108	82.30	83.99	2.01	2.86	50.40	50.58	0.36	0.03
109	82.64	84.48	2.17	3.37	50.64	50.89	0.49	0.06
110	82.99	84.96	2.31	3.86	50.85	51.19	0.67	0.12
111	83.67	85.44	2.07	3.13	51.00	51.49	0.96	0.24
112	84.16	85.91	2.03	3.05	51.21	51.79	1.12	0.34
113	84.37	86.39	2.34	4.10	51.45	52.09	1.24	0.41
114	84.72	86.86	2.47	4.60	51.65	52.38	1.39	0.53
115	85.19	87.32	2.44	4.53	52.01	52.68	1.27	0.45
116	85.67	87.77	2.40	4.42	52.52	52.97	0.86	0.21
117	86.24	88.22	2.25	3.93	52.93	53.26	0.61	0.11
118	86.66	88.67	2.26	4.03	53.10	53.55	0.85	0.21
119	86.87	89.11	2.51	5.01	53.32	53.84	0.96	0.27
120	87.46	89.55	2.33	4.36	53.75	54.13	0.70	0.14
121	87.95	90.00	2.28	4.20	54.12	54.41	0.54	0.09
122	88.25	90.45	2.44	4.86	54.36	54.70	0.62	0.12
123	88.79	90.90	2.32	4.45	54.95	54.98	0.06	0.00
124	89.23	91.35	2.32	4.50	55.13	55.25	0.22	0.01
125	89.62	91.81	2.39	4.79	55.51	55.53	0.03	0.00
126	90.04	92.26	2.41	4.93	55.69	55.80	0.20	0.01
127	90.51	92.70	2.36	4.77	56.07	56.08	0.02	0.00
128	90.80	93.12	2.49	5.37	56.57	56.35	0.38	0.05
129	91.29	93.53	2.39	5.00	56.95	56.62	0.59	0.11
130	91.60	93.93	2.48	5.44	57.28	56.88	0.71	0.16
131	92.03	94.32	2.43	5.23	57.41	57.15	0.46	0.07
132	92.33	94.72	2.53	5.73	57.51	57.41	0.18	0.01
133	92.78	95.12	2.46	5.46	57.76	57.68	0.13	0.01
134	93.21	95.52	2.42	5.35	58.12	57.94	0.31	0.03
135	93.48	95.92	2.55	5.97	58.29	58.19	0.18	0.01
136	93.76	96.33	2.66	6.59	58.29	58.44	0.26	0.02
137	94.14	96.73	2.68	6.71	58.54	58.69	0.25	0.02
138	94.57	97.14	2.64	6.58	58.86	58.94	0.13	0.01
139	94.88	97.54	2.72	7.05	58.98	59.18	0.34	0.04
140	95.31	97.95	2.69	6.96	59.25	59.43	0.31	0.03
141	95.68	98.36	2.72	7.16	59.45	59.68	0.39	0.05
142	95.95	98.76	2.85	7.91	59.79	59.92	0.22	0.02
143	96.50	99.16	2.68	7.06	60.05	60.17	0.20	0.01
144	96.79	99.55	2.77	7.60	60.29	60.41	0.19	0.01
145	97.19	99.94	2.75	7.56	60.56	60.65	0.15	0.01
146	97.51	100.32	2.80	7.91	60.97	60.90	0.11	0.00
147	97.96	100.70	2.72	7.51	61.18	61.14	0.07	0.00
148	98.35	101.08	2.70	7.44	61.71	61.38	0.53	0.11
149	98.49	101.46	2.93	8.84	61.94	61.62	0.52	0.10
150	99.09	101.83	2.69	7.52	62.16	61.86	0.49	0.09
151	99.50	102.21	2.65	7.32	62.52	62.10	0.67	0.18
152	99.94	102.59	2.58	7.01	63.02	62.34	1.09	0.46
153	100.25	102.97	2.64	7.38	63.27	62.57	1.12	0.49
154	100.73	103.34	2.53	6.84	63.52	62.81	1.14	0.51
155	101.11	103.71	2.51	6.75	63.97	63.05	1.46	0.85
156	101.40	104.08	2.58	7.19	64.08	63.28	1.26	0.64
157	101.63	104.45	2.70	7.97	64.48	63.52	1.51	0.92
158	101.99	104.83	2.70	8.04	64.72	63.75	1.52	0.94
159	102.38	105.20	2.68	7.97	64.75	63.98	1.20	0.59

160	102.59	105.56	2.81	8.82	65.13	64.21	1.43	0.84
161	103.09	105.91	2.67	7.97	65.26	64.44	1.27	0.67
162	103.19	106.24	2.87	9.31	65.42	64.67	1.15	0.56
163	103.53	106.57	2.85	9.25	65.84	64.90	1.45	0.89
164	103.78	106.92	2.94	9.87	65.95	65.12	1.28	0.69
165	104.23	107.27	2.83	9.23	66.11	65.35	1.17	0.58
166	104.61	107.65	2.82	9.24	66.54	65.58	1.47	0.92
167	104.85	108.05	2.96	10.22	66.63	65.81	1.25	0.68
168	105.13	108.44	3.06	10.98	67.10	66.03	1.63	1.16
169	105.56	108.84	3.01	10.76	67.28	66.25	1.55	1.06
170	106.02	109.24	2.95	10.40	67.38	66.47	1.37	0.83
171	106.36	109.63	2.98	10.68	67.87	66.70	1.75	1.36
172	106.79	110.01	2.93	10.39	68.01	66.92	1.63	1.19
173	107.11	110.40	2.98	10.81	68.23	67.14	1.63	1.19
174	107.68	110.79	2.81	9.67	68.39	67.36	1.54	1.07
175	107.88	111.17	2.96	10.85	68.56	67.57	1.46	0.97
176	108.36	111.56	2.87	10.25	68.89	67.79	1.62	1.20
177	108.85	111.93	2.76	9.51	69.08	68.02	1.56	1.12
178	109.18	112.30	2.78	9.74	69.22	68.24	1.43	0.96
179	109.50	112.66	2.81	10.00	69.57	68.45	1.64	1.26
180	109.72	113.02	2.92	10.86	69.81	68.67	1.66	1.30
Avg.			2.05	1.79			0.84	0.43

Appendix B

Table B. 1. Moment Curvature for Beam A (Part 1)

Curvature (χ)	Timestep (minute)						
	0	15	30	45	60	75	90
-0.000050	-182.78	-303.51	-246.26	-208.50	-185.68	-166.52	-147.09
-0.000049	-182.73	-303.51	-245.87	-207.89	-184.89	-165.59	-146.02
-0.000048	-182.67	-303.50	-245.46	-207.27	-184.08	-164.62	-144.92
-0.000047	-182.61	-303.46	-245.03	-206.61	-183.24	-163.63	-143.81
-0.000046	-182.55	-303.41	-244.59	-205.94	-182.39	-162.62	-142.66
-0.000045	-182.48	-303.34	-244.13	-205.24	-181.51	-161.59	-141.49
-0.000044	-182.40	-303.26	-243.65	-204.53	-180.60	-160.53	-140.30
-0.000043	-182.33	-303.16	-243.16	-203.79	-179.67	-159.45	-139.08
-0.000042	-182.25	-303.04	-242.66	-203.04	-178.71	-158.34	-137.84
-0.000041	-182.15	-302.89	-242.13	-202.25	-177.72	-157.20	-136.57
-0.000040	-182.05	-302.70	-241.59	-201.44	-176.71	-156.03	-135.28
-0.000039	-181.95	-302.46	-241.02	-200.61	-175.66	-154.83	-133.95
-0.000038	-181.83	-302.17	-240.40	-199.74	-174.58	-153.60	-132.59
-0.000037	-181.72	-301.82	-239.77	-198.85	-173.46	-152.34	-131.19
-0.000036	-181.60	-301.44	-239.09	-197.91	-172.32	-151.04	-129.76
-0.000035	-181.47	-301.03	-238.40	-196.94	-171.13	-149.70	-128.28
-0.000034	-181.34	-300.59	-237.68	-195.93	-169.91	-148.32	-126.78
-0.000033	-181.18	-300.12	-236.93	-194.87	-168.64	-146.91	-125.25
-0.000032	-181.02	-299.61	-236.15	-193.76	-167.32	-145.45	-123.68
-0.000031	-180.84	-299.06	-235.31	-192.60	-165.94	-143.94	-122.07
-0.000030	-180.67	-298.46	-234.44	-191.39	-164.51	-142.38	-120.41
-0.000029	-180.48	-297.81	-233.50	-190.11	-163.01	-140.77	-118.71
-0.000028	-180.30	-297.12	-232.48	-188.76	-161.45	-139.09	-116.95
-0.000027	-180.10	-296.40	-231.39	-187.31	-159.81	-137.35	-115.15
-0.000026	-179.91	-295.61	-230.20	-185.75	-158.09	-135.54	-113.29
-0.000025	-179.71	-294.72	-228.86	-184.05	-156.25	-133.65	-111.36
-0.000024	-179.48	-293.49	-226.62	-182.15	-154.29	-131.67	-109.38
-0.000023	-179.21	-290.17	-222.60	-179.94	-152.18	-129.62	-107.32
-0.000022	-178.93	-285.49	-217.51	-176.91	-149.88	-127.45	-105.20
-0.000021	-178.64	-278.87	-211.28	-172.97	-147.33	-125.17	-103.00
-0.000020	-178.28	-270.69	-204.45	-168.46	-144.33	-122.74	-100.73
-0.000019	-177.91	-262.02	-197.62	-163.39	-140.89	-120.13	-98.36
-0.000018	-177.53	-253.03	-190.79	-158.02	-137.19	-117.33	-95.94
-0.000017	-177.14	-243.51	-183.93	-152.71	-133.29	-114.39	-93.43
-0.000016	-176.71	-233.43	-177.01	-147.44	-129.21	-111.35	-90.88
-0.000015	-174.54	-223.18	-170.14	-142.25	-125.11	-108.19	-88.32
-0.000014	-166.53	-212.84	-163.27	-137.15	-121.04	-104.96	-85.71
-0.000013	-154.83	-202.40	-156.50	-132.08	-116.97	-101.76	-83.07
-0.000012	-143.07	-191.86	-149.71	-126.99	-112.97	-98.61	-80.47
-0.000011	-131.27	-181.18	-142.86	-121.92	-108.99	-95.50	-77.91
-0.000010	-119.43	-170.39	-135.98	-116.92	-105.08	-92.44	-75.40
-0.000009	-107.55	-159.49	-128.90	-111.97	-101.21	-89.40	-72.91
-0.000008	-95.65	-148.46	-121.31	-107.04	-97.34	-86.39	-70.46
-0.000007	-83.73	-137.26	-113.16	-102.07	-93.45	-83.39	-68.00
-0.000006	-71.79	-125.87	-104.58	-97.00	-89.51	-80.38	-65.57
-0.000005	-59.84	-114.21	-95.91	-91.82	-85.53	-77.32	-63.12
-0.000004	-47.88	-102.26	-87.28	-86.49	-81.56	-74.24	-60.67
-0.000003	-35.91	-89.83	-78.69	-80.84	-77.48	-71.14	-58.21

-0.000002	-23.95	-76.62	-70.15	-74.67	-73.26	-67.97	-55.75
-0.000001	-11.98	-62.16	-61.57	-68.02	-68.88	-64.72	-53.24
0	0.00	-42.96	-52.95	-61.12	-64.23	-61.34	-50.67
0.000001	11.96	-20.81	-44.35	-54.19	-59.17	-57.75	-48.01
0.000002	23.92	-0.40	-35.78	-47.29	-53.55	-53.84	-45.27
0.000003	35.87	18.57	-27.23	-40.39	-47.58	-49.42	-42.36
0.000004	47.82	36.44	-18.63	-33.49	-41.57	-44.43	-39.21
0.000005	59.76	53.38	-9.95	-26.56	-35.57	-39.25	-35.65
0.000006	71.70	69.65	-1.11	-19.65	-29.60	-34.07	-31.69
0.000007	83.62	85.10	7.80	-12.76	-23.65	-28.89	-27.64
0.000008	95.53	99.81	16.79	-5.86	-17.68	-23.72	-23.58
0.000009	107.42	114.22	25.99	1.05	-11.71	-18.57	-19.53
0.000010	119.28	128.22	35.54	7.97	-5.74	-13.43	-15.49
0.000011	131.10	141.86	45.78	14.89	0.24	-8.30	-11.47
0.000012	142.89	155.16	56.41	21.80	6.20	-3.15	-7.45
0.000013	154.63	168.10	67.27	28.73	12.16	2.00	-3.45
0.000014	166.31	180.75	78.21	35.70	18.14	7.14	0.55
0.000015	174.40	193.04	89.20	42.70	24.13	12.28	4.55
0.000016	176.69	205.09	100.09	49.78	30.14	17.42	8.53
0.000017	177.13	216.81	110.98	56.91	36.15	22.57	12.51
0.000018	177.51	228.22	121.85	64.13	42.16	27.73	16.48
0.000019	177.89	239.38	132.63	71.45	48.20	32.90	20.46
0.000020	178.26	250.28	143.29	78.88	54.27	38.07	24.44
0.000021	178.63	260.91	153.87	86.54	60.36	43.24	28.42
0.000022	178.93	271.24	164.39	94.61	66.48	48.42	32.40
0.000023	179.20	281.31	174.82	102.87	72.63	53.61	36.38
0.000024	179.48	289.51	185.14	111.34	78.81	58.82	40.36
0.000025	179.71	295.10	194.81	119.85	85.04	64.06	44.33
0.000026	179.91	298.45	202.61	127.72	91.07	69.27	48.19
0.000027	180.10	299.64	208.43	134.73	96.62	74.21	51.80
0.000028	180.29	300.72	212.23	140.68	101.63	78.69	55.05
0.000029	180.48	301.69	215.30	145.63	106.10	82.62	57.91
0.000030	180.66	302.52	218.02	149.98	110.08	86.00	60.45
0.000031	180.84	303.23	220.50	153.91	113.84	88.98	62.77
0.000032	181.01	303.83	222.79	157.53	117.36	91.69	64.92
0.000033	181.17	304.38	224.91	160.89	120.66	94.18	66.91
0.000034	181.33	304.83	226.86	164.06	123.79	96.51	68.79
0.000035	181.46	305.14	228.70	167.05	126.77	98.70	70.56
0.000036	181.59	305.36	230.45	169.86	129.63	100.78	72.24
0.000037	181.71	305.54	232.11	172.52	132.40	102.76	73.83
0.000038	181.83	305.69	233.66	175.05	135.05	104.67	75.35
0.000039	181.94	305.80	235.13	177.48	137.59	106.51	76.79
0.000040	182.04	305.89	236.50	179.81	140.03	108.30	78.18
0.000041	182.14	305.95	237.78	182.04	142.37	110.05	79.51
0.000042	182.24	305.99	238.99	184.19	144.64	111.77	80.79
0.000043	182.32	306.01	240.15	186.25	146.82	113.48	82.00
0.000044	182.39	306.02	241.26	188.22	148.92	115.16	83.12
0.000045	182.47	306.01	242.32	190.13	150.96	116.80	84.19
0.000046	182.53	305.97	243.34	191.97	152.93	118.40	85.21
0.000047	182.59	305.93	244.31	193.75	154.84	119.95	86.21
0.000048	182.65	305.87	245.23	195.47	156.68	121.41	87.18
0.000049	182.71	305.79	246.09	197.13	158.48	122.79	88.11
0.000050	182.76	305.70	246.92	198.72	160.21	124.11	89.02

Table B. 1. Moment Curvature for Beam A (Part 2)

Curvature (χ)	Timestep (minute)					
	105	120	135	150	165	180
-0.000050	-129.68	-113.37	-100.09	-90.39	-79.48	-68.15
-0.000049	-128.58	-112.36	-99.15	-89.53	-78.71	-67.46
-0.000048	-127.47	-111.33	-98.19	-88.65	-77.92	-66.76
-0.000047	-126.33	-110.27	-97.20	-87.76	-77.12	-66.03
-0.000046	-125.17	-109.19	-96.21	-86.85	-76.30	-65.30
-0.000045	-123.99	-108.09	-95.19	-85.92	-75.47	-64.56
-0.000044	-122.78	-106.97	-94.16	-84.97	-74.62	-63.79
-0.000043	-121.54	-105.83	-93.10	-84.00	-73.76	-63.02
-0.000042	-120.27	-104.66	-92.02	-83.01	-72.88	-62.23
-0.000041	-118.98	-103.47	-90.92	-82.01	-71.99	-61.44
-0.000040	-117.65	-102.24	-89.79	-80.98	-71.08	-60.63
-0.000039	-116.29	-100.99	-88.63	-79.93	-70.15	-59.80
-0.000038	-114.91	-99.72	-87.45	-78.86	-69.20	-58.96
-0.000037	-113.50	-98.42	-86.23	-77.76	-68.23	-58.11
-0.000036	-112.06	-97.09	-84.99	-76.63	-67.23	-57.23
-0.000035	-110.59	-95.72	-83.72	-75.47	-66.21	-56.33
-0.000034	-109.09	-94.32	-82.41	-74.29	-65.17	-55.42
-0.000033	-107.56	-92.89	-81.06	-73.07	-64.11	-54.48
-0.000032	-105.99	-91.43	-79.68	-71.81	-63.01	-53.53
-0.000031	-104.39	-89.94	-78.28	-70.51	-61.89	-52.56
-0.000030	-102.76	-88.39	-76.84	-69.19	-60.75	-51.56
-0.000029	-101.09	-86.81	-75.36	-67.84	-59.59	-50.55
-0.000028	-99.39	-85.20	-73.83	-66.44	-58.40	-49.53
-0.000027	-97.65	-83.57	-72.25	-65.01	-57.19	-48.48
-0.000026	-95.86	-81.90	-70.63	-63.52	-55.93	-47.42
-0.000025	-94.01	-80.18	-68.96	-62.00	-54.65	-46.33
-0.000024	-92.12	-78.42	-67.25	-60.46	-53.35	-45.22
-0.000023	-90.18	-76.61	-65.51	-58.90	-52.03	-44.11
-0.000022	-88.19	-74.72	-63.78	-57.33	-50.70	-42.98
-0.000021	-86.14	-72.77	-62.01	-55.75	-49.36	-41.86
-0.000020	-84.05	-70.80	-60.24	-54.17	-48.02	-40.72
-0.000019	-81.90	-68.81	-58.45	-52.61	-46.67	-39.59
-0.000018	-79.72	-66.84	-56.66	-51.04	-45.32	-38.46
-0.000017	-77.52	-64.88	-54.89	-49.49	-44.00	-37.33
-0.000016	-75.34	-62.91	-53.17	-47.95	-42.69	-36.20
-0.000015	-73.15	-60.98	-51.49	-46.47	-41.38	-35.10
-0.000014	-70.95	-59.08	-49.84	-45.02	-40.12	-34.02
-0.000013	-68.78	-57.22	-48.22	-43.60	-38.88	-32.96
-0.000012	-66.61	-55.40	-46.62	-42.21	-37.68	-31.93
-0.000011	-64.45	-53.60	-45.08	-40.81	-36.49	-30.92
-0.000010	-62.32	-51.81	-43.56	-39.45	-35.29	-29.94
-0.000009	-60.25	-50.04	-42.07	-38.14	-34.10	-28.95
-0.000008	-58.19	-48.31	-40.58	-36.83	-32.96	-27.97
-0.000007	-56.19	-46.60	-39.10	-35.54	-31.83	-26.98
-0.000006	-54.20	-44.90	-37.67	-34.26	-30.71	-26.03
-0.000005	-52.21	-43.24	-36.24	-32.99	-29.60	-25.09
-0.000004	-50.21	-41.61	-34.83	-31.75	-28.49	-24.15
-0.000003	-48.20	-39.98	-33.44	-30.50	-27.39	-23.23
-0.000002	-46.17	-38.34	-32.06	-29.27	-26.30	-22.29
-0.000001	-44.14	-36.69	-30.70	-28.05	-25.21	-21.36
0	-42.10	-35.01	-29.33	-26.83	-24.12	-20.43

0.000001	-40.04	-33.30	-27.94	-25.61	-23.02	-19.48
0.000002	-37.93	-31.58	-26.55	-24.38	-21.91	-18.51
0.000003	-35.73	-29.87	-25.12	-23.12	-20.79	-17.52
0.000004	-33.44	-28.11	-23.67	-21.84	-19.64	-16.47
0.000005	-31.01	-26.28	-22.19	-20.52	-18.45	-15.34
0.000006	-28.35	-24.37	-20.68	-19.15	-17.18	-14.00
0.000007	-25.40	-22.33	-19.11	-17.71	-15.83	-12.51
0.000008	-22.26	-20.08	-17.46	-16.17	-14.32	-11.03
0.000009	-19.09	-17.63	-15.67	-14.47	-12.66	-9.54
0.000010	-15.94	-15.17	-13.75	-12.66	-10.98	-8.06
0.000011	-12.79	-12.71	-11.80	-10.85	-9.31	-6.59
0.000012	-9.64	-10.27	-9.86	-9.05	-7.64	-5.12
0.000013	-6.50	-7.83	-7.92	-7.26	-5.99	-3.66
0.000014	-3.37	-5.40	-6.00	-5.48	-4.34	-2.21
0.000015	-0.26	-2.97	-4.09	-3.70	-2.71	-0.77
0.000016	2.84	-0.55	-2.18	-1.92	-1.09	0.68
0.000017	5.94	1.87	-0.28	-0.15	0.53	2.11
0.000018	9.05	4.27	1.62	1.61	2.14	3.53
0.000019	12.14	6.66	3.51	3.37	3.75	4.94
0.000020	15.21	9.05	5.39	5.12	5.36	6.35
0.000021	18.28	11.43	7.25	6.86	6.96	7.75
0.000022	21.35	13.81	9.12	8.59	8.56	9.11
0.000023	24.42	16.18	10.97	10.33	10.15	10.34
0.000024	27.49	18.54	12.82	12.05	11.70	11.41
0.000025	30.54	20.86	14.62	13.70	13.14	12.33
0.000026	33.45	23.06	16.31	15.23	14.44	13.14
0.000027	36.12	25.06	17.85	16.60	15.60	13.88
0.000028	38.51	26.86	19.24	17.83	16.63	14.52
0.000029	40.65	28.50	20.52	18.97	17.55	15.07
0.000030	42.60	30.02	21.73	20.01	18.38	15.54
0.000031	44.42	31.45	22.85	20.95	19.10	15.99
0.000032	46.12	32.81	23.90	21.79	19.75	16.40
0.000033	47.72	34.09	24.86	22.54	20.36	16.78
0.000034	49.25	35.31	25.73	23.23	20.93	17.14
0.000035	50.70	36.43	26.53	23.89	21.47	17.48
0.000036	52.08	37.47	27.27	24.51	21.97	17.80
0.000037	53.39	38.41	27.98	25.10	22.44	18.10
0.000038	54.64	39.29	28.65	25.66	22.90	18.38
0.000039	55.80	40.13	29.29	26.19	23.32	18.65
0.000040	56.85	40.92	29.90	26.71	23.74	18.91
0.000041	57.83	41.68	30.49	27.20	24.13	19.16
0.000042	58.76	42.41	31.05	27.67	24.51	19.40
0.000043	59.65	43.11	31.59	28.12	24.87	19.62
0.000044	60.51	43.78	32.11	28.56	25.23	19.84
0.000045	61.35	44.42	32.61	28.97	25.57	20.06
0.000046	62.15	45.04	33.09	29.37	25.90	20.26
0.000047	62.93	45.64	33.55	29.76	26.21	20.46
0.000048	63.68	46.23	34.00	30.14	26.52	20.65
0.000049	64.40	46.79	34.43	30.50	26.81	20.84
0.000050	65.11	47.34	34.85	30.86	27.10	21.02

Table B. 2. Moment Curvature for Beam B (Part 1)

Curvature (χ)	Timestep (minute)						
	0	15	30	45	60	75	90
-0.000050	-284.14	-636.29	-560.44	-459.13	-329.22	-272.06	-424.78
-0.000049	-284.07	-637.41	-568.07	-473.49	-345.25	-285.64	-424.45
-0.000048	-283.99	-638.48	-574.92	-485.70	-360.35	-298.37	-423.95
-0.000047	-283.91	-639.49	-581.40	-496.12	-374.31	-310.07	-423.29
-0.000046	-283.83	-640.45	-587.23	-505.45	-387.32	-320.69	-422.46
-0.000045	-283.75	-641.36	-592.70	-513.97	-398.91	-330.28	-421.47
-0.000044	-283.67	-642.19	-597.70	-521.63	-409.24	-338.81	-420.32
-0.000043	-283.58	-642.97	-602.20	-528.41	-418.64	-346.32	-418.99
-0.000042	-283.49	-643.70	-606.32	-534.52	-427.18	-353.05	-417.46
-0.000041	-283.40	-644.37	-610.04	-540.10	-434.79	-359.01	-415.73
-0.000040	-283.31	-644.98	-613.46	-545.18	-441.47	-364.11	-413.83
-0.000039	-283.21	-645.54	-616.63	-549.65	-447.23	-368.40	-411.72
-0.000038	-283.11	-646.05	-619.57	-553.56	-452.23	-371.93	-409.34
-0.000037	-283.01	-646.49	-622.26	-557.06	-456.37	-374.49	-406.70
-0.000036	-282.89	-646.88	-624.69	-560.16	-459.66	-376.33	-403.78
-0.000035	-282.77	-647.20	-626.88	-562.88	-462.24	-377.55	-400.57
-0.000034	-282.65	-647.44	-628.87	-565.18	-463.97	-378.10	-397.00
-0.000033	-282.52	-647.61	-630.64	-567.07	-464.87	-377.95	-393.03
-0.000032	-282.38	-647.69	-632.17	-568.55	-464.84	-377.08	-388.62
-0.000031	-282.24	-647.65	-633.45	-569.60	-464.02	-375.56	-383.62
-0.000030	-282.08	-647.50	-634.46	-570.16	-462.44	-373.31	-377.86
-0.000029	-281.92	-647.26	-635.22	-570.08	-460.14	-370.32	-371.06
-0.000028	-281.74	-646.92	-635.71	-568.90	-457.06	-366.63	-362.52
-0.000027	-281.57	-646.45	-635.89	-566.31	-453.15	-362.17	-352.21
-0.000026	-281.39	-645.83	-635.79	-562.33	-448.35	-357.01	-340.35
-0.000025	-281.20	-645.03	-635.36	-556.84	-442.70	-351.03	-327.40
-0.000024	-281.02	-643.98	-634.60	-549.71	-436.22	-344.20	-314.05
-0.000023	-280.83	-642.64	-633.45	-541.56	-428.82	-336.52	-300.30
-0.000022	-280.59	-640.89	-631.76	-532.38	-420.44	-327.85	-286.19
-0.000021	-280.34	-638.71	-629.01	-522.10	-411.03	-318.14	-271.75
-0.000020	-280.08	-636.25	-622.39	-510.63	-400.45	-307.31	-256.97
-0.000019	-279.76	-633.52	-611.79	-497.85	-388.54	-295.13	-241.89
-0.000018	-279.44	-630.29	-597.47	-483.45	-375.03	-281.80	-226.52
-0.000017	-279.12	-626.63	-581.08	-467.12	-360.23	-268.25	-210.84
-0.000016	-278.79	-622.41	-562.49	-449.61	-344.37	-255.29	-194.78
-0.000015	-278.36	-617.78	-542.44	-430.94	-327.46	-243.55	-178.38
-0.000014	-277.90	-612.68	-521.00	-411.12	-309.52	-232.13	-161.87
-0.000013	-277.35	-606.85	-498.24	-390.24	-290.51	-220.45	-146.75
-0.000012	-276.80	-592.10	-474.26	-368.35	-271.37	-208.35	-133.98
-0.000011	-276.14	-562.63	-448.97	-345.35	-254.16	-195.75	-122.34
-0.000010	-275.32	-531.63	-422.46	-321.09	-238.60	-182.64	-111.15
-0.000009	-274.43	-499.67	-394.65	-295.51	-222.89	-168.65	-99.82
-0.000008	-273.31	-466.82	-365.46	-268.81	-206.59	-153.58	-88.40
-0.000007	-271.86	-432.84	-334.95	-240.89	-189.35	-137.35	-76.64
-0.000006	-238.31	-397.85	-302.54	-213.45	-170.52	-119.91	-64.80
-0.000005	-198.66	-361.18	-268.03	-190.23	-150.00	-100.64	-52.43
-0.000004	-158.97	-320.27	-231.28	-166.06	-127.14	-79.37	-39.34
-0.000003	-119.25	-273.99	-191.63	-139.26	-101.28	-55.29	-25.42
-0.000002	-79.51	-223.19	-147.87	-108.10	-71.15	-27.43	-11.36
-0.000001	-39.76	-164.21	-97.48	-69.88	-35.71	3.13	3.84
0	0.00	-81.58	-36.85	-25.25	0.88	33.93	19.76

0.000001	39.74	9.09	20.20	19.59	37.60	64.84	36.49
0.000002	79.46	83.55	71.48	64.22	74.29	95.75	54.45
0.000003	119.18	148.75	115.31	105.58	110.75	126.54	74.01
0.000004	158.88	207.82	153.50	142.69	145.04	156.95	93.40
0.000005	198.55	261.82	187.25	175.86	176.21	185.30	112.04
0.000006	238.16	312.49	218.18	205.66	204.30	211.22	129.71
0.000007	271.80	360.35	247.97	232.69	229.85	235.03	146.25
0.000008	273.29	405.71	283.11	257.24	253.02	256.77	161.65
0.000009	274.42	449.22	319.32	279.75	274.17	276.78	176.31
0.000010	275.32	489.76	353.39	300.58	293.35	295.15	190.08
0.000011	276.14	525.95	385.16	319.93	310.99	311.91	202.70
0.000012	276.80	559.18	414.69	337.70	326.79	327.24	214.65
0.000013	277.36	590.51	442.08	354.45	341.16	341.12	225.82
0.000014	277.90	611.24	467.39	370.72	354.45	353.92	236.38
0.000015	278.37	618.38	490.45	386.75	366.41	365.45	246.52
0.000016	278.80	624.35	511.53	404.33	377.37	375.66	256.17
0.000017	279.13	629.32	530.95	423.11	387.27	384.95	265.36
0.000018	279.45	633.48	548.71	440.68	396.37	393.52	274.11
0.000019	279.77	636.88	564.84	456.84	405.03	401.33	282.67
0.000020	280.09	639.79	579.49	471.69	413.36	408.30	291.19
0.000021	280.36	642.30	592.83	485.30	421.66	414.73	299.89
0.000022	280.60	644.34	604.96	497.66	430.70	420.62	309.30
0.000023	280.84	645.88	615.31	508.92	440.80	426.05	320.13
0.000024	281.04	647.20	622.85	519.17	450.91	431.23	331.57
0.000025	281.22	648.23	627.47	528.38	460.20	436.26	342.65
0.000026	281.40	649.01	630.22	536.64	468.63	441.27	353.32
0.000027	281.58	649.63	632.02	543.90	476.25	446.69	363.68
0.000028	281.76	650.10	633.16	550.33	483.07	452.41	373.73
0.000029	281.93	650.41	633.72	555.84	489.09	458.01	383.49
0.000030	282.09	650.58	633.79	560.49	494.34	463.15	392.93
0.000031	282.25	650.62	633.44	564.05	498.84	467.78	402.02
0.000032	282.39	650.54	632.67	566.52	502.69	471.86	410.12
0.000033	282.53	650.37	631.52	567.94	505.83	475.43	416.77
0.000034	282.65	650.10	630.04	568.34	508.22	478.46	422.10
0.000035	282.78	649.75	628.22	567.75	509.83	480.94	426.71
0.000036	282.90	649.31	626.04	566.38	510.74	482.96	430.79
0.000037	283.01	648.80	623.57	564.44	510.87	484.49	434.45
0.000038	283.11	648.22	620.77	561.94	510.41	485.49	437.79
0.000039	283.21	647.57	617.61	558.87	509.26	485.98	440.81
0.000040	283.31	646.87	614.11	555.28	507.43	485.91	443.53
0.000041	283.40	646.09	610.18	551.16	504.68	485.31	445.89
0.000042	283.49	645.24	605.78	546.37	501.09	484.10	447.98
0.000043	283.58	644.34	600.98	540.87	496.74	482.44	449.91
0.000044	283.67	643.36	595.78	534.82	491.65	480.24	451.69
0.000045	283.75	642.32	590.11	528.08	485.71	477.40	453.34
0.000046	283.83	641.23	584.09	520.81	479.09	473.94	454.84
0.000047	283.91	640.09	577.36	512.48	471.53	469.66	456.22
0.000048	283.99	638.89	569.74	502.92	462.99	464.73	457.48
0.000049	284.07	637.63	561.29	492.56	453.59	459.08	458.65
0.000050	284.14	636.28	552.31	481.22	443.24	452.74	459.72

Table B. 2. Moment Curvature for Beam B (Part 2)

Curvature (χ)	Timestep (minute)					
	105	120	135	150	165	180
-0.000050	-343.01	-291.48	-246.09	-205.36	-171.36	-144.58
-0.000049	-341.17	-289.81	-244.61	-204.05	-170.21	-143.59
-0.000048	-339.25	-288.05	-243.06	-202.69	-169.02	-142.55
-0.000047	-337.23	-286.23	-241.44	-201.27	-167.79	-141.48
-0.000046	-335.13	-284.33	-239.74	-199.81	-166.51	-140.38
-0.000045	-332.94	-282.35	-237.99	-198.27	-165.18	-139.23
-0.000044	-330.64	-280.29	-236.16	-196.68	-163.79	-138.03
-0.000043	-328.24	-278.13	-234.25	-195.02	-162.35	-136.79
-0.000042	-325.73	-275.87	-232.27	-193.29	-160.85	-135.49
-0.000041	-323.09	-273.52	-230.21	-191.48	-159.28	-134.15
-0.000040	-320.34	-271.07	-228.05	-189.59	-157.65	-132.74
-0.000039	-317.45	-268.51	-225.80	-187.62	-155.95	-131.29
-0.000038	-314.45	-265.84	-223.45	-185.57	-154.18	-129.77
-0.000037	-311.32	-263.04	-221.01	-183.43	-152.33	-128.20
-0.000036	-308.05	-260.12	-218.45	-181.21	-150.41	-126.55
-0.000035	-304.60	-257.08	-215.77	-178.89	-148.41	-124.83
-0.000034	-301.02	-253.90	-212.97	-176.46	-146.32	-123.05
-0.000033	-297.24	-250.56	-210.07	-173.92	-144.14	-121.20
-0.000032	-293.25	-247.06	-207.03	-171.27	-141.87	-119.26
-0.000031	-289.05	-243.37	-203.84	-168.50	-139.48	-117.24
-0.000030	-284.61	-239.48	-200.49	-165.59	-136.97	-115.12
-0.000029	-279.90	-235.36	-196.96	-162.53	-134.34	-112.89
-0.000028	-274.86	-231.00	-193.21	-159.30	-131.60	-110.56
-0.000027	-269.46	-226.30	-189.22	-155.91	-128.74	-108.12
-0.000026	-263.58	-221.24	-184.97	-152.32	-125.73	-105.57
-0.000025	-257.09	-215.71	-180.42	-148.50	-122.55	-102.90
-0.000024	-249.78	-209.56	-175.45	-144.39	-119.16	-100.08
-0.000023	-241.14	-202.48	-169.93	-139.95	-115.55	-97.12
-0.000022	-230.12	-193.57	-163.60	-135.07	-111.68	-93.99
-0.000021	-217.23	-182.77	-155.82	-129.54	-107.47	-90.66
-0.000020	-203.33	-170.69	-146.70	-122.89	-102.80	-87.07
-0.000019	-189.43	-158.40	-136.67	-115.25	-97.39	-83.21
-0.000018	-175.53	-146.23	-126.54	-107.03	-91.29	-78.90
-0.000017	-161.58	-134.16	-116.53	-98.85	-84.78	-74.01
-0.000016	-147.66	-122.16	-106.65	-90.81	-78.19	-68.74
-0.000015	-133.88	-110.29	-96.99	-82.84	-71.75	-63.50
-0.000014	-120.15	-98.63	-87.38	-75.11	-65.49	-58.35
-0.000013	-106.55	-87.15	-78.06	-67.55	-59.39	-53.33
-0.000012	-93.06	-75.75	-68.95	-60.19	-53.36	-48.37
-0.000011	-79.78	-64.72	-60.03	-52.94	-47.50	-43.56
-0.000010	-66.59	-53.96	-51.32	-45.95	-41.85	-38.91
-0.000009	-53.72	-43.36	-42.92	-39.16	-36.34	-34.38
-0.000008	-41.13	-33.17	-34.80	-32.64	-31.06	-30.01
-0.000007	-29.35	-23.27	-26.98	-26.33	-25.93	-25.77
-0.000006	-19.48	-13.79	-19.35	-20.15	-20.90	-21.60
-0.000005	-10.82	-4.81	-12.06	-14.27	-16.11	-17.60
-0.000004	-2.82	2.94	-5.02	-8.60	-11.46	-13.71
-0.000003	4.72	9.63	1.64	-3.21	-7.03	-9.99
-0.000002	11.92	15.67	7.78	1.96	-2.79	-6.42
-0.000001	18.86	21.29	13.21	6.94	1.32	-2.96
0	25.55	26.67	18.10	11.68	5.29	0.40

0.000001	32.17	31.78	22.68	16.07	9.18	3.66
0.000002	38.68	36.77	26.85	19.92	12.86	6.90
0.000003	45.06	41.46	30.80	23.47	16.24	10.01
0.000004	51.43	46.00	34.64	26.88	19.42	13.00
0.000005	57.63	50.50	38.39	30.17	22.48	15.97
0.000006	63.79	54.95	42.00	33.32	25.41	19.00
0.000007	70.03	59.28	45.53	36.39	28.30	22.59
0.000008	76.10	63.51	48.97	39.38	31.18	26.41
0.000009	82.05	67.66	52.36	42.31	34.36	30.04
0.000010	87.94	71.77	55.76	45.32	38.05	33.53
0.000011	93.84	75.87	59.15	48.45	41.73	36.91
0.000012	99.66	80.02	62.61	51.94	45.37	40.22
0.000013	105.51	84.21	66.17	55.91	48.97	43.50
0.000014	111.42	88.43	69.94	59.92	52.55	46.75
0.000015	117.55	92.79	74.00	63.94	56.08	49.95
0.000016	123.94	97.34	78.65	67.99	59.58	53.11
0.000017	130.66	102.23	83.55	72.04	63.11	56.25
0.000018	137.74	107.79	88.45	76.12	66.67	58.99
0.000019	145.81	113.85	93.42	80.27	70.20	61.16
0.000020	154.73	120.09	98.45	84.46	73.53	63.07
0.000021	163.59	126.49	103.58	88.65	76.28	64.83
0.000022	172.31	133.03	108.78	92.84	78.61	66.46
0.000023	180.92	139.68	114.06	96.68	80.74	67.85
0.000024	189.48	146.35	119.42	99.91	82.66	69.04
0.000025	198.00	153.05	124.66	102.74	84.28	70.09
0.000026	206.44	159.57	129.17	105.31	85.67	71.00
0.000027	214.38	165.26	133.09	107.54	86.93	71.84
0.000028	221.03	170.05	136.67	109.41	88.07	72.61
0.000029	226.60	174.35	139.83	111.13	89.11	73.32
0.000030	231.58	178.23	142.54	112.74	90.08	73.99
0.000031	236.09	181.55	145.00	114.24	91.00	74.63
0.000032	240.24	184.42	147.22	115.66	91.88	75.24
0.000033	243.87	187.06	149.26	116.97	92.73	75.81
0.000034	247.02	189.46	151.17	118.19	93.51	76.37
0.000035	249.91	191.65	152.95	119.35	94.24	76.89
0.000036	252.59	193.68	154.58	120.45	94.93	77.38
0.000037	255.06	195.57	156.11	121.48	95.58	77.84
0.000038	257.38	197.35	157.54	122.45	96.19	78.27
0.000039	259.58	199.03	158.89	123.36	96.78	78.68
0.000040	261.66	200.62	160.16	124.22	97.33	79.06
0.000041	263.61	202.13	161.37	125.03	97.87	79.43
0.000042	265.44	203.55	162.52	125.80	98.38	79.78
0.000043	267.18	204.90	163.62	126.55	98.87	80.12
0.000044	268.84	206.19	164.66	127.25	99.34	80.45
0.000045	270.43	207.42	165.64	127.92	99.79	80.76
0.000046	271.93	208.58	166.59	128.56	100.21	81.05
0.000047	273.34	209.68	167.49	129.17	100.61	81.33
0.000048	274.67	210.72	168.34	129.75	101.00	81.60
0.000049	275.93	211.73	169.15	130.29	101.37	81.86
0.000050	277.13	212.69	169.92	130.82	101.72	82.11